Automated Construction of Equivalent Electrical Circuit Models for Electromagnetic Components and Systems

Zur Erlangung des akademischen Grades Doktor-Ingenieur (Dr.-Ing.)
genehmigte Dissertation von Felix Traub, M.Sc., aus Stuttgart
April 2014 — Darmstadt — D 17

TECHNISCHE
UNIVERSITÄT
DARMSTADT

Fachbereich Elektrotechnik
und Informationstechnik

Institut für Theorie
Elektromagnetischer Felder (TEMF)

Automated Construction of Equivalent Electrical Circuit Models for Electromagnetic Components and Systems

Genehmigte Dissertation von Felix Traub, M.Sc., aus Stuttgart

1. Gutachten: Prof. Dr. Thomas Weiland
2. Gutachten: Prof. Dr. Albert Ruehli

Tag der Einreichung: 28. Oktober 2013
Tag der Prüfung: 3. Dezember 2013

Darmstadt — D 17

Bitte zitieren Sie dieses Dokument als:
URN: urn:nbn:de:tuda-tuprints-38056

Dieses Dokument wird bereitgestellt von tuprints,
E-Publishing-Service der TU Darmstadt.
http://tuprints.ulb.tu-darmstadt.de
tuprints@ulb.tu-darmstadt.de

Die Veröffentlichung steht unter folgender Creative Commons Lizenz:
Namensnennung-NichtKommerziell-KeineBearbeitung 3.0 Deutschland

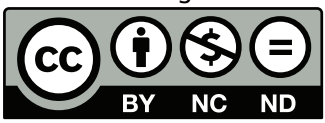

http://creativecommons.org/licenses/by-nc-nd/3.0/de/

Automated Construction of Equivalent Electrical Circuit Models for Electromagnetic Components and Systems

Vom Fachbereich Elektrotechnik und Informationstechnik
der Technischen Universität Darmstadt
zur Erlangung der Würde eines
Doktor-Ingenieurs (Dr.-Ing.)
genehmigte Dissertation

von

Felix Traub, M.Sc.

Geboren am 31. Dezember 1985 in Stuttgart

Referent:	Prof. Dr.-Ing. Thomas Weiland
Korreferent:	Prof. Dr. Albert Ruehli
Tag der Einreichung:	27. Oktober 2013
Tag der mündlichen Prüfung:	3. Dezember 2013

D17
Darmstadt 2014

Abstract

The description of electromagnetic components and systems by electrical circuit models is indispensable for a wide range of applications: In the field of Electromagnetic Compatibility (EMC), electrical circuit models are ideally suited for the detection of EMC coupling paths, which are very difficult to track for 3-dimensional (3D) geometries. In the field of numerical optimization techniques, electrical circuit models offer short simulation times and allow the coupling of the electromagnetic domain to other physical domains. In the field of power electronics, electrical circuit models describe energy dissipation due to parasitic electromagnetic interactions.

Historically, electrical circuits and electromagnetic fields were developed as models for the description of electromagnetic phenomena at about the same time. The description in terms of electromagnetic fields has turned out to be the more general model, electrical circuits being a quasistatic approximation thereof. However, in their range of validity, electrical circuits are intriguingly simple, compact and intuitive description of electromagnetic processes. For purposes of analysis and visualization, a description in terms of electrical circuits is often preferable. If an electromagnetic system can be described in terms of an electrical circuit, the electrical circuit model is called an equivalent electrical circuit.

The construction of an equivalent electrical circuit model is in general cumbersome and less formalized than a description in terms of electromagnetic fields. No general and reliable technique for the automated construction of equivalent electrical circuit models exists. The aim of this thesis is the development of a technique that allows a fully automated construction of equivalent electrical circuit models from 3D geometry information. Instead of constructing the circuit directly from geometry data, our approach consists of reducing a field-theoretical model to an equivalent electrical circuit model. In this way, we exploit the generality of the field-theoretical approach, which can be applied for a wide range of geometries using state-of-the-art simulation techniques. The electromagnetic effects having the largest impact in the frequency range of interest are then used for the construction of the electrical circuit model. The circuit elements can be seen as condensed representations of these field-theoretical processes. The reduction process allows a very direct assessment of the accuracy of the electrical circuit model.

Zusammenfassung

Die Beschreibung elektromagnetischer Komponenten und Systeme durch elektrische Netzwerkmodelle wird in vielen Gebieten erfolgreich angewandt: Im Gebiet der elektromagnetischen Verträglichkeit (EMV) ermöglichen elektrische Netzwerkmodelle die einfache Detektion von EMV Koppelpfaden, die in dreidimensionalen Modellen nur schwer zu identifizieren sind. Für numerische Optimierungsverfahren sind die kurzen Rechenzeiten und die einfache Kopplung zu weiteren physikalischen Domänen attraktiv. Ersatzschaltbilder für leistungselektronische Komponenten und Systeme beschreiben die Verschlechterung der Effizienz durch parasitäre Vorgänge.

Historisch entstanden elektrische Netzwerke und elektromagnetische Felder als Modelle zur Beschreibung elektromagnetischer Phänomene zu derselben Zeit. Die Beschreibung durch elektromagnetische Felder hat sich als sehr allgemein und präzise bewährt. Elektrische Netzwerke bilden eine quasistatische Approximation des allgemeineren Modells. In ihrem Gültigkeitsbereich sind elektrische Netzwerke jedoch sehr einfache, kompakte und intuitive Modelle für elektromagnetische Komponenten und Systeme. Sie eignen sich daher oft besser als feldtheoretische Modelle zur Analyse und Visualisierung der wichtigsten Vorgänge. Solche Netzwerkmodelle werden Ersatzschaltbilder genannt.

Die Erstellung eines Netzwerkmodells ist oftmals mühsam und schwach formalisiert im Vergleich zur feldtheoretischen Darstellung. Es existiert kein allgemein anwendbares und verlässliches Verfahren zur Erstellung solcher Modelle. Im Rahmen dieser Arbeit entwickeln wir ein Verfahren zur automatisierten Erstellung von Netzwerkmodellen aus 3D Geometrieinformation. Anstatt das Netzwerkmodell direkt aus Geometriedaten zu erstellen, kondensieren wir ein feldtheoretische Modell zu einem Ersatzschaltbild. Wir nutzen damit den hohen Formalisierungsgrad der feldtheoretischen Beschreibung. Diese kann durch moderne Simulationsverfahren auf allgemeine Komponenten und Systeme angewandt werden. Zur Erstellung des Ersatzschaltbildmodells werden dann nur diejenigen elektromagnetischen Vorgänge berücksichtigt, die zur Beschreibung in einem gegebenen Frequenzbereich am wichtigsten sind. Das Verfahren erzeugt damit sehr kompakte Modelle. Die Genauigkeit des Netzwerkmodells kann sehr direkt bewertet werden.

Contents

1 Introduction

In 2010, the first Formula 1 car was designed using only computational methods. At around the same time, virtual engineering became more and more a reality even in industries having to comply with strict reliability and security requirements, e.g., the automotive or airplane industry. Very generally, Virtual Engineering covers a wide range of computational methods which are integrated in the product development process in order to design more powerful products in a faster and cheaper way.

The increasing use of computational methods is due to more powerful hardware, with memory availability and computational speed growing exponentially with time, and to more intelligent software, allowing to predict the real behavior of a component or system based entirely on computer simulations. In Fig. 1.1, the conventional design process is shown on the left hand side, while a more advanced design process using virtual engineering is shown on the right hand side. In this realistic depiction of an industrial design process, virtual engineering does not completely replace the conventional process, but it is embedded in order to make best use of its advantages. Virtual engineering allows shorter cycles at earlier stages in the design process. There is no need for expensive and time-consuming testing of prototypes. Design faults can be detected and corrected at an early stage, where a redesign is comparably cheap.

In order for virtual engineering to work efficiently, two ingredients are needed. First, it is indispensable to have at one's hand simulation methods which predict the behavior of the real device with sufficient accuracy and which need minimal time. Second, there must be a way to extract from the simulation results as fast as possible the relevant effects and interactions in order to improve the design in a systematic and targeted way. For the purpose of brevity and illustration, we refer to the first ingredient as **predicting** the behavior and to the second step as **understanding** the behavior.

The work presented in this thesis is set in the framework of industrial development of electromagnetic components and systems. For the purposes of industry, the first ingredient is already available in great abundance in modern commercial and open-source simulation tools. The second ingredient, however, is based almost entirely on the working experience of experts in the field to perform a root-cause analysis of the simulation results, extract the relevant fault mechanisms and propose a redesign which eliminates the fault mechanisms.

The numerical simulations used in the first ingredient are very powerful and general tools. The description of practical electric components or systems in terms of numerical simulations leads to algebraic systems with millions of degrees of freedom. This high complexity makes it very difficult to find the root-cause of unintended behavior, i.e., to understand the interactions leading to unwanted effects. Identifying the root-cause is indispensable before appropriate measures can be defined to restore the desired behavior.

An a priori completely different approach to predicting the electric behavior of electromagnetic components or systems is by way of an electrical circuit model. Electrical circuit models can be seen as condensed descriptions of the physical reality, i.e., the local properties of a complex electromagnetic field configuration are reduced to a small set of effective parameters describing the electromagnetic behavior. A description in terms of electrical circuit model has the following advantages:

- The low complexity of electrical circuit models greatly simplifies root cause analysis. The root cause for unintended behavior can usually be attributed to interactions of few circuit elements only. These interactions can easily be detected and visualized.
- Most electrical engineers are more familiar with electrical circuit models than with field theoretical descriptions of electromagnetic components and systems. Electrical circuits are thus an intuitive way to visualize the functionality as well as parasitic processes.
- The computation times of electrical circuit models are very short. Furthermore, electrical circuit models can be coupled with models from different physical domains (e.g., thermal or mechanical models). This allows to run extensive multi-domain optimization algorithms to find optimal designs for all domains.

For an electrical circuit model to be used in this way, it has to satisfy several properties:

- The **compactness** requirement: The electrical circuit model has to be as compact as possible while reproducing all interactions needed to describe the behavior of the electromagnetic component or system in the domain of operation. In other words, there are no circuit elements which obfuscate analysis while not contributing significantly in the range of operation.
- The **physicality** requirement: The elements of the electrical circuit model can be related to physical properties of the electromagnetic component or

system. For example, each resistor or inductor in the electrical circuit model can be attributed to a conductor while each capacitor can be attributed to local charge accumulations.

- The **accuracy** requirement: An electrical circuit model is a priori a qualitative model for an electromagnetic component or system. We require that the accuracy of the electrical circuit model can be controlled to guarantee user-defined limits on accuracy[1].

While the properties of electrical circuit models are very desirable, their generation is usually very cumbersome. Above, we indicated that electrical circuit models describe both functionality and parasitic processes. This requires that, in general, these processes and interactions already have to be known for the construction of the electrical circuit model. In the literature, the construction of electrical circuits usually is a two-step process: First, a topology is proposed on the basis of some intuitive understanding of the physical processes. Second, the parameters of the electrical circuit are used as fitting parameters to maximize the quantitative agreement with the real component or system. This procedure is little formalized, depends heavily on the intuition of experts, and is the opposite of the ultimate goal, i.e., to generate the understanding on the basis of an electrical circuit model rather than the 3D model.

In this thesis, we propose a method to automatically generate electrical circuit models for arbitrary 3D electromagnetic components or systems with no prior knowledge and understanding of functionality and parasitic processes. Our method is a two-step process:

1. The electromagnetic component or system is analyzed on a 3D basis using electromagnetic field simulations. This analysis is very general. In particular, all physical interactions are included and very good quantitative results can be expected. The 3D interactions are then separated into those interactions which are relevant in the frequency domain of operation, and those interactions which are irrelevant. This step is executed using an eigenmode analysis and a decomposition of the spectrum in relevant and irrelevant eigenmodes.

2. The relevant interactions are modeled using circuit elements, all irrelevant interactions are discarded. Both the topology and the values of the circuit

[1] Improving the accuracy of any physical model always requires increasing the number of degrees of freedom, i.e., shifting from a qualitative model to a quantitative model. Restricting ourselves to limited accuracy allows to keep the number of degrees of freedom small and retain the principal characteristic of electrical circuits, straightforward interpretability.

elements can be derived directly from the 3D eigenmodes. The separation of eigenmodes allows a very direct control of electrical circuit accuracy.

In Sect. 1.1 we illustrate in further detail the importance of electrical circuit models. We show areas of application and summarize the state of the art in the construction of electrical circuit models. In Sect. 1.2 we give a short outline of this thesis.

1.1 Uses of Electrical Circuit Models

The use of electrical circuits is very widespread in industry and in science. In this section, we illustrate in greater detail three main areas of application of electrical circuit models: First, the use of electrical circuit models to perform a root cause analysis or study different design variants. Second, the use of electrical circuits as simple models for complex 3D components and systems. Third, the use of electrical circuits for fast coupled simulations and multi-domain optimizations.

1.1.1 Design Evaluation and Root Cause Analysis

The typical problem in the design process of electromagnetic components is an electromagnetic behavior which differs from the intended behavior. The primary goal in this situation is to quickly determine the root cause for the unintended behavior and to remove it by redesign or suitable filters. Due to their compact size and the limited set of possible interactions, electrical circuits are well suited to perform a root cause analysis.

One of the first systematic applications of electrical circuit models arose in the modeling of interconnects in Very Large Scale Integrated (VLSI) circuits. At high frequencies, inductances of (physically) long interconnects become relevant. Electrical circuit models are used for both quantitative [1] and qualitative [2] analysis. With the Partial Element Equivalent Circuit (PEEC) method [3], a systematic way to construct electrical circuit models for typical integrated circuit structures was introduced.

The use of electrical circuits is very widespread in power electronics. In power electronics applications, the functionality is determined by non-linear lumped circuit elements, e.g., diodes and Insulated-Gate Bipolar Transistor (IGBT). Instead of including the active elements in field simulations or ignoring the distributed circuit design in a pure circuit simulation, the easiest way of describing such a system is by coupling the non-linear circuit elements with an equivalent electrical circuit for

the passive geometry to describe the parasitic impact of the latter, e.g., inductances of busbars [4] and unbalanced current sharing [5]. In [6], electrical circuit models are used to discuss different topologies for resonant switching converters.

One of the main fields of application of electrical circuit models is EMC. EMC deals with the detection and elimination of unintended electromagnetic effects. In [7], the impact of parasitic inductances of the power supply lines on the device behavior is investigated and an optimal strategy for the positioning of decoupling capacitors is derived. For these positions to be well defined physically, the link between geometry (physical positions) and electrical circuit model (inductors) is crucial. In [8], the effect of parasitic couplings in Electromagnetic Interference (EMI) filters is studied using electrical circuit models for different filter topologies.

A very general method for root-cause analysis is a sensitivity analysis which allows to quantify the impact of model parameters on electromagnetic behavior. A general method for a sensitivity analysis of electrical circuits is introduced in [9]. In [10], the method is applied to a circuit of partial inductances generated by the PEEC method.

1.1.2 Simple Description for Complex Processes

The equations of motion of electrical circuits (Chap. 2) contain only a limited set of three basic interactions (resistive, inductive, and capacitive). When large systems of elementary interactions are allowed, the response can nevertheless be very complex. In fact, it can be shown that any system of ordinary differential equations can be written in terms of an equivalent electrical circuit [11]. Equivalently, it can be shown that every system with a response that can be written as a rational function with respect to some parameter (usually the frequency) can be described in terms of an equivalent electrical circuit [12, 13]. In general, these circuits are purely mathematical objects. In this thesis, we restrict ourselves to electrical circuit models which illustrate and reproduce the basic physical processes.

Electrical circuit models can be used for the modeling of frequency-dependent material properties. In [14], an electrical circuit model is used to illustrate the impact of the substrate on the quality factor of spiral inductors for, e.g., Radio-Frequency Identification (RFID) tags. In [15], the impact of patterned shields on the quality factor is studied using an electrical circuit models. The circuits used in these applications are constructed from an existing understanding of physical couplings, the circuit elements are phenomenological descriptions of these processes.

Electrical circuits can also be used to describe different operating conditions of battery systems. The electrical circuits are constructed by first proposing a topology based on the physical processes in the battery and second parametrizing the circuit elements to comply with the real behavior of the battery [16]. The range of applications is very wide and covers runtime effects [17] as well as short-time behavior [18].

1.1.3 Coupled Simulations

The design process of components and systems is never restricted to a single domain. Instead, requirements from different domains, e.g., the electromagnetic, thermal and mechanical domains, have to be met simultaneously. On the computational level, this requires coupling of the physical models. Electrical circuits are very well suited to coupled simulations. Their computation time is low and coupling mechanisms are known for a variety of domains.

Coupling of electromagnetic and mechanical models is important, e.g., in the modeling of piezoelectric devices. The coupling of an electrical circuit model with appropriate mechanical models is described, e.g., in [19, 20].

In power electronics applications, heat management is a crucial factor for good device design and thermo-mechanical breakdown a major factor limiting lifetime, [21]. A very general procedure for the coupling of electrical circuit models and thermal models is presented in [22, 23]. In [24, 25], thermal component models for semiconductor devices are constructed and coupled with electrical circuit models. On the system level, [26] describes the coupling of electrical circuits with thermal models to describe entire power modules. In [27], an inherently coupled problem, a superconducting fault current limiter, is described in terms of an electrical circuit coupled with a corresponding equivalent thermal circuit.

1.2 Outline of the Thesis

In Chap. 2, the electrical circuit model for the description of electromagnetic components and systems is introduced. The equations of motion for electrical circuits are Kirchhoff's equations. Kirchhoff's equations are supplemented by a set of constitutive equations for the circuit elements. The circuit elements are defined using energy concepts. With the Fourier transform, electrical circuit theory can be transformed from the time domain to the frequency domain. Using the theory of graphs, electrical circuit theory can be formulated on a strictly mathematical basis.

It is shown that all information about the electrical circuit is contained in a matrix polynomial in the complex frequency. The coefficient matrices of different orders are directly related to the different types of circuit elements.

In Chap. 3, field theoretical models for electromagnetic components and systems are described. The equations of motion of electromagnetism are the macroscopic Maxwell's equations. The field-theoretical model of Maxwell's equations is compared with the electrical circuit model from the previous chapter. It is shown that electrical circuits cannot describe all electromagnetic phenomena incorporated in Maxwell's equations. We therefore show a quasistatic approximation of Maxwell's equations, Darwin's model, which exhibits the same range of phenomena as electrical circuits. The link between electrical circuit models and the field theoretical Darwin model is established using energy concepts.

In Chap. 4, discretization schemes are introduced which allow to implement and solve electromagnetic systems on a computer. In this thesis, the Finite Element Method (FEM) is mainly used. We also introduce important features of the PEEC Method, which is the state-of-the-art method for the construction of electrical circuit models.

In Chap. 5, the theory of polynomial eigenvalue problems is introduced. In this thesis, the theory of eigenfrequencies and eigenmodes is used to separate relevant from irrelevant phenomena in the frequency range of interest. Neglecting irrelevant phenomena enables us to construct very compact, but still accurate electrical circuit models. We also show how practical eigenvalue problems can be solved using a numerical scheme, the Lanczos method.

In Chap. 6, all concepts from the previous sections will be combined to yield a procedure to automatically construct electrical circuit models for electromagnetic components and systems. The procedure will consist of two steps: In the first step, the component or system is described using a field-theoretical model. The field theoretical model is very general and includes all physical couplings. After performing an eigenmode analysis, irrelevant couplings are automatically removed when all eigenmodes with eigenfrequencies outside the frequency range of interest are discarded. In the second step, the remaining 3D eigenmodes are projected on eigenmodes of an appropriate electrical circuit model. The explicit form of the electrical circuit model can be constructed from its eigenmodes. By construction, the electrical circuit model only contains the most relevant effects in the frequency range of interest and is very compact. The circuit elements can be related to physical quantities and design features. The accuracy of the electrical circuit model can be controlled very directly.

In Chap. 7, our method is tested and applied to realistic examples. As sanity check, we compute electrical circuit models for conductor geometries for which analytical expression are known and prove the validity of both our method and the implementation. Our method is then applied to realistic examples describing real products from an industrial partner, Robert Bosch GmbH, [28].

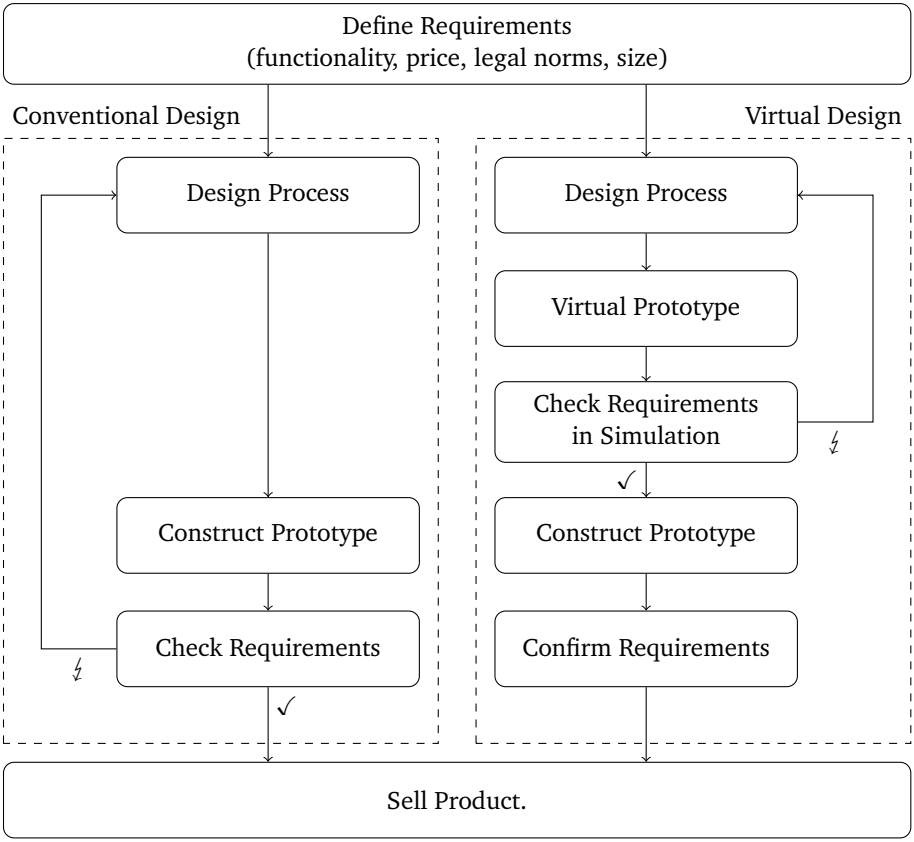

Figure 1.1.: Industrial design process with and without virtual engineering

2 Electrical Circuits

Electrical Circuits are simple but powerful models for the description of electromagnetic components and systems. The equations of motion for electrical circuits are Kirchhoff's equations. Kirchhoff's equations are supplemented by a set of constitutive equations for the circuit elements. The circuit elements are defined using energy concepts. In following chapters, these energy concepts will establish the connection to the field theoretical description. With the Fourier transform, electrical circuit theory can be transformed from the time domain to the frequency domain.

Using the theory of graphs, electrical circuit theory can be formulated on a strictly mathematical basis. It is shown that all information about the electrical circuit is contained in a matrix polynomial in the complex frequency. The coefficient matrices of different orders correspond to the different types of circuit elements. This matrix polynomial will be analyzed in Chap. 6 using the spectral theory of matrix polynomials.

2.1 Electrical Circuit Theory

The subject of electrical circuit theory is the study of the properties of electrical circuits. An electrical circuit is built up from vertices (nodes) which are connected by edges (circuit elements). A generic electrical circuit is shown in Fig. 2.1.

Put very simply, the nodes of the electrical circuit are capable of accumulating electric charge q while the edges are capable of supporting the flow of electric current I from one node to another node. The (differential) charge transfer between the end nodes of an edge is related to the current flowing to the edge by

$$I = \frac{\mathrm{d}q}{\mathrm{d}t}. \tag{2.1}$$

Electric currents result from energy differences. These energy differences are described in terms of voltages. More precisely, if a current I flowing along an edge leads to a (differential) change in electromagnetic energy $\frac{\mathrm{d}E}{\mathrm{d}t}$, the voltage V assigned to the edge is equal to

$$V = \frac{\mathrm{d}E/\mathrm{d}t}{I} = \frac{P}{I}. \tag{2.2}$$

$P = \frac{\mathrm{d}E}{\mathrm{d}t}$ is the power, i.e., the amount of energy per time, flowing through a circuit edge.

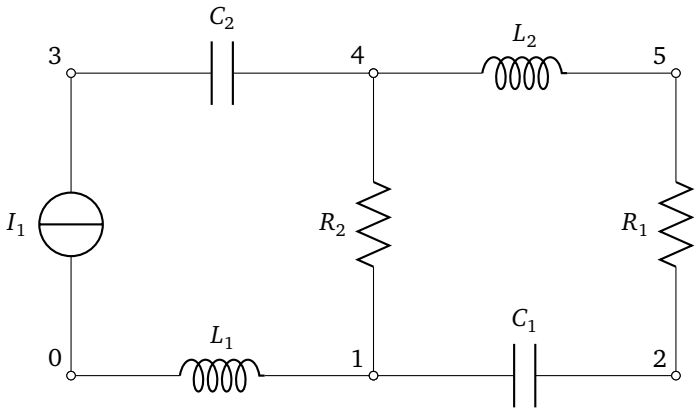

Figure 2.1.: Generic electrical circuit

2.1.1 A List of Circuit Elements

In the previous section, we showed that the currents and the voltages in a circuit edge are not independent. The edges can be assigned different types of circuit elements, each circuit element is characterized by its current-voltage relationship.

Ohmic Resistor

In an Ohmic resistor, electrical energy is dissipated, i.e., it is converted to a different kind of energy, heat. In an ideal Ohmic resistor, the rate of energy conversion, i.e., the power, is proportional to the square of the current flowing though the element

$$P = R \cdot I^2. \tag{2.3}$$

The proportionality constant R is called the resistance, with unit Ohm, $[R] = 1\Omega = 1\,\mathrm{V/A}$. For an ideal Ohmic resistor, it is independent of time and, in particular, independent of current through the element. From the power (2.3), the current-voltage relationship for an ideal Ohmic resistor can be derived using (2.2),

$$V = R \cdot I. \tag{2.4}$$

Eq. (2.4) describes a linear relation between current and voltage. The ideal Ohmic resistor therefore belongs to the group of linear circuit elements. Furthermore, an

Ohmic resistor is a passive device, in which electrical energy can be dissipated, but never generated. In a circuit diagram, such as Fig. 2.1, a resistor is drawn as in Fig. 2.2.

Figure 2.2.: Resistor

Inductor

An inductor stores magnetic energy when there is a current flowing through it. The energy stored in an inductor is proportional to the square of the current

$$E = \frac{L}{2} \cdot I^2. \tag{2.5}$$

The proportionality constant L is called the inductance, with unit Henry, $[L] = 1\,\mathrm{H} = 1\,\mathrm{Vs/A}$. For an ideal inductor, it is independent of time and the current through the element. The current-voltage relationship of an inductor can again be derived using (2.2),

$$P = \frac{\mathrm{d}E}{\mathrm{d}t} = L \cdot I \cdot \frac{\mathrm{d}I}{\mathrm{d}t} \quad \Rightarrow \quad V = L \cdot \frac{\mathrm{d}I}{\mathrm{d}t}. \tag{2.6}$$

For an ideal inductor, the relation between current and voltage is linear, i.e., the ideal inductor belongs to the group of linear circuit elements. An ideal inductor can store or release previously stored magnetic energy. However, energy can neither be generated nor dissipated. It therefore belongs to the group of passive circuit elements. In a circuit diagram, an inductor is drawn as in Fig. 2.3.

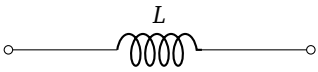

Figure 2.3.: Inductor

Capacitor

A capacitor stores electrical energy when it is loaded with electric charge. The electrical energy is proportional to the square of the charge,

$$E = \frac{1}{2C} \cdot Q^2. \tag{2.7}$$

The proportionality constant C is called the capacitance, with unit Farad, $[C] = 1\,\mathrm{F} = 1\,\mathrm{As/V}$. For an ideal capacitor, it is independent of time and the charge stored in the capacitor.

For purposes of formulation, the charges is usually replaced by a formal current, the displacement current I_C,

$$Q = \int_{-\infty}^{t} I_C(t')\mathrm{d}t'. \tag{2.8}$$

The displacement current I_C is a formal current because, unlike conduction currents, it does not involve the transfer of electric charge. The relationship between current and voltage in a capacitor can again be derived from the power

$$P = \frac{\mathrm{d}E}{\mathrm{d}t} = \frac{1}{C} \cdot I_C \cdot \int_{-\infty}^{t} I_C(t')\mathrm{d}t' \quad \Rightarrow \quad V = \frac{1}{C} \int_{-\infty}^{t} I(t')\mathrm{d}t'. \tag{2.9}$$

For an ideal capacitor, the relation between current and voltage is linear, i.e., the ideal capacitor belongs to the group of linear circuit elements. A capacitor can store or release previously stored electrical energy. However, energy can neither be generated nor dissipated. The capacitor therefore belongs to the class of passive circuit elements. In a circuit diagram, a capacitor is drawn as in Fig. 2.4.

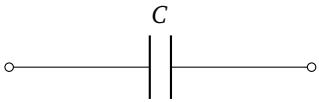

Figure 2.4.: Capacitor

2.1.2 Current and Voltage Sources

An electrical circuit with only passive circuit elements has zero currents and voltages at all times, unless it is excited by a source of electrical energy. The most simple source of electrical energy are ideal current and voltage sources.

As indicated by the name, a current source provides energy by driving an electrical circuit with a (in general time-dependent) source current. This current is independent from the voltage drop needed to keep the current flowing. Similarly, a voltage source provides energy by specifying a (in general time-dependent) voltage between different parts of the electrical circuit. The voltage is independent of the current flow needed to maintain the voltage level.

We emphasize that current and voltage sources do not always provide electrical energy. They can also extract energy from an electrical circuit, which has previously been stored in inductors and capacitors. By definition, current and voltage sources belong to the group of active circuit elements. In a circuit diagram, current and voltage sources are drawn as in Fig. 2.5 and 2.6 respectively.

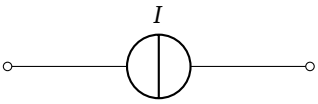

Figure 2.5.: Current source

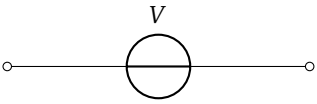

Figure 2.6.: Voltage source

2.1.3 Kirchhoff's Laws

For electrical circuits to form a meaningful physical model, it is essential that the basic principles of physics are respected. In the case of electrical circuit, the principles involved are conservation of charge and conservation of energy. These principles are reflected in the equations of motion of electrical circuits, Kirchhoff's equations:

Kirchhoff's current law is a statement of conservation of charge, [29]. More precisely, it states that electric currents describe the time-rate of change of electric charge and that the total electric charge is constant:

Theorem 2.1. *The algebraic sum of all edge currents leaving a node is zero at all instants of time.*

It is crucial to note that the total current can consist of different contributions, e.g., conduction currents in resistors or inductors, source currents in current and

voltage sources, and displacement currents in capacitors. Kirchhoff's current law, Thm. 2.1, treats all these currents on the same footing, i.e., the total current is the sum from all contributions.

Kirchhoff's second law, also called Kirchhoff's voltage law, is a statement of energy conservation, [29]. By definition in (2.2), the change in electrical energy involved with a current through a circuit element is proportional to the voltage drop along the circuit element. Considering a constant current flowing trough a loop of edges, the power is proportional to the algebraic sum of the corresponding voltages. Energy conservation requires that energy can neither be generated nor destroyed, hence it follows

Theorem 2.2. *The algebraic sum of edge voltages around any loop is zero at all instants of time.*

2.2 The Fourier Transform

Kirchhoff's equations and the constitutive equations of the circuit elements form a system of integro-differential equations with respect to time. For such a system of equations, different approaches are feasible for different situations:

- In order to describe the response of a system with respect to a time-dependent signal, it is feasible to directly solve the integro-differential equations. This requires the specification of boundary conditions in space and time, [30]. For example, in the modeling of an electric discharge process, the test component is excited by a strong current pulse at time zero. The pulse and the subsequent relaxation process to the stationary state is best described in time-domain.

- In order to describe the response of a system with respect to a time-harmonic signal, it is feasible to replace time by frequency as parameter, i.e., to transform the problem into frequency domain. For example, an antenna is driven by a signal which is essentially time-harmonic with weak modulation in frequency or amplitude.

In general, a transform reformulates a mathematical expression in another domain. The importance of transforms stems from the fact that mathematical operations can take different forms in different domains. A suitably chosen transform can greatly simplify the solution of an operator equation.

In this thesis, the frequency domain is described in terms of the Fourier transform. The description starts with a function $f(t)$ in time domain. Formally, this function can be written as a superposition of Dirac delta functions $\delta_{t'}(t) = \delta(t'-t)$ in time,

$$f(t) = \int_{-\infty}^{\infty} f(t')\delta(t'-t)\mathrm{d}t' = \int_{-\infty}^{\infty} f(t')\delta_{t'}(t)\mathrm{d}t'.$$

In other words, $f(t')$ can be interpreted as the coefficient of a basis function, $\delta_{t'}(t) = \delta(t'-t)$. The transformation into frequency domain corresponds to a change of basis functions. More precisely, the basis of delta functions is replaced by a basis of complex exponential functions,

$$f(t) = \frac{1}{2\pi}\int_{-\infty}^{\infty} F(\omega)e^{j\omega t}\mathrm{d}\omega. \tag{2.10}$$

The coefficient function $F(\omega)$ is called the Fourier transform of $f(t)$, $F = \mathscr{F}[f]$. It can be computed from $f(t)$ by

$$\mathscr{F}f(\omega) = F(\omega) = \int_{-\infty}^{\infty} f(t)e^{-j\omega t}\mathrm{d}t. \tag{2.11}$$

We conclude that representations in time and frequency domain are equivalent and can be transformed into one another. In order to simplify notation, we use the complex frequency $s = j\omega$ instead of ω in the following.

The great advantage of the Fourier transform in the study of integro-differential problems is the transformations of the mathematical operations of differentiation or integration in time-domain to algebraic multiplication and division in frequency domain, [31], i.e.,

$$\begin{aligned} g(t) &= \tfrac{\mathrm{d}}{\mathrm{d}t}f(t) && \Leftrightarrow \quad G(s) = sF(s) \\ g(t) &= \textstyle\int_{-\infty}^{t} f(t')\mathrm{d}t' && \Leftrightarrow \quad G(s) = \tfrac{1}{s}F(s). \end{aligned} \tag{2.12}$$

2.3 Electrical Circuit Analysis

In this section we study the properties of electrical circuits in time- and frequency domain. The first step is a mathematical formulation of the circuit theory presented above. This mathematical formulation is based on graph theory and results in a matrix representation of electrical circuits. In a second step, the matrix representation can be studied with the powerful toolset of matrix algebra.

2.3.1 Graph Theory

An electrical circuit is a special form of a oriented graph. An oriented graph $G(V,E)$ consists of a set of vertices, $V = \{v_1, \cdots, v_n\}$, and a set of edges, $E = \{e_1, \cdots, e_m\}$. Each edge is an ordered pair of vertices, $e_k = (v_{k_1}, v_{k_2})$. A generic graph is shown in Fig. 2.7. This graph consists of six vertices, v_1 - v_6, and seven edges, e_1 - e_7. The arrows on the edges indicate the orientation, i.e., $e_1 = (v_1, v_2)$, etc. In the analysis of electrical circuits, the vertices are associated with the nodes of the circuit, the edges are associated with the circuit elements, and the orientation of the edges corresponds with the reference direction for current and voltage.

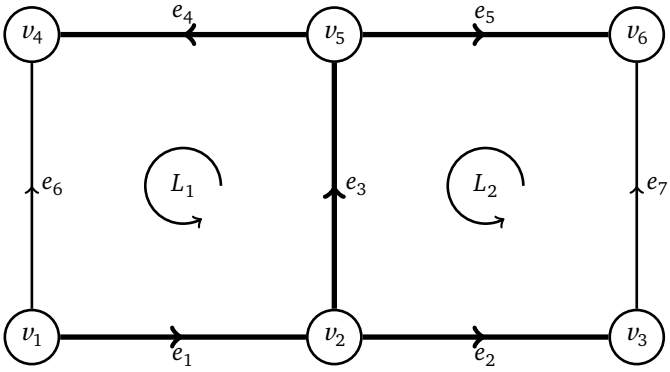

Figure 2.7.: Oriented graph

A chain is an ordered set of edges $(\pm e_{k_1}, \cdots, \pm e_{k_l})$ such that neighbouring edges are adjacent in the same node. The signs of the edges indicate the direction in which they are traversed. A chain which ends at its start vertex is called closed. A closed chain where each vertex is traversed only once is called a loop. In Fig. 2.7, for example, the chain $L_1 = (e_1, e_3, e_4, -e_6)$ forms a loop. A graph is called

connected if for each pair of vertices there exists a chain connecting them. Electrical circuits can in general be assumed to be connected; if they are not, the connected subgraphs can be analyzed separately.

A subgraph $G' = (V', E')$ is a graph with $V' \subset V$ and $E' \subset E$. A subgraph T of G is called a tree if it is connected and does not contain loops. If a tree contains all vertices of the original circuit, it is called spanning. For the graph in Fig. 2.7, the bold edges form a spanning tree. A tree has the important property that whenever an edge of G is added to T, provided it is not already part of T, exactly one loop is formed. This loop is called a fundamental loop. When, for example, the edge e_6 is added to the tree in Fig. 2.7, the fundamental loop L_1 is formed. Similarly, adding the edge e_7 results in the fundamental loop L_2 to be formed. Trees and fundamental loops are important concepts in the study of electrical circuits. It is shown below that the edges of a spanning tree specify all independent voltages while the fundamental loops specify all independent currents.

In the following, we present a mathematical formulation of graphs based on matrix algebra. This formulation allows to use a wide range of already existing work on matrices. The topology of a general graph can be described by the incidence and loop matrices [32]. The incidence matrix $\tilde{\mathbf{A}}$ describes the adjacencies of the edges,

$$\tilde{\mathbf{A}}_{kl} = \begin{cases} +1 & \text{if l-th edge ends at k-th vertex} \\ -1 & \text{if l-th edge starts at k-th vertex} \\ 0 & \text{otherwise} \end{cases} \tag{2.13}$$

As each edge starts and ends at exactly one node, the sum of all columns of the incidence matrix is zero. In order to remove redundant information, one row of the incidence matrix can be deleted. The corresponding vertex is distinguished as a reference vertex. In electrical circuits, the reference vertex corresponds to the ground node. The resulting matrix is called reduced incidence matrix, $\mathbf{A} = \tilde{\mathbf{A}}_{\text{reduced}}$. In the following, when we use the word 'incidence matrix **A**', we always mean the reduced incidence matrix $\tilde{\mathbf{A}}_{\text{reduced}}$. For example, defining v_1 as the reference vertex for the graph in Fig. 2.7, the incicdence matrix reads

$$\mathbf{A} = \begin{pmatrix} 1 & -1 & -1 & 0 & 0 & 0 & 0 \\ 0 & 1 & 0 & 0 & 0 & 0 & -1 \\ 0 & 0 & 0 & 1 & 0 & 1 & 0 \\ 0 & 0 & 1 & -1 & -1 & 0 & 0 \\ 0 & 0 & 0 & 0 & 1 & 0 & 1 \end{pmatrix}.$$

The topology of a graph is completely described by its incidence matrix: The number of vertices is equal to the number of rows of the incidence matrix plus one, the number of edges is equal to the number of columns. Two distinct vertices are connected by an edge if there exists one column in the incidence matrix where the corresponding matrix entries are +1 and -1 respectively. The incidence matrix cannot describe self-loops, i.e., edges starting and ending at the same vertex. However, for electrical circuits, self-loops can be removed from the analysis because the voltage drop along the corresponding edge is always zero.

Similarly, the fundamental loop matrix describes all fundamental loops in a graph. It is defined by

$$\mathbf{B}_{kl} = \begin{cases} +1 & \text{if the k-th loop traverses the l-th edge in positive direction} \\ -1 & \text{if the k-th loop traverses the l-th edge in negative direction} \\ 0 & \text{otherwise} \end{cases} \tag{2.14}$$

The graph in Fig. 2.7, has two fundamental loops, L_1 and L_2. The corresponding fundamental loop matrix reads

$$\mathbf{B} = \begin{pmatrix} 1 & 0 & 1 & 1 & 0 & -1 & 0 \\ 0 & 1 & -1 & 0 & -1 & 0 & 1 \end{pmatrix}.$$

It can be shown, that a graph is also described completely by its fundamental loop matrix, even though reconstructing the actual graph is more difficult, [32]. The fundamental loop matrix cannot describe pendant vertices, i.e., vertices which are not part of any loop. Again, for electrical circuits, pendant vertices can be removed from the analysis because the current flow through the adjacent edge is always zero.

The incidence matrix **A** and the fundamental loop matrix **B** are dual descriptions for the topology of graphs. The incidence matrix is based on the relationship between edges and vertices while the loop matrix is based on the relationship between edges and loops. This duality is reflected by the following theorems, which are very useful in analysis of an electrical circuits.

Theorem 2.3. *Let $G(V,E)$ be a (self-loop free) graph,* **A** *and* **B** *its incidence and fundamental loop matrix respectively. Then, [32],*

$$\mathbf{B}\cdot\mathbf{A}^{\mathrm{T}} = 0 \qquad \mathbf{A}\cdot\mathbf{B}^{\mathrm{T}} = 0. \tag{2.15}$$

Theorem 2.4. *For a connected graph with $n+1$ vertices and e edges, the ranks of the reduced incidence and the fundamental loop matrix are given by, [32],*

$$\operatorname{rank}(\mathbf{A}) = n \qquad \operatorname{rank}(\mathbf{B}) = e - n. \tag{2.16}$$

From the relationship between the incidence and the loop matrices, it follows in particular that

Corollary 2.1. *Let $G(V,E)$ be a connected graph with incidence matrix $\mathbf{A}$ and fundamental loop matrix $\mathbf{B}$. The null space of $\mathbf{B}$ is spanned by the rows of $\mathbf{A}$, the null space of $\mathbf{A}$ is spanned by the rows of $\mathbf{B}$, i.e.,*

$$\mathbf{A}\mathbf{x} = 0 \Leftrightarrow \exists \tilde{\mathbf{x}} : \mathbf{x} = \mathbf{B}^{\mathrm{T}} \tilde{\mathbf{x}} \qquad \mathbf{B}\mathbf{x} = 0 \Leftrightarrow \exists \tilde{\mathbf{x}} : \mathbf{x} = \mathbf{A}^{\mathrm{T}} \tilde{\mathbf{x}}. \tag{2.17}$$

2.3.2 Electrical Circuits in Terms of Graphs

In order to describe electrical circuits as graphs, the circuit quantities have to be identified with objects from graph theory, [33]:

- The set of nodes of an electrical circuit corresponds to the set of vertices of the corresponding graph.
- The set of edges of an electrical circuit corresponds to the set of edges of the corresponding graph.
- The reference directions for voltage and current in an electrical circuit corresponds to the orientations of the edges of the corresponding graph.

Having identified the electrical circuit with a graph, the circuit can be expressed in mathematical form. In particular, it is possible to define the incidence matrix $\mathbf{A}$ and the fundamental loop matrix $\mathbf{B}$ for the circuit. Furthermore, the edge voltages and currents can be expressed in vectorial form, $\mathbf{V}$ and $\mathbf{I}$ respectively. With these definitions, Kirchhoff's current law (Thm. 2.1) reads, [33],

$$\mathbf{A}\mathbf{I} = 0, \tag{2.18}$$

and Kirchhoff's voltage law (Thm. 2.2) reads, [33],

$$\mathbf{B}\mathbf{V} = 0. \tag{2.19}$$

In order to incorporate the constitutive equations, the current and voltage vectors, $\mathbf{I}$ and $\mathbf{V}$ are each decomposed into four parts $\mathbf{I}_R$, $\mathbf{I}_L$, $\mathbf{I}_C$, $\mathbf{I}_s$, $\mathbf{V}_R$, $\mathbf{V}_L$, $\mathbf{V}_C$, and $\mathbf{V}_s$ respectively. $\mathbf{I}_R$, $\mathbf{V}_R$ are all currents and voltages in resistive edges, $\mathbf{I}_L$, $\mathbf{V}_L$ all currents and voltages in inductive edges. $\mathbf{I}_C$ describes the displacement currents in the capacitors, $\mathbf{V}_C$ describes the corresponding capacitor voltages. Furthermore, $\mathbf{I}_s$ and $\mathbf{V}_s$ are the currents and voltages in those edges belonging to current or voltage sources. The total edge current and edge voltage vectors are the direct sums of the subvectors,

$$\mathbf{I} = \mathbf{I}_R \oplus \mathbf{I}_L \oplus \mathbf{I}_C \oplus \mathbf{I}_s \qquad \mathbf{V} = \mathbf{V}_R \oplus \mathbf{V}_L \oplus \mathbf{V}_C \oplus \mathbf{V}_s \,.$$

The constitutive equations for the circuit elements can now be written in both time- and frequency domain in the following vectorial form:

$$\mathbf{V}_R(t) = \mathbf{R}\,\mathbf{I}_R(t) \quad \Leftrightarrow \quad \mathbf{V}_R(s) = \mathbf{R}\,\mathbf{I}_R(s) \tag{2.20}$$

$$\mathbf{V}_L(t) = \mathbf{L}\,\frac{\mathrm{d}\,\mathbf{I}_L(t)}{\mathrm{d}t} \quad \Leftrightarrow \quad \mathbf{V}_L(s) = s\,\mathbf{L}\,\mathbf{I}_L(s) \tag{2.21}$$

$$\mathbf{V}_C(t) = \int_{-\infty}^{t} \mathbf{C}^{-1}\,\mathbf{I}_C(t')\mathrm{d}t' \quad \Leftrightarrow \quad \mathbf{V}_C(s) = \frac{1}{s}\,\mathbf{C}^{-1}\,\mathbf{I}_C(s) \tag{2.22}$$

The resistance and capacitance matrices, $\mathbf{R}$ and $\mathbf{C}$, are diagonal. The inductance matrix L is dense and symmetric. The diagonal elements $L_k = \mathbf{L}_{kk}$ contain the self inductances of all inductors, the off-diagonal elements $M_{kl} = \mathbf{L}_{kl}$ contain the mutual inductances between inductors. The dimensionless coupling factors $K_{kl} = M_{kl}/\sqrt{L_{kk}L_{ll}}$ are smaller than 1 for realistic systems.

The total Ohmic loss rate P, and the total inductive and capacitive energies, E_L and E_C respectively, will play a crucial role in the eigenmode analysis of electrical circuits in later chapters. For future reference, we express these quantities in terms of circuit matrices. In order to generalize (2.3), (2.5), and (2.7) to circuits with many circuit elements, the contributions from the individual circuit elements have to be added. In matrix form, this result can be written in terms of edge currents as

$$P = \mathbf{I}_R^{\mathrm{T}}\,\mathbf{R}\,\mathbf{I}_R \qquad E_L = \frac{1}{2}\,\mathbf{I}_L^{\mathrm{T}}\,\mathbf{L}\,\mathbf{I}_L \qquad E_C = \frac{1}{2s^2}\,\mathbf{I}_C^{\mathrm{T}}\,\mathbf{C}^{-1}\,\mathbf{I}_C, \tag{2.23}$$

or, equivalently, in terms of edge voltages as

$$P = \mathbf{V}_R^{\mathrm{T}}\,\mathbf{R}^{-1}\,\mathbf{V}_R \qquad E_L = \frac{1}{2s^2}\,\mathbf{V}_L^{\mathrm{T}}\,\mathbf{L}^{-1}\,\mathbf{V}_L \qquad E_C = \frac{1}{2}\,\mathbf{V}_C^{\mathrm{T}}\,\mathbf{C}\,\mathbf{V}_C \,. \tag{2.24}$$

2.3.3 The Nodal Approach

In the previous section, electrical circuits were described in terms of algebraic quantities, i.e., in terms of matrices and vectors. In this section, the equations of motion solved, i.e., the current and voltage vectors are computed for a given configuration of current or voltage sources. In the following, only the frequency domain expression will be considered.

First, note that the edge currents can be computed from the edge voltages and vice versa using the constitutive equations of the circuit elements, (2.20)-(2.22). It thus suffices to solve Kirchhoff's equations for one set of either edge currents or edge voltages only. In the nodal approach, only the edge voltages are computed.

Second, it can be shown that even the set of edge voltages does not constitute linearly independent unknowns. This is because the set of solutions is restricted by Kirchhoffs's voltage law, (2.19). Using the relations in Corollary 2.1, there exists a vector Φ such that

$$\mathbf{V} = \mathbf{A}^{\mathrm{T}} \Phi. \tag{2.25}$$

The vector Φ is called the vector of node potentials.

The above relationship can be interpreted such that each node of the electrical circuit is assigned a potential and the voltage drop along an edge between two nodes is equal to the difference in potential between these nodes[1]. Adding the same constant to all node potentials leaves the edge voltages invariant. This arbitrariness is removed in the above scheme by using the reduced incidence matrix. The node which is used to reduce the node incidence matrix is implicitly assigned a zero potential which fixes all other potentials relative to this reference node.

Before continuing the derivation, we decompose the electrical circuit G into subgraphs G_R, G_L, G_C and G_s. The subgraphs are chosen such that G_R contains all edges with resistors, G_L contains all edges with inductors, G_C all edges with capacitors, and G_s contains all edges with current sources. Each subgraph defines its own incidence matrix $\mathbf{A}_R$, $\mathbf{A}_L$, $\mathbf{A}_C$, and $\mathbf{A}_s$ respectively. The incidence matrices of the subgraphs correspond to submatrices of the total incidence matrix,

$$\mathbf{A} = \mathbf{A}_R \oplus \mathbf{A}_L \oplus \mathbf{A}_C \oplus \mathbf{A}_s \,.$$

[1] In vector analysis, it is well known that in any simply connected domain, a conservative vector field is always a gradient field. The established relation between the edge voltages and the node potentials is the equivalent of this statement on the level of graphs.

With this decomposition, the voltages along resistive, inductive, capacitive edges and, in particular, the voltage drops along current sources can be computed,

$$\mathbf{V}_R = \mathbf{A}_R^{\mathrm{T}} \Phi \qquad \mathbf{V}_L = \mathbf{A}_L^{\mathrm{T}} \Phi \qquad \mathbf{V}_C = \mathbf{A}_C^{\mathrm{T}} \Phi \qquad \mathbf{V}_S = \mathbf{A}_S^{\mathrm{T}} \Phi. \tag{2.26}$$

Substituting the new expressions into the constitutive equations yields the corresponding expressions for the currents along these edges,

$$\mathbf{I}_R(s) = \mathbf{R}^{-1} \mathbf{A}_R^{\mathrm{T}} \Phi \qquad \mathbf{I}_L(s) = \frac{1}{s} \mathbf{L}^{-1} \mathbf{A}_L^{\mathrm{T}} \Phi \qquad \mathbf{I}_C(s) = s\, \mathbf{C} \mathbf{A}_C^{\mathrm{T}} \Phi.$$

In (2.24), all energy related quantities, i.e., the Ohmic loss rate and inductive and capacitive energy, are expressed in terms of edge voltages. With the node potential ansatz, (2.26), the Ohmic loss rate and the electrical energy can be reformulated in terms of potentials,

$$P = \Phi^{\mathrm{T}} \mathbf{A}_R^{\mathrm{T}} \mathbf{R}^{-1} \mathbf{A}_R \Phi \qquad E_L = \frac{1}{2s^2} \Phi^{\mathrm{T}} \mathbf{A}_L^{\mathrm{T}} \mathbf{L}^{-1} \mathbf{A}_L \Phi \qquad E_C = \Phi^{\mathrm{T}} \mathbf{A}_C^{\mathrm{T}} \mathbf{C} \mathbf{A}_C \Phi.$$

This expression can be simplified considerably by introducing the circuit matrices

$$\widehat{\mathbf{G}} = \mathbf{A}_R \mathbf{R}^{-1} \mathbf{A}_R^{\mathrm{T}} \qquad \widehat{\mathbf{L}^{-1}} = \mathbf{A}_L \mathbf{L}^{-1} \mathbf{A}_L^{\mathrm{T}} \qquad \widehat{\mathbf{C}} = \mathbf{A}_C \mathbf{C} \mathbf{A}_C^{\mathrm{T}}, \tag{2.27}$$

and rewriting

$$P = \Phi^{\mathrm{T}} \widehat{\mathbf{G}} \Phi \tag{2.28}$$

$$E_L = \frac{1}{2s^2} \Phi^{\mathrm{T}} \widehat{\mathbf{L}^{-1}} \Phi \tag{2.29}$$

$$E_C = \Phi^{\mathrm{T}} \widehat{\mathbf{C}} \Phi. \tag{2.30}$$

Substituting the expression for the edge currents into Kirchhoff's current law (2.18) yields

$$0 = \mathbf{A}_R \mathbf{I}_R + \mathbf{A}_L \mathbf{I}_L + \mathbf{A}_C \mathbf{I}_C + \mathbf{A}_s \mathbf{I}_s \qquad \Rightarrow \qquad \left(\widehat{\mathbf{G}} + \frac{1}{s} \widehat{\mathbf{L}^{-1}} + s \widehat{\mathbf{C}} \right) \cdot \Phi = -\mathbf{A}_s \mathbf{I}_s,$$

The (frequency-dependent) matrix $\mathbf{Y}(s) = \left(\widehat{\mathbf{G}} + \frac{1}{s} \widehat{\mathbf{L}^{-1}} + s \widehat{\mathbf{C}} \right)$ is called the admittance matrix. It serves as the system matrix for the electrical circuit, i.e., it describes the

output (in terms of edge voltages and currents) in terms of general input (in terms of current sources).

Note that if the capacitor currents are again replaced by the charge on the capacitor, Kirchhoff's current law can be written as a continuity equation for the electric charge,

$$\mathbf{A}_R \mathbf{I}_R + \mathbf{A}_L \mathbf{I}_L + \mathbf{A}_s \mathbf{I}_s = -\frac{\mathrm{d}\mathbf{Q}}{\mathrm{d}t}. \tag{2.31}$$

Last but not least, we derive an expression for the impedance matrix $\mathbf{Z}$ from the system matrix. The impedance matrix relates the voltage drops along current sources to the magnitude of the source current. The source network is described by the source current vector, $\mathbf{I}_s$, and the node incidence matrix of the source network, $\mathbf{A}_s$. According to (2.25), the voltage drops along the sources are given by

$$\mathbf{V} = \mathbf{A}_s^{\mathrm{T}} \Phi = -\mathbf{A}_s^{\mathrm{T}} \mathbf{G}^{-1}(s) \mathbf{A}_s \mathbf{I}_s = -s \mathbf{A}_s^{\mathrm{T}} \left(\widehat{\mathbf{L}^{-1}} + s \widehat{\mathbf{G}} + s^2 \widehat{\mathbf{C}} \right)^{-1} \mathbf{A}_s \mathbf{I}_s . \tag{2.32}$$

The impedance matrix $\mathbf{Z}$ is defined as the proportionality matrix between source currents and source voltages, i.e.,

$$\mathbf{Z}(s) = \frac{\mathbf{V}_s}{\mathbf{I}_s} = -s \mathbf{A}_s^{\mathrm{T}} \left(\widehat{\mathbf{L}^{-1}} + s \widehat{\mathbf{G}} + s^2 \widehat{\mathbf{C}} \right)^{-1} \mathbf{A}_s . \tag{2.33}$$

3 Macroscopic Electrodynamics

In this chapter, field theoretical models for electromagnetic components and systems are described. Field theoretical models are the most general descriptions of electromagnetic components and systems. The equations of motion of electromagnetism, the macroscopic Maxwell's equations, are stated. Maxwell's equations are compared with the electrical circuit model from the previous chapter. It is shown that electrical circuits cannot describe all electromagnetic phenomena incorporated in Maxwell's equations. We therefore show a quasistatic approximation, Darwin's model, which exhibits the same range of phenomena as electrical circuits. The link between electrical circuit models and the field theoretical Darwin model is established using energy concepts.

3.1 Maxwell's Equations in Vacuum

The basic physical quantity in electromagnetism is the electric charge. To our best knowledge, electric charge consists of elementary particles with discrete charges. For example, an electron carries an electric charge $q = -1.602 \times 10^{-19}\,\mathrm{C}$. Due to their small magnitude on macroscopic scales, a superposition of many charged elementary particles can be treated with high accuracy as a continuous space charge distribution $\rho(x)$, $[\rho]=1\,\mathrm{C/m^3}$.

An electric charge which is moving through space produces an electric current. For example, an electron moving with speed $\vec{v}$ produces an electric current $\vec{j} = q\vec{v}$. Again, a superposition of the currents produced by many moving elementary charges can be interpreted as a continuous current density $\vec{j}(x)$, $\left[\vec{j}\right] = 1\,\mathrm{C/m^2 s}$.

Charged particles exert force upon each other. The force between charged particles is mediated by electromagnetic fields, the electric field $\vec{E}$ and the magnetic field $\vec{B}$. For a charged particle with charge q and trajectory $x(t)$ in the presence of an electric field $\vec{E}$ and a magnetic field $\vec{B}$, the force is given by

$$\vec{F}(t) = q\vec{E}(x(t), t) + q\dot{x}(t) \times \vec{B}(x(t), t). \tag{3.1}$$

The main difficulty in the analysis of a system of moving charges and fields stems from the fact that fields and charges cannot be treated separately. Moving charges are sources for the electromagnetic fields and they are, at the same time, subject to the force exerted by the electromagnetic fields. It follows that the equations of motion for systems of fields and charges must be a coupled system of fields and

charges. Combining and extending previous work, the equations of motion for the electromagnetic fields were first formulated by the English physicist James Clerk Maxwell and are accordingly called Maxwell's equations. Using modern notation in terms of partial differential equations, they can be written in the following form, [34],

$$\nabla \cdot \vec{D} = \rho \tag{3.2}$$

$$\nabla \cdot \vec{B} = 0 \tag{3.3}$$

$$\nabla \times \vec{E} + \partial_t \vec{B} = 0 \tag{3.4}$$

$$\nabla \times \vec{H} - \partial_t \vec{D} = \vec{j} \tag{3.5}$$

The quantities ρ and $\vec{j}$ are the charge and current densities respectively, the fields $\vec{E}$ and $\vec{B}$ are the electric and the magnetic field respectively. There are two additional fields, the displacement field $\vec{D}$ and the magnetizing field $\vec{H}$. In vacuum, the displacement field and the magnetizing field differ from the electric and magnetic fields due to a conventional scaling factor only. However, when analyzing the interaction of electromagnetic fields with materials on a macroscopic level, the displacement field and the magnetizing field can be complex (i.e., non-linear, frequency-dependent, non-isotropic) functions of the electric and magnetic fields. A simplified model, which nevertheless works well for a wide range of materials, is shown in the next section.

3.2 Macroscopic Maxwell's Equations

The system of Maxwell's equations from the previous section provides a complete description of a system of charges and currents and the forces acting between them on all scales. However, for systems with very complex charge and current distributions, a full solution can be unfeasible or even impossible. Such complex systems are given by, e.g., solid state materials interacting with the electromagnetic fields. The huge amount of particles, the lack of knowledge of the exact charge and current locations and, above all, the presence of quantum effects makes an microscopic analysis in terms of classical electrodynamics impossible.

A much more elegant approach which, above all, leads back to the realm of classical electrodynamics, is to treat macroscopic material distributions in an approximate, statistical manner. More precisely, materials in electromagnetic fields give rise to additional source terms in Maxwell's equations, which are a function of the electromagnetic fields.

For a dielectric material, the interaction of field and material is modeled in terms of a polarization density $\vec{P}$. Intuitively, the phenomenon of polarization can be understood by treating the atomic nucleus and the valence electron as an electric dipole which is aligned by an applied electric field [34]. More rigorously, it can also be derived from quantum-mechanics. Inside the material, the polarization leads to a decrease of the electric field strength,

$$\vec{E} = \frac{1}{\epsilon_0}\left(\vec{D} - \vec{P}\right).$$

$\epsilon_0 = 8.854 \times 10^{-12}$ As/Vm is a conventional scaling factor . As pointed out above, the polarization density can in general be a very complex function of the applied electric field. In this thesis, we restrict ourselves to linear, isotropic, frequency-independent materials. These assumptions are clearly an approximation for real materials and their validity has to be assessed for practical problems. In particular, the assumption of frequency-independence is acceptable only as long as temporal changes are slow or, equivalently, if there is no significant variation of the material parameters in the frequency band of interest. In this case, the polarization can be related to the electric field by the electric susceptibility κ_e, $\vec{P} = \epsilon_0 \kappa_e \vec{E}$. The relation between the electric field and the displacement field reads

$$\vec{D} = \epsilon_0 \vec{E} + \vec{P} = \epsilon_0 (1 + \kappa_e)\vec{E} = \epsilon \vec{E}. \tag{3.6}$$

Under the above assumptions, the permittivity ϵ is a frequency-independent scalar which is in general spatially inhomogeneous, depending on the different material properties at different points in space.

For a magnetic material, the interaction of the field and the material is modeled in terms of a magnetization density $\vec{M}$. Intuitively, the phenomenon of magnetization can be understood by treating the elementary spins of the atoms as magnetic dipoles which are aligned in the presence of an applied magnetic field. A more rigorous derivation again has to include quantum effects. Inside the material, the magnetization can lead to a decrease (for dia-magnetism) or an increase (for para-magnetism) of the magnetic field. The magnetization can in general be a very complex, non-linear (for ferro-magnetism) function of the applied magnetic field. In this thesis, we again restrict ourselves to linear, isotropic, frequency-independent materials. For this approximation, the same considerations as for dielectric materials apply. Similar to the description of dielectric materials, the magnetization can then be related to the magnetic field by the magnetic susceptibility κ_m, $\vec{M} = \kappa_m / \mu_0 \vec{B}$. The relation between the magnetic field and the magnetization field reads

$$\vec{B} = \mu_0(\vec{H} + \vec{M}) = \mu_0(1 + \kappa_m)\vec{H} = \mu\vec{H}. \tag{3.7}$$

The permeability μ is again a frequency-independent scalar which is in general spatially inhomogeneous, depending on the different material properties at different points in space.

Last but not least, in some materials there exist freely moving charged particles, e.g., electrons in the conduction band of metals or ions in fluids. Such materials form conductors. An applied electric field exerts a force on the freely moving charges. The analysis of charge movement on a microscopic level again requires the use of quantum-mechanics. On a macroscopic level, the movement of many elementary charged particles gives rise to a current density. In general, this current density can be written

$$\vec{j} = \sigma\vec{E}. \tag{3.8}$$

σ defines the conductivity of the material. In general, the conductivity can be an arbitrary non-isotropic, frequency-dependent, non-linear function of the applied electric field. In this thesis, all conductivities are assumed isotropic, frequency-independent and independent of the applied field strength. In this case, (3.8) can be viewed as a generalization of Ohm's law (2.4).

The assumption of frequency-independent permittivities, permeabilities, and conductivities is an approximation which is not always satisfied for practical examples. The work presented in this thesis is concerned with the automated construction of an electrical circuit model for a 3D electromagnetic component from geometry and material data. As will be discussed in Sect. 6, classical electrical circuit with frequency-independent circuit elements correspond to frequency-independent material parameters. A generalization of electrical circuits with frequency-dependent circuit elements leads beyond the realm of classical electrical circuit theory.

3.3 Maxwell's Equations in Frequency Domain

In Sect. 2.2, the Fourier transform was introduced to simplify mathematical expressions involving time derivatives. When Maxwell's equations are transformed into frequency domain, the partial derivatives with respect to time can be replaced by algebraic multiplications with the complex frequency. Vectorial quantities, such as the electrical field $\vec{E}$ and the magnetic field $\vec{B}$, can be transformed into frequency domain component-wise,

$$\mathscr{F}\left[\vec{E}\right](x,s)=\frac{1}{2\pi i}\int_0^\infty \vec{E}(x,t)e^{-st}\mathrm{d}t \qquad \mathscr{F}\left[\vec{B}\right](x,s)=\frac{1}{2\pi i}\int_0^\infty \vec{B}(x,t)e^{-st}\mathrm{d}t.$$

with inverse transform

$$\vec{E}(x,t)=\int_{-i\infty}^{i\infty}\mathscr{F}\mathscr{L}\left[\vec{E}\right](x,s)e^{st}\mathrm{d}s \qquad \vec{B}(x,t)=\int_{-i\infty}^{i\infty}\mathscr{F}\left[\vec{B}\right](x,s)e^{st}\mathrm{d}s.$$

The time-domain representations, $\vec{E}(x,t)$ and $\vec{B}(x,t)$ and the frequency-domain representations, $\mathscr{F}\left[\vec{E}\right](x,s)$ and $\mathscr{F}\left[\vec{E}\right](x,s)$, are equivalent expressions for the same electric and magnetic field respectively. As there is no risk of confusion, we will in the following denote the time and the frequency domain representation by the same symbol, $\vec{E}(x,s)=\mathscr{F}\left[\vec{E}\right](x,s)$. The distinction between time and frequency domain can be made from the different representations of differential operators, (2.12). In frequency domain, Maxwell's equations read

$$\nabla\cdot\vec{D}(x,s)=\rho(x,s) \tag{3.9}$$
$$\nabla\cdot\vec{B}(x,s)=0 \tag{3.10}$$
$$\nabla\times\vec{E}(x,s)+s\vec{B}(x,s)=0 \tag{3.11}$$
$$\nabla\times\vec{H}(x,s)-s\vec{D}(x,s)=\vec{j}(x,s). \tag{3.12}$$

The constitutive equations read

$$\vec{D}(x,s)=\epsilon(x)\vec{E}(x,s) \tag{3.13}$$
$$\vec{B}(x,s)=\mu(x)\vec{H}(x,s) \tag{3.14}$$
$$\vec{j}(x,s)=\sigma(x)\vec{E}(x,s)+\vec{j}_s(x,s). \tag{3.15}$$

As pointed out above, a frequency dependence of the material parameters is not taken into account.

3.4 Quasistatic Approximations for Maxwell's Equations

Maxwell's equations are the most general model for the description of electromagnetic systems. For this reason, electrical circuit models should be contained in some sense in Maxwell's equations.

It is well known that classical electrical circuits cannot describe all electromagnetic phenomena. In particular, electrical circuits do not in general describe wave propagation, i.e., electromagnetic fields traveling through vacuum. Furthermore, any change in a source induces a voltage in all circuit elements instantaneously, i.e., there is in general no retardation of electrical signals[1]. The key to understanding the relationship between Maxwell's equations and electrical circuits is that electrical circuits provide an approximation to Maxwell's equations which is valid in the low-frequency domain. To quantify this relation, we discuss in this section low frequency (quasistatic) approximations for Maxwell's equations. A mathematically rigorous discussion can be found in [36].

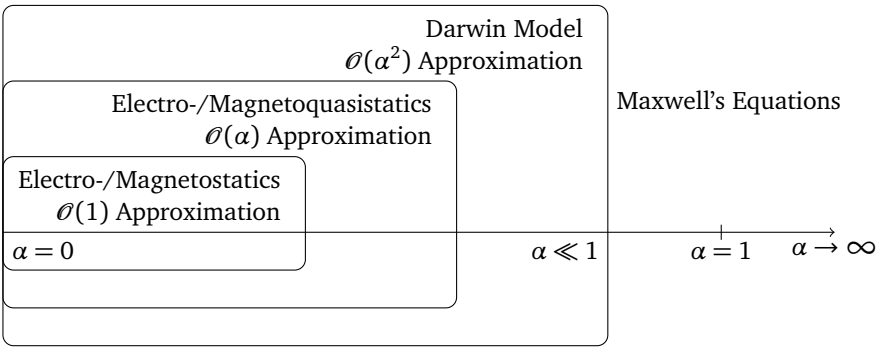

Figure 3.1.: Quasistatic approximations to Maxwell's equations

The first step towards the derivation of quasistatic models is the definition of a dimensionless parameter α which defines the quasistatic region, Fig. 3.1. As α is small in the quasistatic region, it is a suitable expansion parameter for the construction of quasistatic models. The order of the approximation in α further sub-divides the quasistatic region. For the definition of the expansion parameter, all lengths in the application under investigation are expressed in terms of dimensionless parameters t' and x', i.e., $t = Tt'$ and $x = Lx'$, where T is a characteristic time and L is a characteristic length for the application [36]. Maxwell's equations with dimensionless lengths read

[1] There are extensions of classical circuit theory, e.g., [35], including these phenomena.

$$\begin{aligned}
\nabla' \cdot \vec{D} &= L\rho \\
\nabla' \cdot \vec{B} &= 0 \\
\nabla' \times \vec{E} + \frac{L}{T}\partial_{t'}\vec{B} &= 0 \\
\nabla' \times \vec{H} - \frac{L}{T}\partial_{t'}\vec{D} &= L\vec{j}.
\end{aligned}$$

Defining

$$\alpha = \frac{L}{cT} \tag{3.16}$$

with $c = (\epsilon_0\mu_0)^{-1/2}$ the vacuum speed of light, the final system of equations reads

$$\begin{aligned}
\nabla' \cdot \vec{D} &= L\rho \\
\nabla' \cdot \vec{B} &= 0 \\
\nabla' \times \vec{E} + c\alpha\partial_{t'}\vec{B} &= 0 \\
\nabla' \times \vec{H} - c\alpha\partial_{t'}\vec{D} &= L\vec{j}.
\end{aligned}$$

The same considerations can also be made in frequency domain, the characteristic time T then corresponds to a characteristic frequency $S = 2\pi i T^{-1}$. With the characteristic wavelength $\lambda = c/T$, the quasistatic limit $\alpha \ll 1$ corresponds to $L \ll \lambda$, i.e., the wavelengths are much larger than the characteristic length of interest.

With a suitable expansion parameter at hand, the electromagnetic fields can be expanded using a Taylor expansion,

$$\vec{E} = \vec{E}^{(0)} + \alpha\vec{E}^{(1)} + \frac{\alpha^2}{2}\vec{E}^{(2)} + \cdots \qquad \vec{B} = \vec{B}^{(0)} + \alpha\vec{B}^{(1)} + \frac{\alpha^2}{2}\vec{B}^{(2)} + \cdots \tag{3.17}$$

Rather than computing the full electromagnetic field and performing the Taylor expansion coefficients afterward, we want to formulate equations of motion for the expansion coefficients. It will turn out that the equations of motion couple the longitudinal and the transverse parts of the expansion coefficient belonging to different orders. While the magnetic field only has a transverse part, $\nabla \cdot \vec{B} = 0$, the electric field has a longitudinal and a transverse component, $\vec{E} = \vec{E}_L + \vec{E}_T$.

3.4.1 Zeroth Order: Electrostatics and Magnetostatics

To compute the zeroth order, the dimensionless parameter α can be set to zero. The equations of motion then read

$$\begin{aligned} \nabla \cdot \vec{D}_L &= \rho & \nabla \cdot \vec{B} &= 0 \\ \nabla \times \vec{E}_T &= 0 & \nabla \times \vec{H} &= \vec{j} \end{aligned}$$

The same expression results when all fields and sources are assumed to be time-independent in Maxwell's equations. The limit $\alpha = 0$ therefore corresponds to the static limit of Maxwell's equations. In the static limit, the electric and the magnetic fields decouple. The source of the electric field is the electric charge density while the source for the magnetic field is the current density. The transverse component of the electric field vanishes, $\vec{E}_T = 0$.

3.4.2 First Order: Electroquasistatics and Magnetoquasistatics

The first order approximation introduces a unidirectional coupling between the electric and the magnetic field. This results in two sets of equations of motion. The equations of motion for electroquasistatics read

$$\begin{aligned} \nabla \cdot \vec{D}_L &= \rho & \nabla \cdot \vec{B} &= 0 \\ \nabla \times \vec{E}_T &= 0 & \nabla \times \vec{H} &= \vec{j} + \partial_t \vec{D}_L. \end{aligned}$$

The equations of motion for electroquasistatics implicitly contain the continuity equation,

$$\nabla \cdot \vec{j} + \partial_t \rho = 0. \tag{3.18}$$

It is possible therefore to model time-dependent changes in the charge densities. On the level of electrical circuits, such effects correspond to capacitive behavior. On the other hand, Faraday's law of induction is not incorporated in the system of equations. Electroquasistatics therefore cannot be used to describe inductive effects.

The second set of equations, the equations of motion for magnetoquasistatics, read

$$\nabla \cdot \vec{D}_L = \rho \qquad \nabla \cdot \vec{B} = 0$$
$$\nabla \times \vec{E}_T = -\partial_t \vec{B} \qquad \nabla \times \vec{H} = \vec{j}.$$

The equations of motion for magnetoquasistatics do not incorporate the continuity equation. On the other hand, Faraday's law of induction is included. The equations of motion of magnetoquasistatics therefore describe inductive, but not capacitive effects.

3.4.3 Second Order: Darwin's Model

The second order approximation introduces a mutual coupling between the electric and the magnetic fields and results in a single set of equations of motion,

$$\begin{aligned} \nabla \cdot \vec{D}_L &= \rho & \nabla \cdot \vec{B} &= 0 \\ \nabla \times \vec{E}_T &= -\partial_t \vec{B} & \nabla \times \vec{H} &= \vec{j} + \partial_t \vec{D}_L. \end{aligned} \tag{3.19}$$

The second order approximation for Maxwell's equations is called Darwin's model. Darwin's model differs from Maxwell's model in the definition of the displacement current, using only the longitudinal part of the electric field, [37],

$$\vec{j}_{D,Maxwell} = \partial_t \vec{D} = \partial_t (\vec{D}_L + \vec{D}_T) \quad \leftrightarrow \quad \vec{j}_{D,Darwin} = \partial_t \vec{D}_L. \tag{3.20}$$

3.5 The Scalar and Vector Potentials

In many cases, the solution of Maxwell's equations, (3.2)-(3.5), can be simplified considerably if the electromagnetic fields are expressed in terms of auxiliary fields. For suitably chosen auxiliary fields, the number of unknowns may be reduced with respect to the original system, or the equations take a form which can be solved more easily. There is a wide range of auxiliary fields which have been defined in the literature. The most feasible choice depends on the application at hand. In this work, we will use the description in terms of scalar potential ϕ and vector potential $\vec{A}$. This choice of auxiliary fields is motivated by two observations:

- The equations of motion of the quasistatic Darwin model take a very convenient form for subsequent analysis and numerical implementation.

- In Sect. 6, the scalar potential ϕ will be identified as the field-theoretical equivalent to the vector of node potentials of an associated electrical circuit model. This identification will allow a very intuitive scheme for the construction of electrical circuit models from field data.

In order to reformulate Maxwell's and Darwin's equations in terms of scalar and vector fields, we exploit that every transverse field can be written as gradient of a scalar function,

$$\vec{E}_T = -\nabla\phi_E \qquad \vec{B}_T = -\nabla\phi_B, \tag{3.21}$$

and that every transverse field can be written as a curl of a vector field,

$$\vec{E}_R = \nabla\times\vec{A}_E \qquad \vec{B}_T = \nabla\times\vec{A}_B. \tag{3.22}$$

This decomposition of the electromagnetic fields greatly simplifies the solution of Maxwell's equations because some degrees of freedom can at once be eliminated: Inserting (3.21) and (3.22) into the homogeneous Maxwell equations, (3.3) and (3.4), yields:

$$\begin{aligned} \Delta\phi_B = 0 \quad &\Rightarrow \quad \phi_B = 0 \\ \nabla\times\vec{E}_T + \partial_t\nabla\times\vec{A}_B = 0 \quad &\Rightarrow \quad \vec{E}_T = -\partial_t\vec{A}_B. \end{aligned}$$

The homogeneous Maxwell equations allow to discard two unneeded auxiliary fields, the magnetic scalar potential ϕ_B and the electric vector potential $\vec{A}_E$. The formulae for the electromagnetic fields in terms of the electric scalar potential $\phi = \phi_E$ and the vector potential $\vec{A} = \vec{A}_B$ read

$$\begin{aligned} \vec{E} &= -\nabla\phi - \partial_t\vec{A} \\ \vec{B} &= \nabla\times\vec{A}. \end{aligned} \tag{3.23}$$

These formulae for the electromagnetic fields satisfy the homogeneous Maxwell's equations identically. For the scalar potential ϕ and the vector potential $\vec{A}$ to form a Helmholtz decomposition of the electric field, the vector potential has to be transverse, $\nabla\cdot\vec{A} = 0$. This is not generally the case. The definition of the electromagnetic fields in terms of potentials, (3.23), is not unique. More precisely, for any scalar function κ, the transformation

$$\phi \to \phi + \partial_t\kappa \qquad \vec{A} \to \vec{A} - \nabla\kappa. \tag{3.24}$$

leaves the electromagnetic fields invariant. Such a transformation is called a gauge transformation. In Sect. 4 we discuss how the gauge dependence of the potentials in reflected in electrical circuit models. At this point, let us continue with reformulating Maxwell's equations using the potential formulation. Inserting (3.23) into the inhomogenous Maxwell's equations, (3.2) and (3.5) respectively, yields

$$\nabla \cdot (\epsilon \nabla \phi + \epsilon \partial_t \vec{A}) = -\rho \qquad \nabla \times (\frac{1}{\mu} \nabla \times \vec{A}) + \partial_t (\epsilon \nabla \phi + \epsilon \partial_t \vec{A}) = \vec{j} \tag{3.25}$$

In this work, we are interested far more in the quasistatic Darwin model. Inserting the decomposition (3.23) into the equations of motion for the Darwin model, the homogeneous Darwin equations are satisfied identically. The two inhomogeneous Darwin equations read

$$\nabla \cdot (\epsilon \nabla \phi) = -\rho \qquad \nabla \times (\frac{1}{\mu} \nabla \times \vec{A}) + \partial_t (\epsilon \nabla \phi) = \vec{j} \tag{3.26}$$

The difference between the Maxwell and the Darwin model becomes most evident when the gauge is fixed by the Lorenz gauge fixing condition,

$$\nabla \cdot (\epsilon \vec{A}) + \epsilon^2 \mu \partial_t \phi = 0. \tag{3.27}$$

The equations of motion for the potentials for the Maxwell and the Darwin models respectively read:

$$\begin{array}{rrl} \text{Darwin Model} & [\text{Maxwell Model}] & \\ \hline -\nabla \cdot (\epsilon \nabla \phi) & \left[+\epsilon^2 \mu \partial_t^2 \phi\right] & = \rho \\ \nabla \times \left(\frac{1}{\mu} \nabla \times \vec{A}\right) - \frac{1}{\epsilon \mu} \nabla \cdot (\epsilon \vec{A}) & \left[+\epsilon \partial_t^2 \vec{A}\right] & = \vec{j} \end{array} \tag{3.28}$$

From this representation, it can be seen that the equations of motion for Darwin's model correspond to a linear approximation of the equations of motion for Maxwell's model, i.e., the second-order partial derivatives with respect to time are neglected. In frequency domain, the second-order derivatives correspond to terms which are quadratic in the frequency. Performing a study of scales for the equations of motion shows that the second-order derivatives with respect to time are suppressed by α^2 where α is the dimensionless parameter defined in (3.16).

3.6 Green's Functions

In Sect. 2.2, the Fourier transform served as example for a general procedure for the solution of the equations of motion of a given physical system:

1. Specify a set of basis functions for the sources and express all sources in terms of this basis.
2. Solve the equations of motion for each basis function separately.
3. The solution of the equations of motion for a general source corresponds to a linear superposition of the elementary solutions. The coefficients can be obtained from the expansion of the source in terms of basis functions.

In the example of the Fourier transform, the basis functions correspond to exponentials, $f_s(t) = e^{st}$. A differential equation in time domain corresponds to an algebraic equation in frequency domain, which can be solved very easily for each basis function separately.

In this section, a similar procedure is applied for the solution of partial differential equations. Consider a Dirac delta function in time and space, $\delta_{(x',t')}(x,t) = \delta^3(x-x')\delta(t-t')$. Any function in space-time can be expressed in terms of Dirac delta functions by

$$f(x,t) = \int\int f(x',t')\delta_{(x',t')}(x,t)\mathrm{d}^3x'\mathrm{d}t'. \tag{3.29}$$

In this expansion, $f(x',t')$ has to be interpreted as coefficient belonging to the basis function $\delta_{(x',t')}$.

Consider next the equations of motion for the Maxwell and the Darwin model in terms of scalar and vector potential. For spatially homogeneous material distributions, the equations of motion read

Darwin Model	Maxwell Model
$\Delta\phi = -\frac{\rho}{\epsilon}$	$\Delta\phi - \frac{1}{c^2}\partial_t^2\phi = -\frac{\rho}{\epsilon}$
$\Delta\vec{A} = -\mu\vec{j}$	$\Delta\vec{A} - \frac{1}{c^2}\partial_t^2\vec{A} = -\mu\vec{j}.$

(3.30)

where $\Delta = \nabla^2$ is the Laplace operator, $c = (\epsilon\mu)^{-1/2}$ is the speed of light in the homogeneous material. For the Darwin model, the fields and their sources are

connected by the Laplace operator which is time independent. It follows that there is an instantaneous relationship between the sources and the fields. The Laplace operator has a simple analytical solution for the basis functions $\delta_{(x',t')}$, [34],

$$\Delta G_{(x',t')} = \delta_{(x',t')} \quad \Leftrightarrow \quad G_{(x',t')}(x,t) = \frac{1}{4\pi|x-x'|}. \tag{3.31}$$

The function $G_{(x',t')}(x,t)$ is the Green function of the Laplace operator. For the Maxwell model, the fields and their sources are connected by a wave equation which is time-dependent. The effect of the time-derivative becomes obvious when the corresponding Green function is computed, [34]:

$$(\Delta - \frac{1}{c^2}\partial_t^2)G_{(x',t')} = \delta_{(x',t')} \quad \Leftrightarrow \quad G_{(x',t')}(x,t) = \frac{\delta((t-t')-|x-x'|/c)}{4\pi|x-x'|}. \tag{3.32}$$

The Green function for the wave equation differs from the Green function for the Laplace operator by an additional delta function in the nominator. This delta function introduces retardation in the physical model, i.e., a source at position x and time t does not influence the fields at position x' before a time $t' = t + |x-x'|/c$.

Using the Green functions for the Laplace equation and the wave equation, (3.31) and (3.32) respectively, together with an expansion of the charge and current densities according to (3.29), the scalar and vector potentials can be expressed in terms of sources by an integral equation,

Darwin Model	Maxwell Model
$\phi(x,t) = -\frac{1}{4\pi\epsilon}\int \frac{\rho(x',t)}{\lvert x-x'\rvert}\mathrm{d}^3x$	$\phi(x,t) = -\frac{1}{4\pi\epsilon}\int \frac{\rho(x',t-\frac{\lvert x-x'\rvert}{c})}{\lvert x-x'\rvert}\mathrm{d}^3x$
$\vec{A}(x,t) = -\frac{\mu}{4\pi}\int \frac{\vec{j}(x',t)}{\lvert x-x'\rvert}\mathrm{d}^3x$	$\vec{A}(x,t) = -\frac{\mu}{4\pi}\int \frac{\vec{j}(x',t-\frac{\lvert x-x'\rvert}{c})}{\lvert x-x'\rvert}\mathrm{d}^3x.$

(3.33)

An explicit expression for the Green functions for the Darwin and Maxwell models can in general be formulated only under the assumption of spatially homogeneous media. If needed in the general case of spatially inhomogeneous media, the Green function has to be computed numerically.

3.7 Energy in the Electromagnetic Fields and the Definitions of Resistance, Capacitance and Inductance

The total force exerted by the electromagnetic fields on charged particles, (3.1), leads to an expression for the work done by the electromagnetic field, i.e., for the rate of conversion from electromagnetic energy into other (e.g. mechanical or thermal) forms of energy. In [34], the following expression is derived

$$P = \int \vec{j}(x) \cdot \vec{E}(x) \mathrm{d}^3 x. \tag{3.34}$$

This expression is reformulated using Maxwell's equations in order to derive an expression for energy conservation in the electromagnetic fields,

$$P = -\partial_t \int u_{Maxwell}(x) \mathrm{d}^3 x \quad \text{where} \quad u_{Maxwell}(x) = \frac{1}{2}\vec{E} \cdot \vec{D} + \frac{1}{2}\vec{B} \cdot \vec{H}. \tag{3.35}$$

In (3.35), $u_{Maxwell}(x)$ is the energy density of the electromagnetic field, i.e., it can be interpreted as energy stored in the electromagnetic fields.

In this thesis, we concentrate on deriving and analyzing an expression for the electromagnetic field energy in the Darwin model. We will show that the energy can be broken into several contributions which correspond to similar contributions to the total energy in an electrical circuit. Using the expression (3.23) for the electric field in terms of scalar and vector potential and the Darwin equations of motion (3.26) for the potentials, the work (3.34) can be reformulated

$$P = -\frac{\mathrm{d}}{\mathrm{d}t} \int \underbrace{\frac{1}{2}\left([-\phi(\nabla \cdot \epsilon \nabla \phi)] + \left[\vec{A} \cdot \left(\nabla \times \left(\frac{1}{\mu} \nabla \times \vec{A} \right) \right) - \vec{A} \cdot \left(\frac{1}{\epsilon\mu} \nabla \cdot (\epsilon \vec{A}) \right) \right] \right)}_{u_{Darwin}(x)} \mathrm{d}^3 x \tag{3.36}$$

In the derivation, we assume time-independent materials and that all fields, charges and currents vanish at infinity. $u_{Darwin}(x)$ can be interpreted as the energy stored in the electromagnetic fields. While this expression is rather complicated in its general form, it can be simplified considerably when spatially homogeneous materials are assumed for simplicity. In this case, $u_{Darwin}(x)$ in (3.36) simplifies to

$$u(x) = -\frac{\epsilon}{2}\phi \Delta \phi - \frac{1}{2\mu}\vec{A} \Delta \vec{A}. \tag{3.37}$$

The negative-definiteness of the Laplace operator directly implies the positive-definiteness of the electromagnetic energy. In the next sections, we are going to discuss in detail the terms in (3.36) and establish the connection to electrical circuit theory.

Before plunging into the detailed analysis, we compare u_{Darwin} with the definition of electromagnetic energy density in the Maxwell model, $u_{Maxwell}$. Transforming both expressions, (3.36) and (3.35), into frequency domain and subtracting yields the following result:

$$\Delta u = u_{Maxwell} - u_{Darwin} = -\frac{s^2}{2c} \int \left[2\epsilon \phi^2 + \frac{1}{\mu} |\vec{A}|^2 \right] \mathrm{d}^3 x = \mathcal{O}\left(s^2\right). \tag{3.38}$$

As expected, the difference in electromagnetic field energy is a quadratic function of frequency which becomes negligible at low frequencies, i.e., in the frequency domain of validity of Darwin's model. Furthermore the energy density in the Maxwell model is always higher than the energy density in the Darwin model. The missing energy stems from the neglected s^2 terms in the equations of motion, i.e., the missing energy is the energy stored in propagating electromagnetic waves.

3.7.1 Resistance

We start our discussion with the term on the left-hand side of (3.36). For some volume V with conductivity σ, the total dissipated power is given by

$$P = \int_V \vec{j}(x) \cdot \vec{E}(x) \mathrm{d}^3 x = \int_V \frac{1}{\sigma(x)} \left| \vec{j} \right|^2 \mathrm{d}^3 x.$$

The total power is thus proportional to the square of the total current I,

$$P = \left(\underbrace{\int_V \frac{1}{\sigma(x)} \left| \frac{\vec{j}}{I} \right|^2 \mathrm{d}^3 x}_{R} \right) I^2. \tag{3.39}$$

R is a geometry-dependent coefficient which is independent of the magnitude of the current. Comparing (3.39) with (2.3) reveals a similar structure to the Ohmic losses in a lumped resistor. We thus interpret R as the field-theoretical equivalent to an Ohmic resistor.

In the simple case of a straight conductor of length l, with constant cross section A, conductivity σ, and homogeneous current density $\vec{j}$, the resistance takes a very simple expression

$$R = \frac{d}{A\sigma}.$$

3.7.2 Capacitance

The first term on the right-hand side of (3.36) describes a change of electrical energy stored in a distribution of electric charges,

$$E_C = -\int_V \frac{1}{2}\phi \cdot (\nabla \cdot \epsilon \nabla \phi) \mathrm{d}^3x = \int_V \frac{1}{2}\vec{E}_C \cdot \vec{D}_C \mathrm{d}^3x \tag{3.40}$$

Decomposing the total charge distribution into disjoint sets with total charges Q_k, i.e.,

$$\rho(x) = \sum_{k=1}^{n} Q_k \tilde{\rho}_k(x)$$

where $\int_V \tilde{\rho}_k \mathrm{d}^3x = 1$, and writing the potential in terms of Green's function for the Coulomb equation[2], we can write

$$E_C = \sum_{k,l=1}^{n} Q_k Q_l \int_{V_k}\int_{V_l} G(x,x')\tilde{\rho}_k(x)\tilde{\rho}_l(x')\mathrm{d}^3x\mathrm{d}^3x' = \mathbf{Q}^{\mathrm{T}}\mathbf{P}\mathbf{Q}. \tag{3.41}$$

The matrix $\mathbf{P}$ is called the potential matrix, P_{kl} are called the coefficients of potential,

$$P_{kl} = \int_{V_k}\int_{V_l} G(x,x')\tilde{\rho}_k(x)\tilde{\rho}_l(x')\mathrm{d}^3x\mathrm{d}^3x'. \tag{3.42}$$

Comparing (3.41) and (2.7), we are led to define the capacitance matrix

[2] For spatially homogeneous materials, an explicit expression exists, (3.31). The formalism remains valid for spatially inhomogeneous materials, even though no explicit expression for the Green's function can be provided.

$$\mathbf{C} = \mathbf{P}^{-1}. \tag{3.43}$$

In practical cases, the normalized density functions $\tilde{\rho}$ are not known a priori. Instead, only the total charges on a set of disjoint conductors are prescribed. The distribution functions $\tilde{\rho}$ are subject to a boundary condition at the positions of the conductors, namely the requirement for the conductors to form equipotential volumes. The concept of capacitance is also valid in this case, as it only depends on the linear relationship between the charges ρ and the scalar potential ϕ. For complex geometries, the values of capacitance can be computed numerically [38, 39, 40]. Last but not least, we emphasize that even though we used the scalar potential for the derivation starting at (2.30), the coefficients of capacitance are well-defined physical quantities. In particular, they are independent of the choice of gauge.

3.7.3 Inductance

The second term on the right-hand side of (3.36) describes a change of electrical energy stored in a distribution of electric currents,

$$E_B = \int_V \vec{A} \cdot \vec{j} \mathrm{d}^3x = \int_V \vec{H} \cdot \vec{B} \mathrm{d}^3x. \tag{3.44}$$

Decomposing the total current density into disjoint closed current paths $\vec{\gamma}_k$,

$$\vec{j} = \sum_{k=1}^{n} I_k \vec{\gamma}_k, \tag{3.45}$$

where $\nabla \cdot \vec{\gamma}_k = 0 \forall k$, and writing the vector potential $\vec{A}$ for given $\vec{j}$ in terms of Green's functions,

$$E_B = \sum_{k,l=1}^{n} I_k I_l \int_V \int_V G(x, x') \vec{\gamma}_k \cdot \vec{\gamma}_l \mathrm{d}^3x \mathrm{d}^3x = \mathbf{I}^{\mathrm{T}} \mathbf{L} \mathbf{I}. \tag{3.46}$$

The matrix L is called the inductance matrix. The coefficients L_{kk} and L_{kl} are called self and mutual inductances respectively,

$$L_{kl} = \int_{V_k} \int_{V_l} G(x, x') \vec{\gamma}_k \cdot \vec{\gamma}_l \mathrm{d}^3x \mathrm{d}^3x'. \tag{3.47}$$

Comparing (3.46) and (2.5), we are led to interpret **L** as the field-theoretical equivalent for the lumped inductance matrix.

In practical cases, the normalized current density functions $\tilde{\gamma}$ are not known a priori. Two different situations have to be distinguished: At very low frequencies, the current distribution is determined by Ohmic properties of the conductors. The current density function can be computed as solution to the scalar diffusion equation [41]. For high frequencies, the current distribution for given total current is given such that the inductive energy is minimized, leading to skin and proximity effects. For complex geometries, the values of inductance have to be computed numerically, [1, 42]. Last but not least, we emphasize that even though we used the vector potential for the derivation starting at (2.29), the coefficients of inductance are well-defined physical quantities. In particular, they are independent of the choice of gauge.

Closing Remarks

As the coefficients of capacitance and inductance can be derived from energy concepts, it is obvious that they are well-defined physical quantities. In particular, they are gauge independent. This is true also for the formulations in terms of scalar and vector potentials. In Sect. 4.4.1 we are going to discuss a generalization of the concepts of resistance, capacitance, and inductance by introducing partial resistances, capacitances and inductances. These partial elements can be assigned to small parts (filaments) of conductors. In general, partial circuit elements depend on the choice of gauge.

The total energy density u_{Darwin} in (3.36) treats the inductive energy and the capacitive energy on equal footings. This implies that energy can be exchanged dynamically between the two forms of energy. In particular, this enables resonant behavior where energy resonates between the two forms. This is the equivalent to LC resonances in lumped electrical circuits.

4 Discrete Electrodynamics

Maxwell's equations describe electromagnetic components and systems by a set of partial differential equations. Unfortunately, for most practical applications, it is impossible to solve the set of equations analytically. In this chapter, we describe discretization schemes which allow to solve the electromagnetic equations of motion on a computer.

The range of numerical techniques available today is very wide. In this thesis, we only show two of them: The FEM has been shown to be a very general, robust and powerful method and is mainly used in this work. The PEEC method is the state-of-the-art method for the construction of electrical circuit models and is mainly introduced for purposes of comparison with our method.

4.1 Discretization Techniques

Maxwell's equations are a set of partial differential equations for the description of electromagnetic systems. In general, a set of partial differential equations is described by a differential operator $\mathscr{D}$ acting on the unknown function f, and a given source function u. f need not be a scalar function, it can also be a vector-valued function or describe a set of coupled functions, e.g., the scalar and vector potential of Darwin's model, (3.26). The source function u describes the excitation of the system. The partial differential equation is augmented by boundary conditions on the boundary $\partial\Omega$ of the domain of definition Ω. Mathematically,

$$\begin{aligned} \mathscr{D} f &= u \\ f|_{\partial\Omega} &= f_b. \end{aligned} \tag{4.1}$$

Eqn. (4.1) describes a continuous system with, in general, an infinite number of degrees of freedom. This infinite number of degrees of freedom is reflected by an infinite dimensional vector space $\mathscr{H}(\Omega)$ of functions defined on Ω. The solution f is the unique function in $\mathscr{H}(\Omega)$ satisfying (4.1). For an numerical implementation on a real computer with finite memory capacity, the number of degrees of freedom has to be restricted to a finite number, i.e., the space $\mathscr{H}(\Omega)$ has to be **discretized**. The discrete vector space $\mathscr{H}^{\mathrm{D}}(\Omega)$ then serves as a set of basis functions and the numerical solution f^{D} is a superposition of basis functions, $f^{\mathrm{D}} \in \mathscr{H}^{\mathrm{D}}(\Omega)$. The accuracy of the discretization depends most strongly on the choice of basis functions.

For best accuracy, the basis functions should be chosen such that both the expected solution and the boundary conditions can be described as accurately as possible.

With only a finite set of basis functions, it is impossible in general to satisfy the continuous equations (4.1) exactly, i.e., f^{D} cannot be chosen to make the residual

$$r = \mathscr{D} f^{\mathrm{D}} - u \tag{4.2}$$

vanish everywhere. Instead of trying to solve the continuous set of equations with a discrete set of basis functions, we have to devise a testing scheme, i.e., approximating the solution of the differential equation by a discrete set of equations. In the following, we show two popular testing schemes:

- The point collocation method, [43], requires the exact solution of (4.1) at a discrete set of points only. While the implementation is straightforward, the accuracy of the method can be very low.
- The method of weighted residuals defines a discrete set of weight functions $g^{\mathrm{D}} \in \mathscr{G}^{\mathrm{D}}(\Omega)$ and solves (4.1) by zeroing the weighted residuals,

$$\langle g^{\mathrm{D}}, \mathscr{D} f^{\mathrm{D}} \rangle = \int_\Omega (g^{\mathrm{D}})^\dagger \mathscr{D} f^{\mathrm{D}} \mathrm{d}^3 x = 0, \qquad \forall g^{\mathrm{D}} \in \mathscr{G}^{\mathrm{D}}(\Omega). \tag{4.3}$$

  The best accuracy is reached in general by Galerkin's choice, [43], $\mathscr{G}^{\mathrm{D}}(\Omega) = \mathscr{H}^{\mathrm{D}}(\Omega)$, i.e., the weighting functions are chosen equal to the basis functions.

Using the discretization procedure above, the equations of motion can be written as a matrix system of equations. Assume that the basis functions are chosen such that the boundary conditions can be satisfied exactly. Let $\{f_i, i = 1, \cdots, N\}$ be a basis for $\mathscr{H}^{\mathrm{D}}(\Omega) = \mathscr{G}^{\mathrm{D}}(\Omega)$, let $f^{\mathrm{D}} = \sum_{i=1}^{N} a_i f_i$. The discretized equations of motion then read

$$\langle f_i, \mathscr{D} \sum_{j=1}^{N} a_j f_j \rangle = \sum_{j=1}^{n} \langle f_i, \mathscr{D} f_j \rangle a_j = \langle f_i, u \rangle = u_i. \tag{4.4}$$

In matrix form,

$$\mathbf{M}\mathbf{f} = \mathbf{u}, \qquad \mathbf{M}_{ij} = \langle f_i, \mathscr{D} f_j \rangle = \int_\Omega f_i^\dagger \mathscr{D} f_j \mathrm{d}^3 x. \tag{4.5}$$

To sum up, we reiterate the three basic steps for the discretization of partial differential equations:

1. Define a set of basis functions f_i. The discrete solution f^{D} is a linear combination of basis functions, $f^{\mathrm{D}} = \sum_{i=1}^{N} a_i f_i$.

2. Define a testing scheme. When using the method of weighted residuals, define a set of testing functions g_i.

3. Reformulate the system of partial differential equations as a matrix system of equations, (4.4), and solve the matrix system of equations.

4.2 The Finite Element Method

The Finite Element Method, [44], is one of the most general discretization techniques and can be applied in general to all differential equations. In this section, we repeat the most important definitions and properties of the FEM for scalar partial differential equations. The structure of this section follows the steps in Sect. 4.1.

Let $\mathscr{D}$ be a scalar partial differential operator, for simplicity, $\mathscr{D} = \Delta$. Furthermore, let Ω be the computational domain, $\partial\Omega = \Gamma$ the boundary with, for simplicity, Dirichlet boundary conditions. Let f be the unknown scalar field, u the scalar source field. The equations of motion read

$$\begin{aligned} \Delta f &= u \\ f|_\Gamma &= f_\Gamma. \end{aligned} \tag{4.6}$$

4.2.1 Basis Functions for the Finite Element Method

The basis functions for the standard FEM are piecewise polynomials. The supports of the basis functions are given by simple geometric entities, e.g., linear and curved polyhedra. Each such polyhedron is called an element and lends the method its name. The decomposition of the computational domain into elements allows to describe spatially inhomogeneous material properties very easily.

Different formulations of the FEM are classified according to the maximum polynomial degree of the basis functions, and the maximum polynomial degree of the Lagrangian interpolation polynomial describing the elements.

- In sub-parametric elements, the order of the interpolation polynomials is smaller than the order of the basis functions. Such an implementation is useful when the geometry is rectangular in character and can be described using, e.g., linear interpolation functions only. On the other hand, many degrees of freedom are available for describing the fields. In this work, sub-parametric elements were used.

- In iso-parametric elements, the order of the interpolation polynomials is equal to the order of the basis functions. Higher order interpolation functions very accurately describe curvilinear geometries using a small number of elements only.

- In super-parametric elements, the order of the interpolation polynomials is higher than the order of the basis functions. Super-parametric elements have little importance in literature.

A major advantage of the FEM is the fact that the different formulations can be combined to very efficiently. First, even without changing the order of the interpolation polynomials, the size of the elements can be adapted to the problem (h-refinement, [45]). The mesh can also be refined locally during the computation, [46]. Second, the order of the implementation functions can be adapted locally, e.g., in order to describe a curved surface. Third, the order of the basis functions can be chosen differently for each element (p-refinement, [47]). Last but not least, the aforementioned techniques can be combined (hp-refinement, [48]).

We start with linear polynomials on linear tetrahedra. In a local coordinate system ξ, ζ, η for a tetrahedron, the corners correspond to the points $(0,0,0)$, $(1,0,0)$, $(0,1,0)$, and $(0,0,1)$. A basis for the space of piecewise polynomials of degree ≤ 1 is given by

$$\phi_0 = 1-\xi-\zeta-\eta \quad \phi_1 = \xi \quad \phi_2 = \zeta \quad \phi_3 = \eta. \tag{4.7}$$

The basis functions are chosen such that each basis function is one at exactly one corner of the tetrahedron and zero at all other corners. A formulation of the basis functions in terms of global coordinates can be obtained by expressing the local coordinates ξ, ζ, η in terms of global coordinates. The explicit form of the basis functions will never be needed, it can be found, e.g., in [44].

The set of all basis functions f_i is given by the ϕ_i for all elements. In the conformal FEM, continuity of the solution is enforced by combining two basis functions which belong to the same node, but are defined on different elements. The support of the basis functions of the conformal FEM extend over multiple elements.

If continuity is not enforced strictly, the resulting version of the FEM is called a Discontinuous Galerkin (DG) method, [49, 50].

Higher order nodal basis functions can be constructed accordingly by restricting the support of higher order polynomials to the elements. For example, quadratic basis functions can be written in local coordinates as

$$\phi_5 = \xi^2 \quad \phi_6 = \xi\eta \quad \phi_7 = \xi\zeta \quad \phi_8 = \eta^2 \quad \phi_9 = \eta\zeta \quad \phi_1 0 = \zeta^2. \tag{4.8}$$

4.2.2 Testing Scheme

In the conformal FEM, the basis functions are reused as basis for the weighted residuals. This corresponds to the Galerkin ansatz. For linear tetrahedral elements, all resulting integrals can be computed using the formula, [44],

$$\int_{V_\Delta} \phi_0^k(x)\phi_1^l(x)\phi_1^m(x)\phi_1^n(x)\mathrm{d}^3x = 6V_\Delta \frac{k!l!m!n!}{(k+l+m+n+3)!}. \tag{4.9}$$

As an example, consider the integral appearing in the discretization of the Laplace operator. This integral can be solved by transformation of variables to a local coordinate systems and using (4.9),

$$\begin{aligned}
\langle \phi_i, \Delta\phi_j \rangle &= \int_{V_\Delta} \phi_i(x)\Delta\phi_j(x)\mathrm{d}^3x = -\int_{V_\Delta} (\nabla\phi_i(x))^{\mathrm{T}}(\nabla\phi_j(x))\mathrm{d}^3x \\
&= -\int_0^1\int_0^1\int_0^1 (\mathbf{J}^{\mathrm{T}}\nabla\phi_i(\xi,\zeta,\eta))^{-1}(\mathbf{J}^{\mathrm{T}}\nabla\phi_j(\xi,\zeta,\eta))\frac{\mathrm{d}\xi\mathrm{d}\zeta\mathrm{d}\eta}{|\det(\mathbf{J})|} \\
&= -\mathrm{Tr}\left[\frac{\mathbf{J}\mathbf{J}^{\mathrm{T}}}{|\det(\mathbf{J})|}\left(\int_0^1\int_0^1\int_0^1 (\nabla\phi_i(\xi,\zeta,\eta))(\nabla\phi_i(\xi,\zeta,\eta))\mathrm{d}\xi\mathrm{d}\zeta\mathrm{d}\eta\right)\right].
\end{aligned}$$

The last integral has to be solved only once for a standard tetrahedron,and an analytical solution exists. The solution for an arbitrary tetrahedron can be computed using the Jacobian of the variable transformation,

$$\mathbf{J} = \frac{\partial(\xi,\zeta,\eta)}{\partial(x,y,z)} = \begin{pmatrix} \partial_x\xi & \partial_y\xi & \partial_z\xi \\ \partial_x\eta & \partial_y\eta & \partial_z\eta \\ \partial_x\zeta & \partial_y\zeta & \partial_z\zeta \end{pmatrix}.$$

4.2.3 Setting up the Matrix System of equations

With the set of basis functions and testing functions, the equations of motion can be discretized. With an expansion of the unknown function, $f^{\mathrm{D}} = \sum_{i=1}^{N} a_i \phi_i$, the discretized equations of motion for, e.g., the scalar Laplace equation read

$$\langle \phi_i, \Delta \sum_{j=1}^{N} a_j \phi_j \rangle = \sum_{j=1}^{N} \langle \phi_i, \Delta \phi_j \rangle i_j = \langle \phi_i, u \rangle, \qquad \forall i = 1, \cdots, N.$$

In order to define the coefficient matrix $\mathbf{M}$, $M_{ij} = \langle \phi_i, \Delta \phi_j \rangle$ the basis functions have to be associated with global degrees of freedom. In order to ensure continuity of the solution, basis functions belonging to the same node are associated with the same degree of freedom. The solution of the local integrals is shown in 4.2.2.

4.3 The Finite Element Method for Electromagnetism

In the previous section, we introduced the FEM along the lines of the scalar Laplace equation. Before applying the FEM to discretize the equations of motion of electromagnetism, a mathematical formulation has to be chosen. In order to use the same formulation for Maxwell's and Darwin's model, the formulation in terms of scalar and vector potential is used, (3.28). While the scalar potential can be discretized using nodal elements, discretizing the vector potential is not so easy.

The main difference between the scalar Laplace equation and the equations of motion for the vector potential is the inherent vectorial character of the latter. Treating each component of the vector field separately, i.e., separately discretizing each component using nodal elements has been proven unfeasible due to the emergence of spurious, i.e., unphysical solutions [51, 52, 53, 54]. The emergence of spurious solutions has been traced back to a numerical violation of the $\nabla \cdot (\nabla \times \vec{v}) = 0$ relationship, [55]. Another disadvantage of nodal based elements is a bad reproduction of continuity requirements of the fields at material interfaces, [56]. To sum up, nodal basis functions adapt very badly to the requirements of intrinsically vectorial problems.

The vector potential is governed by a double curl equation, it thus belongs to the function space

$$\mathscr{H}(curl, \Omega) = \left\{ \vec{v} : \nabla \times \vec{v} \in \mathscr{L}^2(\Omega) \right\} = \left\{ \vec{v} : \int_{\Omega} |\nabla \times \vec{v}|^2 \mathrm{d}^3 x < \infty \right\}.$$

A discretization of the function space $\mathscr{H}(curl, \Omega)$ which provides a significantly better approximation of the physical solution is provided by edge basis functions, [57, 58]. It has been noted that the new basis functions do not produce spurious solutions, [59, 60]. They also offer a better modeling of vector field continuity at material interfaces, [61].

Like nodal basis functions, edge basis functions are in general vector valued polynomials. The lowest order basis functions are linear polynomials and are given by

$$\vec{v}_{ij} = \phi_i \nabla \phi_j - \phi_j \nabla \phi_i. \tag{4.10}$$

The scalar functions ϕ are exactly the nodal basis functions. The name of the edge elements indicates that each basis function is associated with two nodes i and j, or, equivalently, to the edge connecting the nodes.

Extending vector basis functions to higher orders is also possible. The set of basis functions then also comprises higher order vector-valued polynomials. Unlike for nodal elements, this extension is not straightforward in order to retain a good approximation of $\mathscr{H}(curl, \Omega)$. Several extensions are compared in [62]. In this work, a formulation of quadratic edge basis functions from [63] is used.

The edge basis functions (4.10) have originally been derived in order to discretize the electric vector field $\vec{E}$. As the vector potential $\vec{A}$ belongs to the same function space $\mathscr{H}(curl, \Omega)$ and satisfies identical continuity requirements at material interfaces, they can also be used for the discretization of the vector potential $\vec{A}$ for Maxwell's or Darwin's model respectively, [64]. In order to discretize the scalar potential ϕ, the standard nodal basis functions are used.

4.3.1 Software used in this work

Based on the theory presented above, a program for the solution of the equations of motion of Darwin's system using the FEM was implemented by the author. The implementation is based on commercial and open-source software:

- For geometry preprocessing and generation of a linear tetrahedral mesh, the commercial software CST Microwave Studio ® (CST MWS), [65], and the open-source program GMSH, [66], were used.
- In order to set up the matrix system of equations, the Portable Extensible Toolkit for Scientific Computation (PETSc), [67, 68, 69], was used. PETSc is

linked to the Intel Math Kernel Library (MKL), [70], and the Message Passing Interface (MPI) library from the Microsoft High-Performance Computing (HPC) Pack, [71].

- The matrix system of equation was solved using the parallel direct solver SuperLU_Dist, [72, 73].

4.4 The Partial Element Equivalent Circuit method

The PEEC method, [3], is a numerical method for the solution of electromagnetic problems. The standard PEEC method uses an integral formulation of Darwin's model, however it can also be formulated for the full-wave model described by Maxwell's equations [35]. As the name indicates, the PEEC method discretizes the geometry into elementary geometric entities, usually cubes and assigns to each elementary entity values for inductance, resistance, and capacitance. Current and voltage sources can be included on both the 3D level and the circuit level. The discretization procedure results in a very large equivalent electrical circuit which can be solved with standard circuit solvers such as LT SPICE [74] or SABER [75].

For simplicity, in all following sections, we assume that the geometry consists of one or multiple conductors of finite conductivity σ which are placed in infinite vacuum space, i.e. $\epsilon_r(x) = \mu_r(x) = 1$ everywhere. In this case, Green's function for the Laplace equation, $G(x, x')$, has an explicit form (3.31),

$$G(x, x') = \frac{1}{4\pi} \frac{1}{|x - x'|}. \tag{4.11}$$

4.4.1 Partial Circuit Elements

Partial Resistances

Consider a conductor of cross section area A, length l, and spatially homogeneous conductivity σ. When a homogeneous current density $\vec{j} = \frac{I}{A}\vec{e}_l$ flows through the cube, the rate of energy dissipation is given by (3.39). The corresponding resistance can be computed explicitly to yield

$$R = \frac{l}{\sigma A}. \tag{4.12}$$

For practical geometries, e.g., bent wires, there usually does not exist a simple formula for the total resistance such as (4.12). However, even a complex geometry can be imagined to consist of many elementary cubes such that the above assumptions are satisfied for each elementary cube. Each elementary cube is then assigned a resistance according to (4.12). The total resistance can be computed from the resistances of the elementary cubes using the laws of circuit theory. The resistances of the elementary cubes can be seen as part of the total resistance, they are called partial resistances accordingly.

Partial Capacitance

Consider next two homogeneously charged rectangular surfaces S_1 and S_2, carrying total charges Q_1 and Q_2 respectively[1]. In Sect. 3.7.2 we derived an expression for the total capacitive energy of the system, (3.41), and an integral equation for the coefficient of potential (3.42). For the two plates, the coefficient of potential reads

$$P_{kl} = (C^{-1})_{kl} = \frac{1}{\epsilon_0 S_1 S_2} \int_{S_1} \int_{S_2} \frac{1}{4\pi} \frac{1}{|x - x'|} \mathrm{d}a \mathrm{d}a'. \tag{4.13}$$

A closed form solution of (4.13) is computed in [38]. For practical geometries, there exists no simple formula for the total coefficient of potential such as (4.13). However; as above, we can imagine a complex surface as consisting of elementary rectangles. The total coefficient of potential can be computed from the coefficients of the elementary plates using the laws of circuit theory. As the coefficients of potential of the elementary surfaces can be seen as part of the total coefficients of potentials, they are called partial coefficients of potential accordingly.

Partial Inductance

In the two previous sections, we introduced the concepts of partial resistance and partial capacitance by decomposing the total resistance and the total capacitance into parts, which we assigned to simple geometric entities. In this section, we aim at a similar procedure for the inductors, i.e., to decompose the total inductance of a solenoidal current density into parts, to which we assign partial inductances.

[1] At practical time-scales or frequencies, the electric charge can be approximated as a pure surface charge density. The charge density inside conductors or dielectrics is zero with very good approximation [41].

There is a significant difference to the previous cases, however. When a solenoidal current density is broken into several parts, the parts are not necessarily solenoidal themselves. The magnetic field, and thus the definition (3.44), is not well-defined for non-solenoidal current densities. We therefore cannot use (3.44) to define partial inductances.

On the other hand, (3.46) can be generalized to arbitrary current densities. We can thus define partial inductances for, e.g., a system of two cubes V_1 and V_2 carrying homogeneous current densities in directions $\vec{e}_1$ and $\vec{e}_2$ respectively,

$$L_{kl} = \frac{\mu_0}{A_1 A_2} \int_{V_1} \int_{V_2} \frac{\vec{e}_1 \cdot \vec{e}_2}{4\pi|x - x'|} \mathrm{d}^3x \mathrm{d}^3x'. \tag{4.14}$$

A_1 and A_2 are the cross section areas of the cubes normal to $\vec{e}_1$ and $\vec{e}_2$ respectively. A closed form solution of (4.14) is provided in [1]. For $k \neq l$, L_{kl} is called the partial mutual inductance between the k-th and the l-th inductor, for $k = l$, $L_k = L_{kk}$ is the partial self-inductance of the k-th inductor. For practical multiconductor geometries, the inductance matrix (3.46) cannot be computed analytically. However, we can again imagine a complex geometry as consisting of many small cubes, for which the partial self and mutual inductances can be computed. The total inductance can be computed by combining the partial self and mutual inductances according to the laws of circuit theory.

The definition of partial inductances is closely connected to the gauge-dependent vector potential $\vec{A}$. This fact leads to some properties of partial inductances which have to be considered with care:

- The relationship between the vector potential $\vec{A}$ and the current density $\vec{j}$ is subject to the gauge condition (3.24). The values of the partial inductances depend on the gauge [76] and (4.14) is only one possible definition. The original definition is derived using the Lorenz gauge (3.27). A gauge transformation $\vec{A} \to \vec{A} - \nabla\kappa$ changes

$$L = \frac{1}{I^2} \int \vec{A} \cdot \vec{j} \mathrm{d}^3x \to \frac{1}{I^2} \int \left(\vec{A} - \nabla\kappa\right) \vec{j} \mathrm{d}^3x = L + \int \kappa(\nabla \cdot \vec{j}) \mathrm{d}^3x. \tag{4.15}$$

  If the current density is solenoidal, $\nabla \cdot \vec{j} = 0$, the definition of inductance is gauge-independent. It follows, in particular, that when several gauge-dependent partial inductances are combined to compute a loop inductance, this loop inductance is gauge independent as it should be.

- It is shown in Sect. 6.2.4 that in the definition of partial inductances, the open current paths are closed implicitly by a generic current return path,

$$\vec{j}_{\text{return}} = \epsilon \nabla g \quad \text{where} \quad \nabla \cdot \epsilon \nabla g = -\nabla \cdot \vec{j}.$$

  With this return current, $\nabla \cdot (\vec{j} + \vec{j}_{\text{return}}) = 0$ and the partial inductance is really the self inductance of a solenoidal current density.

- A geometrically motivated interpretation of partial inductance is shown in [1]. The partial inductance is related to self and mutual inductances of closed current loops which extend to infinity. An experimental setup approximating current loops extending to infinity is used in [77], where the authors claim to have measured partial inductances. However, their method really measures the mutual inductances of two perpendicular current loops which agrees in this simple case with the definition (4.14) for partial inductance. In general, partial inductances are gauge-dependent quantities and cannot be measured.

To sum up, we emphasize that unlike the concepts of partial resistance and partial capacitance, the concept of partial inductance is a mathematical rather than a physical concept. Whenever partial inductances are used, the physical current return path has to be included in the circuit representation and has also to be modeled by means of partial inductances.

4.4.2 The Partial Element Equivalent Circuit Method for the Solution of Electromagnetic Field Problems

In Sect. 4.4.1, we derived the concepts of partial resistance, partial capacitance and partial inductance based on the assumption that the charge and current densities ρ and $\vec{j}$ are known. This is in general not the case. Instead, charges and currents interact with the electromagnetic fields and their distribution can only be solved using a self-consistent system of equations describing at the same time the charges, currents, electromagnetic fields, and their mutual interactions. Such a system is given, e.g., by Maxwell's equations or Darwin's equations. The PEEC method discretizes such a self-consistent system of equations and expresses the discretized system in terms of partial circuit elements.

In Sect. 4.1, we developed the three steps needed for the discrete description of a physical system - defining the equations of motion, specifying a discrete set

of basis functions, specifying a discrete set of testing functions, and setting up the matrix system of equations. We are going to introduce the PEEC method along these steps.

Equations of Motion

The standard PEEC method [3] is formulated for the quasistatic Darwin's model (Sect. 3.4.3) because it allows for a simple implementation and interpretation as an equivalent electrical circuit. There exist also variants of the PEEC method (Retarded Partial Element Equivalent Circuit (rPEEC), [35]) which use Maxwell's equations as equations of motion.

The PEEC method is an integro-differential equation method, i.e., it starts from an integro-differential formulation of the equations of motion. The charge and current densities from a linearly independent set of unknowns from which all other quantities are computed. The interactions between charges and currents, mediated by the electromagnetic fields, are described in terms of Green's functions (Sect. 3.6).

The integro-differential formulation of Darwin's equations used in the PEEC method is given by [3]

$$\vec{j}(x) = \sigma(x)\vec{E}(x) = \sigma\left(-\partial_t \vec{A} - \nabla\phi\right) \tag{4.16}$$

$$\partial_t \rho = \nabla \cdot \vec{j} \tag{4.17}$$

$$\phi(x) = \frac{1}{\epsilon_0}\int_V \rho(x')G(x,x')\mathrm{d}^3x' \tag{4.18}$$

$$\vec{A}(x) = \mu_0 \int_V \vec{j}(x')G(x,x')\mathrm{d}^3x'. \tag{4.19}$$

Eq. (4.16) is the constitutive equation for conductors. Eq. (4.17) is the continuity equation for the electric charge. Eqs. (4.18) and (4.19) are integral expressions for the equations of motions of the scalar and vector potentials, (3.28).

Discretization

The system of equations (4.16)-(4.19) is discretized by specifying a set of basis functions for the unknown functions $\rho(x)$ and $\vec{j}(x)$. The standard PEEC method

[3] uses two sets of basis functions: In order to approximate the current density, all conductors are decomposed into cubes and a constant current density flowing along each cube is assumed. Each cube (more precisely, each current basis function associated to a cube) is called a current cell. For the k-th current cell with current flow direction $\vec{e}_k$, cross section A_k, and volume V_k, the current basis function is defined by

$$\vec{m}_k(x) = \frac{1}{A_k}\vec{e}_k\chi_{V_k}, \tag{4.20}$$

and χ_{V_k} is the characteristic function of the k-th cube. By construction, each current cell supports current in one direction only. In order to reproduce the real current flow with high accuracy, current cells that support current flowing in mutually orthogonal directions are allowed to overlap. This implies, again, that current cells should be interpreted in terms of basis functions rather than geometric entities.

In order to discretize the charge density, the conductor surfaces are decomposed into rectangles and a constant surface charge density in the rectangles is assumed. Each rectangle (more precisely, each charge basis function associated to a rectangle) is called a charge cell. For the l-th charge cell with surface S, the charge basis function is given by

$$v_l = \frac{1}{S_l}\chi_{S_l}. \tag{4.21}$$

Charge and current cells are usually not chosen independently. A simple implementation results when the charge cells are chosen at the two ends of the current cells that are distinguished by the current flow direction[2]. Overlapping current cells lead to overlapping charge cells. These charge cells are united into one single charge cell, consisting of two or three rectangles. The structure of PEEC current and charge cells is illustrated at a simple example in Fig. 4.1.

In principle, it is possible to eliminate the potentials ϕ and $\vec{A}$ from the PEEC system of equations by inserting (4.18)-(4.19) into (4.16)-(4.17). For easier interpretation of the resulting discrete system as an electrical circuit model, we omit this step. The charge basis functions are then reused to discretize the scalar-valued potential ϕ, the charge basis functions are reused to discretize the vector-valued potential $\vec{A}$.

[2] The four other surfaces cannot carry charge by definition because by construction, the current basis functions prescribes zero divergence at these surfaces.

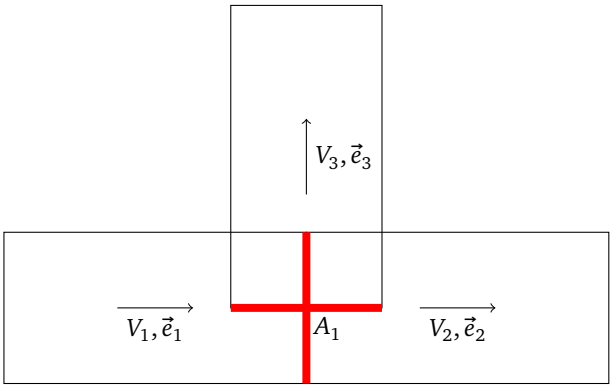

Figure 4.1.: Three PEEC current cells (thin, black) and one PEEC charge cell (thick, red)

Testing

With only a discrete set of basis functions, it is impossible in general to solve the system of equations (4.16)-(4.19) exactly. The problem is circumvented by a suitable testing scheme. For the PEEC method, two testing schemes are commonly used

- The collocation method, [78], forces (4.16)-(4.19) to hold only at selected points. Usually, the centers of the current and charge cells are chosen. The main advantage of the collocation method is its simplicity, the main disadvantage a comparatively low accuracy and stability issues [79, 80].
- The Galerkin method uses test basis functions which are equal to the basis functions and minimizes (4.16)-(4.19) with respect to the standard inner product. The evaluation of the inner product requires further integrals and thus leads to more complicated expression. However, this method leads to a much better accuracy. This is the method used in the standard formulation of the PEEC method [3].

Setting up the Matrix System of Equations

The equations of motion are discretized by inserting the basis functions (4.20) and (4.21) into (4.16)-(4.19). Starting with (4.18), we obtain:

$$\begin{aligned}\Phi_i = \langle v_i, \sum_{j=1}^{N_n} \Phi_j v_j \rangle &= \langle v_i, \int \frac{\sum_{j=1}^{N_n} Q_j v_j}{4\pi\epsilon_0 |x - x'|} \mathrm{d}^3 x' \rangle \\ &= \sum_{j=1}^{N_n} Q_j \left[\frac{1}{\epsilon_0 S_i S_j} \int_{S_i} \int_{S_j} \frac{\mathrm{d}a\mathrm{d}a'}{4\pi|x - x'|} \right].\end{aligned} \tag{4.22}$$

Comparing the last term in (4.22) and (4.13), we recover the partial coefficients of potential for the i-th and j-th charge cells. In matrix form, (4.22) can be written

$$\Phi = \mathbf{P}\mathbf{Q} \quad \Leftrightarrow \quad \mathbf{Q} = \mathbf{C}\Phi \tag{4.23}$$

In order to discretize (4.16), we express the vector potential $\vec{A}$ in terms of the current using (4.19) and obtain

$$\begin{aligned} I_i \left[\int_{V_1} \frac{\mathrm{d}^3 x}{A_i^2 \sigma} \right] &= \langle \vec{m}_i, \sum_{j=1}^{N_b} \frac{I_j}{\sigma_j} \vec{m}_j \rangle \\ &= \langle \vec{m}_i, \int \frac{\mu_0 \sum_{j=1}^{N_b} \frac{\mathrm{d}I_j}{\mathrm{d}t} \vec{m}_j}{4\pi|x - x'|} \mathrm{d}^3 x' \rangle + \langle \vec{m}_i, \sum_{j=1}^{N_n} \Phi_j \nabla v_j \rangle \\ &= \sum_{j=1}^{N_b} \frac{\mathrm{d}I_j}{\mathrm{d}t} \left[\frac{\mu_0}{A_i A_j} \int_{V_i} \int_{V_j} \frac{\vec{e}_1 \cdot \vec{e}_2}{4\pi|x - x'|} \mathrm{d}^3 x \mathrm{d}^3 x' \right] + [\Phi_{i+} - \Phi_{i-}], \end{aligned} \tag{4.24}$$

where Φ_{i+} and Φ_{i-} are the coefficients belonging to the charge cells the end faces of the i-th current cell. Comparing the bracketed term on the left hand side and (4.12), we recover the partial resistance. Comparing the bracketed integral on the right hand side and (4.14), we recover the partial inductance for the i-th and j-th cubes. In matrix form, (4.24) thus takes the form

$$\mathbf{A}^{\mathrm{T}} \Phi = \mathbf{R} \cdot I + \mathbf{L} \cdot \frac{\mathrm{d}I}{\mathrm{d}t}, \tag{4.25}$$

where $\mathbf{R}$ is the diagonal matrix of partial resistances, $\mathbf{L}$ is the matrix of self and mutual inductances. $\mathbf{A}$ describes the incidences of the charge cells into current cells. Mathematically,

$$\mathbf{A}_{ij} = \int_V \vec{m}_j \cdot \nabla v_i \mathrm{d}^3x = \int_V v_i \cdot (-\nabla \cdot \vec{m}_j)\mathrm{d}^3x$$
$$= \begin{cases} +1 & \text{if j-th current cell ends at i-th charge cell} \\ -1 & \text{if j-th current cell starts at i-th charge cell} \\ 0 & \text{otherwise.} \end{cases} \tag{4.26}$$

Interpreting the current cells as edges of a graph and the charge cells as nodes, it is identical to the node incidence matrix (2.13). Last but not least, it remains to discretize the continuity equation (4.17),

$$\frac{\mathrm{d}Q_i}{\mathrm{d}t} = \langle v_i, \sum_{j=1}^{N_n} \frac{\mathrm{d}Q_j}{\mathrm{d}t} v_j \rangle = \langle v_i, \sum_{j=1}^{N_b} I_j (\nabla \cdot \vec{m}_j) \rangle$$
$$= \sum_{j=1}^{N_b} \frac{\mathrm{d}Q_j}{\mathrm{d}t} \left[\int_{V_i} \int_{V_j} v_i (\nabla \cdot \vec{m}_j) \mathrm{d}^3x \mathrm{d}^3x' \right]. \tag{4.27}$$

In matrix form, this equation reads

$$\frac{\mathrm{d}\mathbf{Q}}{\mathrm{d}t} = -\mathbf{A}\mathbf{I}. \tag{4.28}$$

Interpreting the System of Equations as an Equivalent Electrical Circuit

As the name indicates, the PEEC method describes an complex electromagnetic system in terms of a large equivalent electrical circuit. With the following identifications, the discetized field equations have the same form as circuit equations:

- The charge cells form the nodes of the equivalent circuit.
- The current cells form the edges of the equivalent circuit.
- The **A** matrix in (4.26) agrees with the node incidence matrix (2.13) of the equivalent electrical circuit.
- Eq. (4.25) assigns to the i-th current cell a series connection of an inductor L_{ii} and a resistor R_{ii}. Between the i-th and the j-th current cell exists a mutual inductance L_{ij}.

- Eq. (4.23) assigns to each pair of charge cells an inductance. Eq. (4.28) allows to express the charges on the capacitors in terms of capacitor currents as in (2.8).

The size of the electrical circuit directly depends on the mesh size: The number of nodes is equal to the number of charge cells, the number of edges is equal to the number of current cells. For practical geometries, the number of circuit elements can thus be very large.

4.4.3 PEEC Formulations for Different Physical Models

The standard PEEC method [3] uses the Darwin system of equations (4.16)-(4.19) as equations of motion. The discretization technique is more general and can also be applied to different sets of equations of motion. Our investigation reveals interesting relationships between different quasistatic models for Maxwell's equations (Sect. 3.4) and electrical circuits.

- If the set of PEEC basis functions is used to discretize the equations of motion of electroquasistatics, the resulting circuit consists of a resistance matrix and a capacitance matrix only, [81]. Electroquasistatics cannot describe inductive effects. An implementation of the PEEC method for electrostatics is provided by the open-source tool FastCap [39].

- If the set of PEEC basis functions is used discretize the equations of motion of magnetoquasistatic, the resulting circuit consist of a resistance matrix and an inductance matrix only, [81]. Magnetoquasistatics cannot describe capacitive effects. An implementation of the PEEC method for magnetoquasistatics is provided by the open-source tool FastHenry [42].

- If the set of PEEC basis functions is used to discretize the full Maxwell's equations, the Green's functions, i.e., the kernels of the integrals, have to be replaced by their full-wave counterparts, [35]. In this case, the discretized equations of motion are still in the form of circuit equations. However, the circuit elements become retarded or, in the frequency domain, frequency dependent.

This overview confirms the analysis in Sect. 3.4. The equations of motion of electro(quasi)statics and magneto(quasi)statics describe some effects which are also described by electrical circuits, but not all of them. Maxwell's equations require circuit elements which differ from their classical definitions and describing all effects of electromagnetism leads beyond the realm of electrical circuits. The exact counterpart of circuit theory in the 3D domain is Darwin's model.

4.4.4 Inclusion of Dielectric and Magnetic Materials in the PEEC method

Spatially inhomogeneous dielectric and magnetic materials cannot easily be incorporated in the PEEC formalism. This is because there exists no trivial generalization of the Green's function (3.31) to the case of spatially inhomogeneous materials. In practice, two approaches are possible

- The direct approach is to compute the generalized Green's function which is valid also in the presence of inhomogeneous materials. For some simple geometries, such an approach has been proven feasible [82, 83]. In [84], the Green's functions in the presence of materials are computed numerically. From the point of view of circuit interpretation, the main advantage of this approach is that all when all material information is incorporated in the Green's functions, it only alters the circuit element values without changing the topology of the circuit. However; the absence of analytical expressions for general material distributions and the huge work needed for a numerical construction of the Green's function disqualify this approach for practical applications.

- The widely used approach for the description of inhomogeneous materials is to treat the electric and magnetic polarizations as additional unknowns, i.e., to include them explicitly instead of removing them by means of the constitutive equations. The polarizations densities are then discretized using the PEEC basis functions. On the level of electrical circuits, they additional unknowns require additional circuit elements, e.g., excess capacitances or controlled sources. The main advantage of this approach is that it can be applied to arbitrary material distributions and to a broad class of materials, e.g., dielectric materials [85, 86], magnetic materials [87, 88, 89], lossy materials [90] or dispersive materials [91]. On the other hand, the numerical cost is significantly higher because the dielectric and magnetic materials have to be discretized and assigned degrees of freedom. From the point of view of circuit interpretation, the additional circuit elements make the link between the circuit elements and the basic physical processes more difficult.

4.4.5 PEEC Models of Current Sources

To complete the derivation of the PEEC method, excitations for the discretized model have to be defined. We restrict ourselves to current sources, which are needed for the definition of the impedance. In the classical PEEC method, [3],

current sources are not modeled in the 3D domain. Instead, current sources are added to the discretized model on the circuit level. In this section, we discuss the implicit assumptions underlying this model.

In the physical reality, a source current has to be treated on equal footing with the conduction currents. This means that in (4.17) and (4.19), the conduction currents $\vec{j}$ of the 3D model have to be augmented by the source current density $\vec{j}_s$. The source current density can then be discretized with the same set of basis functions, (4.20), as the conduction current density. The discretized continuity equation (4.17) then reads

$$\frac{\mathrm{d}\mathbf{Q}}{\mathrm{d}t} = -\mathbf{A}\mathbf{I} - \mathbf{A}\mathbf{I}_s \,. \tag{4.29}$$

When the discretized system is interpreted as an electrical circuit, $\mathbf{A}\mathbf{I}_s$ corresponds to a classical current source term. More precisely, if an edge of the electrical circuit corresponds to a current cell used for the discretization of a the source current, the edge is assigned a current source. In order to also discretize the modified equation of motion for $\vec{A}$, (4.19), we have to compute the contribution of the source current to the vector potential. Consider a source current which is modeled by a single current cell, $\vec{j}_s = I_s \vec{m}_s$. Then, according to (4.24), the voltage induced in the i-th current cell is given by

$$V_i = \langle \vec{m}_i, \frac{\mathrm{d}I_s}{\mathrm{d}t} \int \frac{\mu_0 \vec{m}_s}{4\pi|x-x'|} \mathrm{d}^3x' \rangle = \frac{\mathrm{d}I_s}{\mathrm{d}t} \left[\int_{V_i} \int_{V_s} \frac{\mu_0 \vec{e}_i \cdot \vec{e}_s}{4\pi|x-x'|} \mathrm{d}^3x \mathrm{d}^3x' \right] = \frac{\mathrm{d}I_s}{\mathrm{d}t} L_{si}.$$

More generally and in matrix form, $\mathbf{A}^{\mathrm{T}} \Phi = \mathbf{L}_s \frac{\mathrm{d}\mathbf{I}_s}{\mathrm{d}t}$. On the level of electrical circuits, this implies that there exist mutual inductances between the conduction current cells and the source current cells. In the classical PEEC method, when modeling current sources by lumped sources, these inductances are defined. This is justified when $\mathbf{L}_s$ is small, i.e., when the physical length of the current sources is small.

Up to this point of the section, we discussed the discretized form of field-theoretical current sources in the PEEC method. In the remaining part of the section, we discuss the opposite situation, i.e., a field-theoretical form of lumped current sources. This discussion is motivated by a problem in later chapters: In Chap. 6, we formulate a field-theoretical model for lumped current sources. The definition in Chap. 6 will be derived using a different reasoning, however, the result will be shown to be equivalent.

The field-theoretical formulation of lumped current sources can be found by reversing the discretization procedure in Sect. 4.4.2, i.e.,

$$\begin{aligned}
\mathbf{A}^{\mathrm{T}}\Phi = \mathbf{R}\mathbf{I} + \mathbf{L}\frac{\mathrm{d}\mathbf{I}}{\mathrm{d}t} \quad &\Rightarrow \quad \begin{cases} \vec{j} &= \sigma(-\partial_t \vec{A} - \nabla\phi) \\ \vec{A} &= \mu_0 \int \vec{j}(x')G(x,x')\mathrm{d}^3x' \end{cases} \\
\frac{\mathrm{d}\mathbf{Q}}{\mathrm{d}t} = -\mathbf{A}\mathbf{I} - \mathbf{A}\mathbf{I}_s \quad &\Rightarrow \quad \partial_t \rho = -\nabla\cdot\vec{j} - \nabla\cdot\vec{j}_s \\
\Phi = \mathbf{P}\mathbf{Q} \quad &\Rightarrow \quad \phi(x) = \frac{1}{\epsilon_0}\int \rho(x')G(x,x')\mathrm{d}^3x'.
\end{aligned}$$

This set of equations[3] differs from the homogeneous equations of motion for the PEEC model, (4.16)-(4.19), in the inclusion of the divergence of the source current, $\nabla\cdot\vec{j}_s$. In the simple case that the source current consists of a single filament γ_s starting at x_0 and ending at x_1, the divergence is given by

$$\nabla\cdot\vec{j}_s = I_s\nabla\cdot\gamma_s = -I_s(\delta^{(3)}(x-x_1) - \delta^{(3)}(x-x_0)) = -I_s\delta.$$

The points x_0 and x_1 are the 3D equivalents to the end nodes of the current source. We appropriately call these points electrodes. In order to study the impact of the additional term on the scalar and vector potential, we compute

$$\nabla\cdot\vec{A} = -\mu_0\int(\nabla\cdot\vec{j})G(x,x')\mathrm{d}^3x' = \mu_0\partial_t\int\rho G(x,x')\mathrm{d}^3x' + \mu_0\int(\nabla\cdot\vec{j}_s)G(x,x')\mathrm{d}^3x'.$$

The first term is exactly the time-derivative of the scalar potential, $-\epsilon_0\mu_0\partial_t\phi$. The second term can be expressed in terms of an auxiliary field g,

$$\int(\nabla\cdot\vec{j}_s)G(x,x')\mathrm{d}^3x' = \epsilon_0 g \qquad \Leftrightarrow \qquad \epsilon_0\Delta g = \nabla\cdot\vec{j}_s = I_s\delta.$$

The auxiliary field g will play an important role in our field-theoretical formulation of lumped current sources in Sect. 6.2.1. To sum up, we repeat the two different ways of incorporating current sources. On the left hand side, we assume an impressed source current density $\vec{j}_s$. On the right hand side, we rephrase the model for lumped current sources:

[3] Note that this set of equations is also equivalent to the PEEC equations of motion using the modified nodal analysis [92].

3D Current Sources		PEEC Current Sources	
$\Delta\vec{A}+\mu_0\vec{j}_\sigma$	$=-\mu_0\vec{j}_s$	$\Delta\vec{A}+\mu_0\vec{j}_\sigma$	$=0$
$\nabla\cdot\vec{A}+\epsilon_0\mu_0\partial_t\phi$	$=0$	$\nabla\cdot\vec{A}+\epsilon_0\mu_0\partial_t\phi$	$=\epsilon_0\mu_0 g$
$\vec{j}_\sigma+\sigma(\partial_t\vec{A}+\nabla\phi)$	$=0$	$\vec{j}_\sigma+\sigma(\partial_t\vec{A}+\nabla\phi)$	$=0.$

(4.30)

5 Spectral Theory

When an electromagnetic system is excited by a time-harmonic signal, the response can be very violent if the frequency of excitation is close to a natural frequency of oscillation, an eigenfrequency. The importance of finding the eigenfrequencies cannot be overestimated: We will show that from the eigenfrequencies of a physical system, the response to an arbitrary excitation can be computed. In particular, the response can be divided into relevant and irrelevant contributions depending on whether the eigenfrequencies are close to or far away from the frequency range of interest. The mathematical background, spectral theory of matrix and operator polynomials, is presented in this chapter.

It is impossible to analytically compute the natural frequencies and the associated natural modes of oscillation for practical systems. We therefore rely on computational schemes and show how a numerical implementation can be obtained.

5.1 Polynomial Eigenvalue Problems

5.1.1 Definition

Let $\mathscr{X}$ be a linear space over the complex numbers $\mathbb{C}$. Let $\mathscr{L}(\mathscr{X})$ be the algebra of linear operators on $\mathscr{X}$, $\mathscr{L}(\mathscr{X}) = \{f : \mathscr{X} \to \mathscr{X}, f \text{ linear}\}$. For simplicity, we restrict ourselves to finite-dimensional spaces[1], and we can identify $\mathscr{X} \simeq \mathbb{C}^n$ for some n. When $\mathscr{X}$ is equipped with a basis, $\mathscr{L}(\mathscr{X})$ is the algebra of complex $n \times n$ matrices acting on $\mathbb{C}^n$.

Consider next a function $\mathbf{L} : \mathbb{C} \to \mathscr{L}(\mathscr{X})$. In the course of this thesis, we have encountered such functions frequently: The equations of motion for electrical circuits (Sect. 2) or Maxwell's and Darwin's equations for the electromagnetic fields (Sect. 3) in the frequency domain are exactly such maps from $\mathbb{C}$, the complex frequency, to the algebra of complex-valued matrices. In the absence of complicated, frequency-dependent materials, we can restrict ourselves to functions which are

[1] For the description of electromagnetic systems in terms of field equations, $\mathscr{X}$ really is the infinite-dimensional space of vector fields on $\mathbb{R}^3$, and $\mathscr{L}(\mathscr{X})$ is the algebra of differential operators on $\mathscr{X}$. In this case, we interpret $\mathscr{X}$ and $\mathscr{L}(\mathscr{X})$ in their discetized form, e.g., using the FEM.

polynomials in the complex frequency s. We therefore define matrix polynomials $\mathbf{L}$ by

$$\mathbf{L}(s) = \sum_{k=0}^{l} s^k \mathbf{A}_k. \tag{5.1}$$

As in the scalar case, we call $\mathbf{A}_l \neq 0$ the leading coefficient.

In the following, we restrict ourselves to regular matrix polynomials, i.e. $\mathbf{L}(s)$ is regular for almost all $s \in \mathbb{C}$[2]. The following definition describes all complex numbers where the matrix polynomial becomes singular:

Definition 5.1. *Let $\mathbf{L} : \mathbb{C} \to \mathscr{L}(\mathscr{X})$ be a matrix polynomial. The complex number s_0 is called an eigenvalue if $\dim\ker(L(s_0)) \geq 1$. The (right) eigenspace T associated to the eigenvalue s_0 is the corresponding null space, $T = \ker(L(s_0))$. The dimension $\beta_0 = \dim(T)$ of the eigenspace is called the geometric multiplicity. A vector $\mathbf{x} \in T$ is called (right) **eigenvector**. The pair $(\mathbf{x}, s_0)$ is called a (right) eigenpair.*

Left eigenspaces and left eigenvectors can be defined similarly by exchanging $L(s_0) \to L(s_0)^\dagger$ in Def. 5.1.

For a matrix polynomial of degree l acting on an n-dimensional vector space, the characteristic polynomial $p(s) = \det(\mathbf{L}(s))$ is a polynomial in s of degree $\leq nl$, with equality if the leading coefficient A_l is invertible. Using standard methods, the characteristic polynomial can be decomposed into a product of nl linear factors[3],

$$p(s) = \prod_{k=1}^{K} (s - s_k)^{\alpha_k}, \tag{5.2}$$

where $\sum_{k=1}^{K} \alpha_k = nl$. The roots s_k of the characteristic polynomial are exactly the eigenvalues of the matrix polynomial. The numbers α_k are called algebraic multiplicities. Generally, $\beta_k \geq 1 \Leftrightarrow \alpha_k \geq 1$ and $\alpha_k \geq \beta_k$. These relations between geometric and algebraic multiplicites allow the following configurations:

- If $\alpha_k = \beta_k = 1$, the corresponding eigenvalue s_k is said to be simple.
- If $\alpha_k = \beta_k > 1$, the corresponding eigenvalue s_k is said to be semisimple or degenerated.
- If $\alpha_k > \beta_k$, the corresponding eigenvalue s_k is said to be defective.

[2] It will turn out that for finite-dimensional $\mathscr{X}$, if $\mathbf{L}(s)$ is regular for at least one $s \in \mathbb{C}$, then $\mathbf{L}(s)$ is singular for a discrete set of complex values only.

[3] We omit an unimportant, constant scaling factor.

5.1.2 Spectral Theory

For finite-dimensional, polynomial, regular eigenvalue problems, the roots of the characteristic polynomial, i.e., the eigenvalues, form a discrete set. The set of eigenvalues is called the spectrum of the matrix polynomial,

$$\sigma(L) = \{s : \det(\mathbf{L}(s)) = 0\} = \{s_1, \cdots, s_K\}. \tag{5.3}$$

In this section, we discuss the properties of the spectrum. In particular, we exhibit in more detail the relation between geometric and algebraic multiplicities. Furthermore, we derive an expression for the **resolvent form** $\mathbf{L}(s)^{-1}$ in terms of eigenvalues and eigenvectors of the matrix polynomial. Most properties will be derived by reformulating a polynomial eigenvalue problem as a linear eigenvalue problem, using a linearization procedure.

Linearization

Let $\mathbf{L}(s)$ be a matrix polynomial of degree l on $\mathbb{C}^n$.

Definition 5.2. *Let* $\mathbf{E}(s)$, $\mathbf{F}(s)$ *be regular matrix polynomials on* $\mathbb{C}^{nl}$*, with constant determinants,* $\det(\mathbf{E}(s)) = E \neq 0$, $\det(\mathbf{F}(s)) = F \neq 0$[4]*. The pair* $(\mathbf{E}(s), \mathbf{F}(s))$ *is called a linearization of* $\mathbf{L}(s)$ *if [93]*

$$\mathbf{L}(s) \oplus \left(\oplus_{k=1}^{l-1} \mathbf{1}_{n\times n}\right) = \mathbf{E}(s)\,(\mathbf{A} - s\mathbf{1})\,\mathbf{F}(s) \tag{5.4}$$

As the name indicates, a linearization transforms a polynomial eigenvalue problem of degree l to a linear eigenvalue problem. However, while the original matrix polynomial acts on an n-dimensional linear space, the linearized polynomial acts on an nl-dimensional linear space.

From the range of linearizations [94, 95, 96], two are particularly important and are almost exclusively used in practice:

- Let

[4] Matrix polynomials with constant determinant are called unimodular.

$$\mathbf{E}(s) = \begin{pmatrix} B_{l-1} & -\mathbf{B}_{l-2} & \cdots & -\mathbf{B}_1 & -\mathbf{B}_0 \\ \mathbf{1} & 0 & \cdots & 0 & 0 \\ 0 & \mathbf{1} & \cdots & 0 & 0 \\ \vdots & \vdots & \ddots & \vdots & \vdots \\ 0 & 0 & \cdots & \mathbf{1} & 0 \end{pmatrix}$$

$$\mathbf{F}(s) = \begin{pmatrix} \mathbf{1} & 0 & 0 & \cdots & 0 \\ s\mathbf{1} & \mathbf{1} & 0 & \cdots & 0 \\ s^2\mathbf{1} & s\mathbf{1} & \mathbf{1} & \cdots & 0 \\ \vdots & \vdots & \vdots & \ddots & \vdots \\ s^{l-1}\mathbf{1} & s^{l-2}\mathbf{1} & s^{l-3}\mathbf{1} & \cdots & \mathbf{1} \end{pmatrix} \tag{5.5}$$

where $\mathbf{B}_k = \sum_{m=0}^{k} s^m \mathbf{A}_{l-k+m}$. The pair $\mathbf{E}(s), \mathbf{F}(s)$ is a linearization for $\mathbf{L}(s)$ with

$$\mathbf{A} = \mathbf{C}_1 = \begin{pmatrix} 0 & \mathbf{1} & 0 & \cdots & 0 \\ 0 & 0 & \mathbf{1} & \cdots & 0 \\ \vdots & \vdots & \vdots & \ddots & \vdots \\ 0 & 0 & 0 & \cdots & \mathbf{1} \\ -\mathbf{A}_l^{-1}\mathbf{A}_0 & -\mathbf{A}_l^{-1}\mathbf{A}_1 & -\mathbf{A}_l^{-1}\mathbf{A}_2 & \cdots & -\mathbf{A}_l^{-1}\mathbf{A}_{l-1} \end{pmatrix} \tag{5.6}$$

The linearization provided by $\mathbf{E}(s)$ and $\mathbf{F}(s)$ is called the first companion form. As $\mathbf{F}(s)$ can be easily inverted, the first companion form is especially suitable for the study of right-hand eigenvectors.

- Let

$$\mathbf{E}(s) = \begin{pmatrix} \mathbf{1} & s\mathbf{1} & s^2\mathbf{1} & \cdots & s^{l-1}\mathbf{1} \\ 0 & \mathbf{1} & s\mathbf{1} & \cdots & s^{l-2}\mathbf{1} \\ 0 & 0 & \mathbf{1} & \cdots & s^{l-3}\mathbf{1} \\ \vdots & \vdots & \vdots & \ddots & \vdots \\ 0 & 0 & 0 & \cdots & \mathbf{1} \end{pmatrix}$$

$$\mathbf{F}(s) = \begin{pmatrix} -\mathbf{B}_{l-1} & \mathbf{1} & 0 & \cdots & 0 \\ -\mathbf{B}_{l-2} & 0 & \mathbf{1} & \cdots & 0 \\ \vdots & \vdots & \vdots & \ddots & \vdots \\ -\mathbf{B}_1 & 0 & 0 & \cdots & \mathbf{1} \\ -\mathbf{B}_0 & 0 & 0 & \cdots & 0 \end{pmatrix} \tag{5.7}$$

where $\mathbf{B}_k$ is as defined above. The pair $\mathbf{E}(s), \mathbf{F}(s)$ is a linearization for $\mathbf{L}(s)$ with

$$\mathbf{A} = \mathbf{C}_2 = \begin{pmatrix} 0 & 0 & \cdots & 0 & -\mathbf{A_l}^{-1}\mathbf{A}_0 \\ \mathbf{1} & 0 & \cdots & 0 & -\mathbf{A}_1\mathbf{A_l}^{-1} \\ 0 & \mathbf{1} & \cdots & 0 & -\mathbf{A}_2\mathbf{A_l}^{-1} \\ \vdots & \vdots & \ddots & \vdots & \vdots \\ 0 & 0 & \cdots & \mathbf{1} & -\mathbf{A}_{l-1}\mathbf{A_l}^{-1} \end{pmatrix} \tag{5.8}$$

The linearization provided by $\mathbf{E}(s)$ and $\mathbf{F}(s)$ is called the second companion form. In this case, $\mathbf{E}(s)$ can be easily inverted, the second companion form is therefore especially suitable for the study of left-hand eigenvectors.

The matrices $\mathbf{C}_1$ and $\mathbf{C}_2$ are similar, $\mathbf{C}_2\mathbf{B} = \mathbf{B}\mathbf{C}_1$, with similarity transformation

$$\mathbf{B} = \begin{pmatrix} \mathbf{A}_1 & \mathbf{A}_2 & \cdots & \mathbf{A}_{l-1} & \mathbf{A}_l \\ \mathbf{A}_2 & \mathbf{A}_3 & \cdots & \mathbf{A}_l & 0 \\ \vdots & \vdots & \iddots & \vdots & \vdots \\ \mathbf{A}_{l-1} & \mathbf{A}_l & \cdots & 0 & 0 \\ \mathbf{A}_l & 0 & \cdots & 0 & 0 \end{pmatrix}. \tag{5.9}$$

Using a linearization, e.g. the first or second companion form, the polynomial eigenvalue problem is reduced to a standard eigenvalue problem. We can then borrow methods from the spectral theory of matrices. In particular, every matrix is similar to a matrix in Jordan normal form, i.e., there exists a Jordan matrix

$$\mathbf{J} = \oplus_{k=1}^{K} \mathbf{J}_k \qquad \mathbf{J}_k = \begin{pmatrix} \lambda_k & 1 & & & \\ & \lambda_k & 1 & & \\ & & \ddots & \ddots & \\ & & & \lambda_k & 1 \\ & & & & \lambda_k \end{pmatrix}, \tag{5.10}$$

and there exist matrices $\tilde{\mathbf{X}}$ and $\tilde{\mathbf{Y}}$ such that[5]

$$\mathbf{C}_1 = \tilde{\mathbf{X}}\mathbf{J}\tilde{\mathbf{X}}^{-1} \qquad \mathbf{C}_2 = \tilde{\mathbf{Y}}^{-1}\mathbf{J}\tilde{\mathbf{Y}}. \tag{5.11}$$

From the structure of $\mathbf{C}_1$ and $\mathbf{C}_2$, it can be concluded [93] that $\tilde{\mathbf{X}}$ and $\tilde{\mathbf{Y}}$ must be of the form

$$\tilde{\mathbf{X}} = \begin{pmatrix} \mathbf{X} \\ \mathbf{X}\mathbf{J} \\ \vdots \\ \mathbf{X}\mathbf{J}^{l-1} \end{pmatrix} \qquad \tilde{\mathbf{Y}} = \begin{pmatrix} \mathbf{Y}^{\dagger} & \mathbf{J}\mathbf{Y}^{\dagger} & \cdots & \mathbf{J}^{l-1}\mathbf{Y}^{\dagger} \end{pmatrix}, \tag{5.12}$$

and

$$\sum_{k=0}^{l} \mathbf{A}_k \mathbf{X} \mathbf{J}^k = 0 \qquad \sum_{k=0}^{l} \mathbf{J}^k \mathbf{Y}^{\dagger} \mathbf{A}_k = 0. \tag{5.13}$$

Furthermore, the similarity transformation $\mathbf{B}$ connecting $\mathbf{C}_1$ and $\mathbf{C}_2$ can be used to construct the relationship

$$\tilde{\mathbf{Y}}\mathbf{B}\tilde{\mathbf{X}} = \mathbf{1}_{nl \times nl}. \tag{5.14}$$

The triple $(\mathbf{X}, \mathbf{J}, \mathbf{Y})$ is called a canonical triple (or Jordan triple) for the matrix polynomial $\mathbf{L}(s)$.

[5] $\mathbf{C}_1$ and $\mathbf{C}_2$ are similar to the same Jordan matrix because they are similar according to (5.9).

Jordan Triples, Eigenvalues, and Eigenvectors

Consider a polynomial eigenvalue problem $\mathbf{L}(s)$ with canonical triple $(\mathbf{X}, \mathbf{J}, \mathbf{Y})$. The characteristic polynomial is given by

$$p(s) = \det(\mathbf{L}(s)) = \det(\mathbf{J} - s\mathbf{1}) = \prod_{k=1}^{K} \det(\mathbf{J}_k - s\mathbf{1}) = \prod_{k=1}^{K} (\lambda_k - s)^{\alpha_k}. \qquad (5.15)$$

The diagonal elements of the Jordan blocks, (5.10), are thus exactly the eigenvalues of the matrix polynomial $\mathbf{L}(s)$, $s_k = \lambda_k$. The sum of the sizes of all Jordan blocks with the same eigenvalue λ_k determines the algebraic multiplicity of the eigenvalue.

Furthermore, consider the columns $\left(\mathbf{x}_{k,1}, \mathbf{x}_{k,2}, \cdots, \mathbf{x}_{k,\alpha_k}\right)$ of $\mathbf{X}$ corresponding to the k-th Jordan block. It can be shown that [93]

$$\sum_{j=0}^{i} \frac{1}{j!} \frac{\mathrm{d}^j \mathbf{L}}{\mathrm{d}s^j}(s_k)\mathbf{x}_{i-j+1} = 0, \qquad i = 0, \cdots, \alpha_k - 1.$$

The series $\left(\mathbf{x}_{k,1}, \mathbf{x}_{k,2}, \cdots, \mathbf{x}_{k,\alpha_k}\right)$ forms a (right) Jordan chain of length α_k. In particular, $\mathbf{x}_{k,1}$ is a right eigenvector with eigenvalue s_k. Similarly, the corresponding series of columns $\left(\mathbf{y}_{k,\alpha_k}, \mathbf{y}_{k,\alpha_k-1}, \cdots, \mathbf{y}_k\right)$ of $\mathbf{Y}$ forms a left Jordan chain and $\mathbf{y}_{k,\alpha_k}$ is a left eigenvector with eigenvalue s_k.

If all Jordan chains have length 1, the matrix polynomial is called diagonalizable. In this case, the Jordan blocks $\mathbf{J}_k$ all have lenght 1, the Jordan matrix $\mathbf{J}$ is diagonal. However, diagonalizability cannot be assumed and has to be proven for a specific matrix polynomial.

The Resolvent Form

The inverse of a matrix polynomial, $\mathbf{L}(s)^{-1}$, is called the resolvent form for the matrix polynomial $\mathbf{L}(s)$. The resolvent form can only be defined for all complex values s which are not contained in the spectrum, $s \notin \sigma(\mathbf{L})$. The resolvent form is crucial for the analysis of many physical systems, as it is provides the response of the system to a general excitation. The resolvent form can be computed from a Jordan triple using the following theorem, [97],

Theorem 5.1. *Let* $\mathbf{L}(s)$ *be a matrix polynomial with invertible leading coefficient,* $(\mathbf{X},\mathbf{J},\mathbf{Y})$ *be its canonical triple. The resolvent form* $\mathbf{L}(s)^{-1}$ *is given by*

$$\mathbf{L}(s)^{-1} = \mathbf{X}(\mathbf{J}-s\mathbf{1})^{-1}\mathbf{Y}^{\dagger} \qquad \forall s \notin \sigma(\mathbf{L}). \tag{5.16}$$

The inverse Jordan matrix in (5.16) can be computed using

$$(\mathbf{J}-s\mathbf{1})^{-1} = \oplus_{k=1}^{K}(\mathbf{J}_k - s\mathbf{1})^{-1}.$$

In the important special case where the matrix polynomial is diagonalizable, the following relation holds

$$\mathbf{L}(s)^{-1} = \sum_{k=1}^{K} \frac{1}{s_k - s}\mathbf{x}_k\mathbf{y}_k^{\dagger}. \tag{5.17}$$

Stability

In Sect. 2.2 we introduced the Fourier transform, and specified transformations between frequency and time domain. With the change of variables $s \to \frac{\mathrm{d}}{\mathrm{d}t}$, $\mathbf{L}(\frac{\mathrm{d}}{\mathrm{d}t})$ can be viewed as l-th order system of ordinary differential equations in t. The general solution can be written in terms of the Jordan triple $(\mathbf{X},\mathbf{J},\mathbf{Y})$ by, [98],

$$f(t) = \mathbf{X}e^{\mathbf{J}t}f_0, \tag{5.18}$$

and f_0 is determined by the the initial condition at $t = 0$. More precisely, the Green's function for the differential operator $\mathbf{L}(\frac{\mathrm{d}}{\mathrm{d}t})$ is given by, [98],

$$G(t,t') = \mathbf{X}e^{\mathbf{J}(t-t')}\mathbf{Y}^{\dagger}. \tag{5.19}$$

A physical system is defined to be stable if the solution decays to zero, regardless of the initial configurations. It has been shown [98, 99] that the system is stable if and only if $\Re(s_k) < 0, \forall k$.

5.1.3 Special Matrix Polynomials

- A matrix polynomial $\mathbf{L}$ is self-adjoint with respect to a scalar product $\langle \circ, \circ \rangle$, if $\mathbf{L}(s)$ is self-adjoint for all $s \in \mathbb{R}$. In a basis which is orthonormal with respect to the scalar product, this is equivalent to the requirement that all coefficient matrices are hermitian, i.e., $\mathbf{A}_k = \mathbf{A}_k^\dagger$. If $\mathbf{x}$ is a right eigenvector of a self-adjoint matrix polynomial with eigenvalue s, then a left eigenvector with eigenvalue $\bar{s}$ is given by $\mathbf{y} = \lambda \mathbf{x}$ and λ is an arbitrary scaling parameter.

- A matrix polynomial $\mathbf{L}$ is real if $\mathbf{L}(s)$ is real for all $s \in \mathbb{R}$, i.e., if all coefficient matrices are real. If $\mathbf{x}, \mathbf{y}$ are right and left eigenvectors respectively with eigenvalue s, then $\bar{\mathbf{x}}, \bar{\mathbf{y}}$[6] are right and left eigenvectors respectively with eigenvalue $\bar{s}$.

- A matrix polynomial $\mathbf{L}$ is real symmetric if it is real and hermitian. From the properties of real and hermitian matrix polynomials, it follows that if $\mathbf{x}$ is a right eigenvector of a real symmetrix matrix polynomial with eigenvalue s, then a left eigenvector with eigenvalue s is given by $\mathbf{y} = \lambda \bar{\mathbf{x}}$ and λ is again an arbitrary scaling parameter.

5.1.4 Linear Matrix Polynomials

In the previous sections, we developed a spectral theory for matrix polynomials of arbitrary degree. In the following sections, we discuss the important special cases needed in this work, linear and quadratic matrix polynomials. The simplest nontrivial polynomial eigenvalue problem reads

$$\mathbf{A}\mathbf{x} = s\mathbf{x},$$

and is a special case of the theory developed above with $\mathbf{A}_0 = -\mathbf{A}$ and $\mathbf{A}_1 = \mathbf{1}$. We restrict our investigation to real symmetric matrices $\mathbf{A}$. Symmetric matrices are self-adjoint with respect to the standard real scalar product $\langle \circ, \circ \rangle : \langle \mathbf{x}, \mathbf{y} \rangle = \mathbf{x}^\mathrm{T} \mathbf{y}$. Then the following theorem holds, [100],

Theorem 5.2. *Let $\mathbf{A}$ be a real symmetric $n \times n$ matrix. Then the matrix polynomial $s\mathbf{1} - \mathbf{A}$ is diagonalizable. All eigenvalues and eigenvectors are real. The left eigenvectors are proportional to the right eigenvectors.*

[6] With $\bar{\mathbf{x}}$ we denote the vector where all vector entries are complex conjugated.

The proportionality can be expressed by a diagonal matrix $\Lambda = \mathrm{diag}(\lambda_1, \cdots, \lambda_n)$, $\mathbf{Y} = \mathbf{X}\Lambda$. Applying (5.14) with $\mathbf{A}_l = \mathbf{A}_1 = \mathbf{1}$ and $\mathbf{Y} = \mathbf{X}\Lambda$ yields

$$\mathbf{X}^{\mathrm{T}}\mathbf{Y} = \mathbf{X}^{\mathrm{T}}\mathbf{X}\Lambda = \mathbf{1},$$

i.e., the eigenvectors can be chosen orthogonal, $\langle \mathbf{x}_k, \mathbf{x}_l \rangle = \lambda_k^{-1}\delta_{kl}$.

More generally, we can consider the generalized linear eigenvalue problem

$$\mathbf{A}\mathbf{x} = s\mathbf{B}\mathbf{x}, \tag{5.20}$$

with complex $n \times n$ matrices $\mathbf{A}$ and $\mathbf{B}$. This corresponds to a polynomial eigenvalue problem with $\mathbf{A}_0 = -\mathbf{A}$, $\mathbf{A}_1 = \mathbf{B}$. Again, we restrict ourselves to real symmetric matrices $\mathbf{A}$ and $\mathbf{B}$. Furthermore, we require $\mathbf{B}$ to be positive definite, i.e., $\langle \mathbf{x}, \mathbf{B}\mathbf{x} \rangle \geq 0, \forall \mathbf{x} \neq 0$. In this case, a scalar product $\langle \circ, \circ \rangle_{\mathbf{B}} = \langle \circ, \mathbf{B}\circ \rangle$ can be defined. The generalized linear eigenvalue problem (5.20) can be transformed into a standard linear eigenvalue problem $\tilde{\mathbf{A}}\mathbf{x} = \mathbf{B}^{-1}\mathbf{A}\mathbf{x} = s\mathbf{x}$ and $\tilde{\mathbf{A}}$ is self-adjoint with respect to the scalar-product $\langle \circ, \circ \rangle_{\mathbf{B}}$. The following theorem is a generalization of results for standard linear eigenvalue problems:

Theorem 5.3. *Let* $\mathbf{A}$, $\mathbf{B}$ *be real symmetric* $n \times n$ *matrices,* $\mathbf{B}$ *be positive definite. Then, the matrix polynomial* $s\,\mathbf{B} - \mathbf{A}$ *is diagonalizable. All eigenvalues and eigenvectors are real. The left eigenvectors are proportional to the right eigenvectors.*

The spectral properties of generalized linear eigenvalue problems are thus very similar to the spectral properties of standard linear eigenvalue problems. The main difference is in the normalization condition: We again introduce a diagonal proportionality matrix $\Lambda = \mathrm{diag}(\lambda_1, \cdots, \lambda_n)$ such that $\mathbf{Y} = \mathbf{X}\Lambda$. Applying the normalization condition (5.14) yields

$$\mathbf{X}^{\mathrm{T}}\mathbf{B}\mathbf{Y} = \mathbf{X}^{\mathrm{T}}\mathbf{B}\mathbf{X}\Lambda = \mathbf{1}, \tag{5.21}$$

i.e., the eigenvectors can be chosen orthogonal with respect to the scalar product $\langle \circ, \circ \rangle_{\mathbf{B}}$, $\langle \mathbf{x}_k, \mathbf{x}_l \rangle_{\mathbf{B}} = \langle \mathbf{x}_k, \mathbf{B}\mathbf{x}_l \rangle = \lambda_k^{-1}\delta_{kl}$.

In both cases, the resolvent form of the matrix polynomial can be computed according to (5.16), which reads in the linear case

$$(\mathbf{A} - s\,\mathbf{B})^{-1} = \sum_{k=1}^{n} \frac{1}{s_k - s}\,\mathbf{x}_k\,\mathbf{y}_k^{\mathrm{T}} = \sum_{k=1}^{n} \frac{\lambda_k}{s_k - s}\,\mathbf{x}_k\,\mathbf{x}_k^{\mathrm{T}}. \tag{5.22}$$

5.1.5 Quadratic Matrix Polynomials

Let $\mathbf{A}_0$, $\mathbf{A}_1$, $\mathbf{A}_2$ be $n \times n$ matrices. We again restrict our analysis to real symmetric matrix polynomials, i.e., $\mathbf{A}_k$ is real symmetric for $k = 0, 1, 2$. The quadratic eigenvalue problem reads

$$\mathbf{A}_0 \mathbf{x} + s \mathbf{A}_1 \mathbf{x} + s^2 \mathbf{A}_2 \mathbf{x} = 0.$$

According to Sect. 5.1.3, the eigenvalues of a real symmetric matrix polynomial are real or come in complex conjugate pairs. If $\mathbf{x}$ is a right eigenvector with eigenvalue s, then the corresponding left eigenvector with eigenvalue s, is given by $\lambda \bar{\mathbf{x}}$ and λ is an arbitrary scaling coefficient.

Quadratic matrix polynomials with only real eigenvalues are called hyperbolic. It has been shown that all eigenvalues of hyperbolic polynomials are semisimple [99]. In particular, hyperbolic pencils are diagonalizable. Quadratic pencils with nonreal eigenvalues are called elliptic. The main difficulty in the spectral analysis of elliptic eigenvalue problems stems from the fact that the linearizations do not respect the symmetry of the problem. In general, the simple relationship $\mathbf{X}\Lambda = \mathbf{Y}$ between left and right eigenvectors has to be replaced by the more complicated relationship, [99],

$$\mathbf{Y} = \mathbf{X}\mathbf{P}\Lambda. \tag{5.23}$$

where $\mathbf{P}$ is a matrix of +1, -1, and 0, called the sign characteristic, [101]. The sign characteristic is an invariant of the matrix polynomial.

In the following, we restrict ourselves to the important special case of real symmetric matrix polynomials which are diagonalizable. In this case, the relation between left and right eigenvectors can be written as

$$\mathbf{Y} = \bar{\mathbf{X}}\Lambda,$$

and Λ is a diagonal proportionality matrix. Inserting this expression into the normalization condition (5.14) yields

$$\mathbf{1} = \mathbf{X}^{\mathrm{T}} \mathbf{A}_1 \mathbf{X} \Lambda + \mathbf{X}^{\mathrm{T}} \mathbf{A}_2 \mathbf{X} \Lambda \mathbf{J} + \mathbf{J} \mathbf{X}^{\mathrm{T}} \mathbf{A}_2 \mathbf{X} \Lambda. \tag{5.24}$$

For the individual generalized eigenvectors, this relationship reads

$$\mathbf{x}_k^{\mathrm{T}} \mathbf{A}_1 \mathbf{x}_l + 2 s_k \mathbf{x}_k^{\mathrm{T}} \mathbf{A}_2 \mathbf{x}_l = \lambda_k^{-1} \delta_{kl}. \tag{5.25}$$

With the normalization (5.24), the resolvent form reads

$$(\mathbf{A}_0 + s\,\mathbf{A}_1 + s^2\,\mathbf{A}_2)^{-1} = \sum_{k=1}^{2n} \frac{\lambda_k}{s_k - s}\,\mathbf{x}_k\,\mathbf{x}_k^{\mathrm{T}}. \tag{5.26}$$

5.1.6 Infinite Eigenvalues

In the previous sections, we always assumed that the leading coefficient $\mathbf{A}_l$ was regular. This will not always be the case for the physical systems discussed in this thesis. The properties of the spectrum in this case can best be explained when the reverse polynomial is introduced,

$$\mathscr{R}[\mathbf{L}](s) = s^l\,\mathbf{L}(\frac{1}{s}) = \sum_{k=0}^{l} s^l\,\mathbf{A}_{l-k} = \mathbf{A}_l + s\,\mathbf{A}_{l-1} + \cdots + s^l\,\mathbf{A}_0\,. \tag{5.27}$$

If $\mathbf{x}$ is an eigenvector of $\mathbf{L}(s)$ with eigenvalue $s \neq 0$, then it is also an eigenvector of $\mathscr{R}[\mathbf{L}](s)$ with eigenvalue $1/s$. As long as $\mathbf{A}_l$ is regular, there is no eigenvalue of $\mathscr{R}[\mathbf{L}](s)$ at $s = 0$. If $\mathbf{A}_l$ becomes singular, however, there are eigenvalues of $\mathscr{R}[\mathbf{L}]$ at $s = 0$. These eigenvalues formally corresponds to eigenvalues of $\mathbf{L}(s)$ at $s = \infty$, they are therefore called infinite eigenvalues.

Studying the spectral properties of polynomial eigenvalue problems with singular leading coefficient is simplified when the spectrum is broken into two parts: In order to determine the finite part of the spectrum, the original polynomial $\mathbf{L}(s)$ is studied with the methods developed in the previous sections. In order to determine the infinite part of the spectrum, the eigenvalues at 0 of the reverse polynomial are studied. More precisely, instead of one Jordan triple $(\mathbf{X}, \mathbf{J}, \mathbf{Y})$, there are two Jordan triples [102]

$$(\mathbf{X}_f, \mathbf{J}_f, \mathbf{Y}_f) \qquad (\mathbf{X}_\infty, \mathbf{J}_\infty, \mathbf{Y}_\infty), \tag{5.28}$$

such that $(\mathbf{X}_f, \mathbf{J}_f, \mathbf{Y}_f)$ comprises all Jordan blocks and associated vectors in $\mathbf{X}$ and $\mathbf{Y}$ corresponding to the finite eigenvalues of $\mathbf{L}$. On the other hand, $(\mathbf{X}_\infty, \mathbf{J}_\infty, \mathbf{Y}_\infty)$ comprises all Jordan blocks and associated vectors corresponding to zero eigenvalues of the reverse polynomial $\mathscr{R}\,\mathbf{L}$. In particular, $\mathbf{X}_\infty$ and $\mathbf{Y}_\infty$ satisfy the normalization condition

$$\left(\mathbf{Y}_\infty^\dagger, \cdots, \mathbf{J}_\infty^{l-1}\mathbf{Y}_\infty^\dagger\right) \cdot \begin{pmatrix} \mathbf{A}_{l-1} & \cdots & \mathbf{A}_0 \\ \vdots & \iddots & \vdots \\ \mathbf{A}_0 & \cdots & 0 \end{pmatrix} \cdot \begin{pmatrix} \mathbf{X}_\infty \\ \vdots \\ \mathbf{X}_\infty \mathbf{J}_\infty^{l-1} \end{pmatrix} = \mathbf{1}. \tag{5.29}$$

The resolvent form then consists of two contributions from the finite and infinite Jordan triples,

$$\mathbf{L}(s)^{-1} = \mathbf{X}_f \left(\mathbf{J}_f - s\mathbf{1}\right)^{-1} \mathbf{Y}_f^\dagger + \mathbf{X}_\infty \left(\mathbf{1} - s\,\mathbf{J}_\infty\right)^{-1} \mathbf{Y}_\infty^\dagger . \tag{5.30}$$

In the important special case of a diagonalizable matrix polynomial, this result reads

$$\mathbf{L}(s)^{-1} = \sum_{k=1}^{m} \frac{1}{s_k - s}\, \mathbf{x}_{f,k}\, \mathbf{y}_{f,k}^\dagger + \sum_{k=1}^{nl-m} \mathbf{x}_{\infty,k}\, \mathbf{y}_{\infty,k}^\dagger . \tag{5.31}$$

The infinite eigenmodes lead to an offset of the resolvent form without changing the structure. If, e.g., the resolvent form has a physical meaning as transfer function of an electrical circuit, this offset corresponds to a correction of the values for inductance at low frequencies.

5.2 Numerical Solution of Eigenvalue Problems

For the analysis of the spectral properties of practical matrix polynomials, e.g., polynomials arising from the discretization of electromagnetic field problem, a numerical approach is the only feasible way due to the large size of the matrices. Even though there exist algorithms to compute the Jordan normal form for matrices, [103], or algorithms for the computation of the Jordan canonical form of matrix polynomials, [104], the numerical computation of the Jordan form is in general not feasible. It can be shown analytically that the Jordan matrix depends discontinuously on the original matrix, [105], the conditioning of the numerical problem can be very bad.

In this thesis, we therefore restrict ourselves to diagonalizable matrix polynomials. Computing the Jordan normal form is then equivalent to computing numerically the eigenvectors and eigenvalues of a large matrix. For this problem, fast and powerful algorithms exist and will be explained below. The set of algorithms can be divided into two large groups, designed for specific eigenvalue problems:

- The first group of algorithms computes all eigenvalues and corresponding eigenvectors for a given matrix. Such algorithms are generally called direct eigenvalue solvers. As the eigenvectors of sparse matrices are in general dense, these algorithms can be used for small to medium size matrices only due to memory restrictions.

- The second group of algorithms computes few eigenvalues and corresponding eigenvectors for large matrices, which are typically sparse. Most algorithms in the this group compute eigenvalues iteratively according to a projection procedure, i.e., the matrix is projected onto a suitably constructed sub-vector space which contains the eigenvectors.

It has to be noted, that most algorithms in the second group do not actually solve the eigenvalue problem. Instead, by means of projection they reduce a large-scale eigenvalue problem to a small-scale eigenvalue problem which can be solved with a direct solver.

5.2.1 Direct Solvers

One of the most widely used direct algorithm is the QR algorithm, [106]. In order to compute the eigenvalues and eigenvectors of a matrix $\mathbf{A}$, a series of matrices $\mathbf{A}_0, \mathbf{A}_1, \mathbf{A}_2, \cdots$ is defined iteratively. In the k-th step, the QR decomposition of the k-th matrix is computed, $\mathbf{A}_k = \mathbf{Q}_k \mathbf{R}_k$, where $\mathbf{Q}_k$ is an orthogonal matrix and $\mathbf{R}_k$ is an upper triangular matrix. The series of matrices $\mathbf{A}_k$ then converges towards a triangular matrix with the eigenvalues on the diagonal [107].

The classical implementation for symmetric matrices can be improved considerably, if the matrix $\mathbf{A}$ is transformed to tridiagonal form[7] prior to starting the QR algorithm. In the classical algorithm, computing the QR decomposition in each step requires $\mathcal{O}(n^3)$ operations. Computing the QR decomposition of a tridiagonal matrix requires only $\mathcal{O}(n)$ operations. Another $\mathcal{O}(n^3)$ operations for tridiagonalization have to be spent only once, [108].

Furthermore, the convergence rate of the classical QR algorithm can be increased significantly if the definition of the matrix $\mathbf{A}_k$ takes into account approximate information about the eigenvalues which can be computed from the not yet converged matrix $\mathbf{A}_{k-1}$. Such adaptions of the classical QR algorithm are called shifted QR algorithms, e.g., [109, 110].

[7] More generally, a matrix can be transformed to Hessenberg form. The Hessenberg form for symmetric matrices is a tridiagonal matrix.

In this work, we use the Lanczos procedure described in 5.2.3 in order to project a large-dimensional eigenvalue on a low-dimensional eigenvalue problem. The low-dimensional eigenvalue problem is then solved using an implementation of the QR algorithm in LAPACK, [111]: First we use the routine *xgehrd* in order to transform a symmetric matrix to tridiagonal form. We then use the routine *xhseqr* in order to compute the eigenvalues of the tridiagonal matrix using a multi-shift QR algorithm.

5.2.2 Iterative Solvers

For large eigenvalue problems, computing all eigenvalues and associated eigenvectors becomes prohibitively expensive. Fortunately, in practice, only few of the eigenvalues and eigenvectors are needed. Such eigenvalue problems can be solved very efficiently in an iterative way.

For purposes of illustration, consider the standard eigenvalue problem $\mathbf{A}\,\mathbf{x} = s\,\mathbf{x}, \mathbf{x} \in \mathbb{C}^n$. Further consider an m-dimensional subspace $V \subset \mathbb{C}^n$. Any vector $\mathbf{y} \in V$ can be written

$$\mathbf{y} = \mathbf{V}\tilde{\mathbf{y}},$$

where $\tilde{\mathbf{y}} \in \mathbb{C}^m$ and the columns of $\mathbf{V}$ are basis vectors for V. An eigenvector $\mathbf{x}$ of $\mathbf{A}$ with eigenvalue s is contained in the subspace if there exists $\tilde{\mathbf{x}} \in \mathbb{C}^m$ such that

$$(\mathbf{AV})\,\tilde{\mathbf{x}} = s\mathbf{V}\tilde{\mathbf{x}}. \tag{5.32}$$

The eigenvector $\mathbf{x}$ is then given by $\mathbf{x} = \tilde{\mathbf{V}}\tilde{\mathbf{x}}$. In general, it is impossible to construct a subspace which contains the eigenvector exactly. Instead, the iterative projection methods generate a series of subspaces $V_1, V_2, \cdots$ such that each subspace contains a better approximation of the eigenvector than the previous subspaces. In this case, for all subspaces V_k the projected eigenvalue equation (5.32) is over-determined and cannot be solved exactly. In order to render (5.32) regular, a testing scheme has to be applied, i.e., the solution is also restricted to an m-dimensional subspace W. Eq. (5.32) then reads

$$\left(\mathbf{W}^{\mathrm{T}}\mathbf{AV}\right)\tilde{\mathbf{x}} = \tilde{s}\mathbf{W}^{\mathrm{T}}\mathbf{V}\tilde{\mathbf{x}}. \tag{5.33}$$

where the columns of $\mathbf{W}$ form a basis for W. The simplest choice $W = V$ corresponds to the Galerkin scheme familiar to us from the discretization of partial differential equations in Chap. 4. The projection procedure is then called the

Rayleigh-Ritz procedure. An eigenvalue $\tilde{s}$ of (5.33) is called a Ritz value, an eigenvector $\tilde{\mathbf{x}}$ is called a Ritz vector. Due to the low dimension of the projected eigenvalue problem in (5.33), the Ritz values and Ritz vectors can be computed using a direct method.

A priori, the Ritz values and Ritz vectors are not related to the eigenvalues and eigenvectors of the original problem. However, for suitably chosen subspaces V, the Ritz values and Ritz vectors can be shown to be good approximations for the eigenvalues and eigenvectors of the original problem. An efficient iterative projection method is capable of constructing very low-dimensional subspaces V which nevertheless contain good approximations of the eigenvalues and eigenvectors of the original problem. One such method will be presented in the following section.

5.2.3 The Lanczos Method for Eigenmode Computation

The Lanczos method for the solution of generalized eigenvalue problems is one of the most important iterative projection techniques. The subspace V used for the projection is chosen equal to a Krylov space, [112]:

$$V_k = \mathscr{K}_k(\mathbf{A}, \mathbf{x}) = \text{span}(\mathbf{x}, \mathbf{A}\,\mathbf{x}, \mathbf{A}^2\,\mathbf{x}, \cdots, \mathbf{A}^{k-1}\,\mathbf{x}). \tag{5.34}$$

The Krylov method can therefore be seen as a generalization of the power iteration method, [105], where $V_k = \text{span}(\mathbf{A}^{k-1}\,\mathbf{x})$. It is well known that the power iteration method converges to the subspace spanned by the eigenvector with largest absolute eigenvalue. Similarly, the Lanczos method produces good approximations of eigenvalues at either end of the spectrum within few iterations. Such eigenvalues are called exterior eigenvalues. On the other hand, many iterations are necessary to produce good approximations of interior eigenvalues, [105].

In this section, we restrict ourselves to linear, real symmetric eigenvalue problems. The Lanczos method can also be generalized to non-symmetric (or, more generally, non-hermitian eigenvalue problems). It is then called the Arnoldi method [113]. Eigenvalue problems of higher degree (e.g., quadratic eigenvalue problems) can be solved using the linearization procedure shown in Sect. 5.1.2.

The Lanczos Algorithm for Standard Eigenvalue Problems

With the specification of the projection space V_k in the previous section, the projection method is in principle fully defined. However, it remains to specify a basis for the projection space which makes the method as numerically stable as possible and at the same time allows for an efficient implementation.

In practice, each Lanczos iteration produces one more basis vector for the projection space, thereby increasing the dimension of the projection space by one. In order to minimize the effect of rounding errors, it is advisable to orthonormalize each new basis vector with respect to all previous basis vectors using the modified Gram-Schmidt procedure. One nice feature about the Lanczos method is that due to the construction of the projection space as a Krylov space, each new Lanczos basis vector has to be orthogonalized with respect to the two previous basis vectors only. It is orthogonal to all previous basis vectors by construction, [105].

Furthermore, instead of explicitly projecting the eigenvalue problem onto the Krylov space, the projected eigenvalue problem can be constructed implicitely during the orthonormalization process. In particular, if the basis vectors are computed

as described above, the projected eigenvalue problem consists of computing the eigenvalues of a tridiagonal matrix.

Plugging everything together, the Lanczos algorithm in each step computes a matrix A_k corresponding to the projection of the original matrix $\mathbf{A}$ on the Krylov space of degree k. The convergence of the Ritz values of the projected matrix is monitored and the iteration is stopped when a satisfying accuracy is reached.

Algorithm 5.1. *The Lanczos Method for Hermitian Eigenvalue Problems*
Input: *Matrix* $\mathbf{A}$*, Initial Vector* $\mathbf{x}$*, Maximum Number of Iterations* N

$\mathbf{x}_1 = \mathbf{x}, o_1 = \sqrt{\mathbf{x}_1^\dagger \mathbf{x}_1}$
for $k = 1 : N$ ***do***
  $\mathbf{x}_k = \mathbf{x}_k / o_k$
  $\mathbf{x}_{k+1} = \mathbf{A}\mathbf{x}_k$
  $\mathbf{x}_{k+1} = \mathbf{x}_{k+1} - o_k \mathbf{x}_k$
  $d_k = \mathbf{x}_k^\dagger \mathbf{x}_{k+1}$
  $o_{k+1} = \sqrt{\mathbf{x}_{k+1}^\dagger \mathbf{x}_{k+1}}$
  Construct projected matrix:

$$\mathbf{A}_k = \begin{pmatrix} d_1 & o_2 & 0 & \cdots & 0 \\ o_2 & d_2 & o_3 & \cdots & 0 \\ \vdots & \vdots & \vdots & \ddots & \vdots \\ 0 & 0 & 0 & \cdots & d_k \end{pmatrix}$$

  Compute Ritz values $\tilde{s}_l$ *and Ritz vectors* $\tilde{\mathbf{x}}_l$
  if *Converged* ***then***
    Break
  end if
end for
Compute eigenvalues and eigenvectors of original problem:
$s = \tilde{s}$, $\mathbf{x} = \mathbf{V}\tilde{\mathbf{x}}$

The Lanczos Algorithm for Generalized Hermitian Eigenvalue Problems

In this work, instead of the standard eigenvalue problem, we usually have to deal with generalized linear eigenvalue problems, $\mathbf{A}\mathbf{x} = s\,\mathbf{B}\mathbf{x}$. We restrict ourselves to real symmetric (or, more generally, hermitian) eigenvalue problems. The spectral properties of the generalized eigenvalue problem in comparison to the standard eigenvalue problem are discussed in detail in Sect. 5.1.4. In particular, it is shown that when the generalized eigenvalue is reformulated as a standard eigenvalue

problem, $\mathbf{B}^{-1}\mathbf{A}\mathbf{x} = s\,\mathbf{x}$, the matrix $\mathbf{B}^{-1}\mathbf{A}$ is self-adjoint with respect to the scalar product defined by B, $\langle \mathbf{x}, \mathbf{y} \rangle_{\mathbf{B}} = \langle \mathbf{x}, \mathbf{B}\mathbf{y} \rangle$. In order to apply the Lanczos algorithm to generalized linear eigenvalue problems, we therefore only have to replace $\mathbf{A}$ by $\mathbf{B}^{-1}\mathbf{A}$ and the standard inner product $\langle \circ, \circ \rangle$ by the $\mathbf{B}$ inner product $\langle \circ, \circ \rangle_{\mathbf{B}}$:

Algorithm 5.2. *The Lanczos Method for Hermitian Eigenvalue Problems*

Input: *Matrices* $\mathbf{A}$, $\mathbf{B}$, *Initial Vector* $\mathbf{x}$, *Maximum Number of Iterations* N

$\mathbf{x}_1 = \mathbf{x}, \mathbf{y}_1 = \mathbf{B}\,\mathbf{x}_1, o_1 = \sqrt{\mathbf{x}_1^\dagger\,\mathbf{y}_1}$

for $k = 1 : N$ ***do***

$\mathbf{x}_k = \mathbf{x}_k\,/o_k, \mathbf{y}_k = \mathbf{y}_k\,/o_k$

$\mathbf{y}_{k+1} = \mathbf{A}\,\mathbf{y}_k$

$\mathbf{y}_{k+1} = \mathbf{y}_{k+1} - o_k\,\mathbf{y}_k$

$d_k = \mathbf{x}_k^\dagger\,\mathbf{y}_{k+1}$

$x_{k+1} = \mathbf{B}^{-1}\,\mathbf{y}_{k+1}$

$o_{k+1} = \sqrt{\mathbf{x}_{k+1}^\dagger\,\mathbf{y}_{k+1}}$

Construct projected matrix:

$$\mathbf{A}_k = \begin{pmatrix} d_1 & o_2 & 0 & \cdots & 0 \\ o_2 & d_2 & o_3 & \cdots & 0 \\ \vdots & \vdots & \vdots & \ddots & \vdots \\ 0 & 0 & 0 & \cdots & d_k \end{pmatrix}$$

Compute Ritz values $\tilde{s}_l$ *and Ritz vectors* $\tilde{\mathbf{x}}_l$

if *Converged* ***then***

Break

end if

end for

Compute eigenvalues and eigenvectors of original problem:

$s = \tilde{s},\ \mathbf{x} = \mathbf{V}\,\tilde{\mathbf{x}}$

Block Lanczos Algorithm

In the previous versions of the Lanczos algorithm, the Krylov spaces were built from one single starting vector. This leads to poor convergence when searching for closely clustered eigenvalues [114]. Even worse, if there are multiple eigenvectors with the same eigenvalue, only one of them will be found by the Lanczos procedure.

All above mentioned problems can be solved by initializing the Lanczos procedure with multiple starting vectors instead of a single starting vector [114, 115]. The standard Lanczos procedure has to be altered in the following way:

- In each Krylov iteration, instead of a single new Krylov vector, a block of new Krylov vectors is generated.
- Instead of orthonormalizing the new Krylov vector with respect to the two previous Krylov vectors, each new Krylov vector has to be orthonormalized with respect to the two previous blocks of Krylov vectors.
- When the matrix is projected onto the block Krylov space, the resulting matrix is no longer tridiagonal. Instead, it is block tridiagonal and the lengths of the blocks are equal to the Krylov block sizes.
- The standard Krylov method breaks down when the new Krylov vector is linearly dependent to the already existing Krylov space. In this case, the Krylov sequence is exhausted. In the block Lanczos method, when only one new Krylov vector is linearly dependent, the Krylov iterations can continue. However, the linearly dependent Krylov vector has to be removed from the Krylov space. This process is called deflation, [105].
- When deflation occurs, the block tridiagonal form of the projected matrix is destroyed by the appearence of fully populated rows and columns corresponding to the last linearly independent Krylov vector in the Krylov sequence, [105].

Orthonormalization Schemes

In the standard Lanczos algorithm, a new Krylov vector is only orthonormalized with respect to the previous two Krylov vectors (or blocks of Krylov vectors for the block Lanczos procedure). By construction, the new Krylov vector is already orthogonal to all previous Krylov vectors. However, this analytical result holds true for infinite arithmetic only. Numerically, there is an increasing loss of orthogonality between new Krylov vectors and old Krylov vectors, i.e., new Krylov vectors are orthogonal to the newer Krylov vectors only, while orthogonality may be lost completely with respect to very old Krylov vectors, [116]. Even worse, as soon as an eigenpair has converged, numerical perturbations will tilt the new Krylov vectors in the direction of the converged eigenvector, leading to the multiple appearence of the same eigenvalue and eigenvector, [117].

The simplest solution is to perform in each step a full reorthonormalization, [105]. The modified algorithm can be implemented with minor changes to the original algorithm, however, as the workload increases quadratically with the number

of Krylov vectors, it is practical for small Krylov spaces only. An more efficient alternative is provided by selective reorthonormalization schemes, [118, 119], where the new Krylov vector is orthonormalized with respect to selected Krylov vectors only.

Finally, it is also possible to allow orthonormality to be lost and to remove duplicate copies of the eigenvectors by analysing the spectral properties of the projected matrix, [120].

In this work, we use the full reorthonormalization scheme in combination with a restart scheme (see below) in order to keep the size of the Krylov space small.

Restarts

The numerical experience with the Lanczos method shows that the total number of Krylov vectors is generally much larger than the number of converged eigenvectors. Hoewever, large Krylov spaces are undesirable due to memory requirements, excessive computational loss and the loss of orthogonality in long Krylov iterations.

This numerical experience can be understood from the fact that the initial vector is in general a linear combination of many eigenvectors from all parts of the spectrum and (in infinite precision) the Krylov iteration will not stop until all eigenvectors present in the start vectors have been recovered. In practical situations, however, we are interested in few eigenvectors from a small part of the spectrum only. Ideally, the initial vector should thus be a linear combination of the the good eigenvectors, i.e., the eigenvectors of interest, only.

It is impossible in general to construct such an initial vector. However, it is possile to compute a crude approximation of these eigenvectors by a few steps of the Lanczos procedure and construct the initial vector of a new Krylov space from the crude approximations. In other words, after a few Krylov iterations, all unwanted Ritz vectors are discarded from the Krylov space and a new initial vector is constructed from the remaining Ritz vectors, [105, 121]. Because the Lanczos procedure is started several times with different start vectors, it is called restarted Lanczos method. In this work, a block variant of the simple explicit restart scheme is employed. Instead of a single restart vector, all Ritz vectors which are in the desired part of the spectrum are used for the restart.

A more sophisticated technique for the restart of the Lanczos procedure is given by implicit restart schemes, [122, 123]. In the implicit restart schemes, the shifted QR iteration is used to discard the bad part of the Ritz spectrum and compress the

good part of the Ritz spectrum in a smaller subspace. Another more recent technique for the implicit restart of the Lanczos method is called thick restarts, [124]. In the thick restart technique, the set of Ritz vectors is also divided into wanted and unwanted Ritz vectors. The unwanted Ritz vectors are discarded. Instead of using the wanted Ritz vectors as initialization for a new Lanczos run, the Krylov space is built on top of the existing Ritz vectors.

Shift-and-Invert Lanczos

The Lanczos method provides fast convergence to exterior eigenvalues whereas convergence to interior eigenvalues is very slow. In particular, it is impossible to directly compute all eigenvalues within a certain part of the spectrum. However, using suitable spectral transformations, this part of the spectrum can be turned inside out, i.e., interior eigenvalues can be made exterior eigenvalues.

More precisely, consider a matrix $\mathbf{A}$ with spectrum S. Imagine that we want to compute all eigenvalues in the spectral region nearest to s_0. Now consider the matrix

$$\tilde{\mathbf{A}} = (\mathbf{A} - s_0\mathbf{1})^{-1}$$

It can be shown, [105], that if $\mathbf{x}$ is an eigenvector of $\tilde{\mathbf{A}}$ with eigenvalue $1/(s-s_0)$, then $\mathbf{x}$ is an eigenvector of $\mathbf{A}$ with eigenvalue s. In other words, the eigenvalues of $\mathbf{A}$ nearest to s_0 are exactly the exterior eigenvalues of $\tilde{\mathbf{A}}$. Instead of starting the Lanczos iterations with the matrix $\mathbf{A}$, convergence can be sped up by starting the Lanczos iterations with the matrix $\tilde{\mathbf{A}} = (\mathbf{A} - s_0\mathbf{1})^{-1}$. The resulting variant of the Lanczos algorithm is called Shift-and-Invert Lanczos (SI Lanczos).

The SI Lanczos method allows to compute selected interior eigenvalues. For generalized eigenvalue problems, a matrix inversion is needed in any case and the numerical workload does not increase. A staggered procedure for the computation of interior eigenvalues is shown in [125]. Instead of directly applying the SI Lanczos procedure, the matrix is first projected on a very large Krylov space using the standard Lanczos method. The SI Lanczos algorithm is then applied in order to compute interior eigenvalues of the reduced matrix. This procedure removes the need to directly invert a very large matrix.

6 A Method for the Automated Construction of Equivalent Electrical Circuit Models

In the previous chapters, we showed two different models for electromagnetic systems: a description in terms of electrical circuits (Chap. 2) and a description in terms of electromagnetic fields (Chap. 3). In this chapter, we discuss in detail the connection of the two models. The discussion in this chapter leads to a very natural and general procedure for the construction of electrical circuit models.

In order to construct electrical circuit models, three basic questions have to be answered. The questions will be discussed and answered in Sect. 6.1-6.3 respectively:

1. *What information is needed in order to construct unique, physical electrical circuit models for an electromagnetic component or system?*
2. *How can this information be obtained?*
3. *How does the information have to be used in order to construct the electrical circuit model?*

Having answered the three questions, we propose a procedure for the automated construction of physical equivalent electrical circuits in Sect. 6.4. We compare the procedure with existing techniques, such as the PEEC method. We discuss in detail the properties of the electrical circuits generated by our procedure, especially the size of the circuit model and its accuracy.

6.1 Information for the Construction of Electrical Circuit Models

In this section we discuss the minimal information needed for the construction of an electrical circuit model. More precisely, we discuss how an electrical circuit can be constructed from a given impedance function and how much information is needed for this circuit to be unique. The choice to construct an electrical circuit from an impedance function is motivated by the fact that characterization of an electromagnetic component or system in terms of the impedance function is a very general concept which has been formulated for many different models, most importantly, electrical circuit models and field-theoretical models, and by the fact that the impedance function is a physically well-defined quantity, i.e., it is in principle also accessible in measurements.

In general, the impedance function of an electrical circuit model is a function of the complex frequency s and can be written in the form of a rational function

$$\mathbf{Z} = \sum_{k=1}^{n} \frac{1}{s_k - s} \mathbf{Z}^{(k)}. \tag{6.1}$$

The $\mathbf{Z}$ matrix stores all impedance functions in matrix form. Eq. (6.1) will be discussed in more detail in Sect. 6.1.1. At present, it is important to note only that the impedance function is fully characterized if the pole frequencies s_k and the residues of the poles $\mathbf{Z}^{(k)}$ are known.

6.1.1 Eigenmode Analysis of Electrical Circuits

In Sect. 2.3 we introduced electrical circuits and expressed the impedance function in terms of circuit matrices (2.33),

$$\mathbf{Z} = -s\,\mathbf{A}_s^{\mathrm{T}} \left(\underbrace{\mathbf{A}_L\,\mathbf{L}^{-1}\,\mathbf{A}_L^{\mathrm{T}}}_{\widehat{\mathbf{L}^{-1}}} + s \underbrace{\mathbf{A}_R^{-1}\,\mathbf{R}^{-1}\,\mathbf{A}_R^{\mathrm{T}}}_{\widehat{\mathbf{G}}} + s^2 \underbrace{\mathbf{A}_C\,\mathbf{C}\,\mathbf{A}_C^{\mathrm{T}}}_{\widehat{\mathbf{C}}} \right)^{-1} \mathbf{A}_s\,. \tag{6.2}$$

The $\mathbf{A}_s, \mathbf{A}_L, \mathbf{A}_R, \mathbf{A}_C$ matrices are the node incidence matrices of the source, inductive, resistive and capacitive networks respectively. They describe the topology of the electrical circuit. The circuit element matrices $\mathbf{L}, \mathbf{R}, \mathbf{C}$ contain the circuit element values. The circuit matrices $\widehat{\mathbf{L}^{-1}}, \widehat{\mathbf{G}}, \widehat{\mathbf{C}}$ have the following important properties

- They are real, symmetric and independent from s.
- They are positive (semi-) definite. More precisely, the dimensions of the null spaces of the $\widehat{\mathbf{L}^{-1}}, \widehat{\mathbf{G}}, \widehat{\mathbf{C}}$ are equal to the dimensions of the null spaces of $\mathbf{A}_L, \mathbf{A}_R, \mathbf{A}_C$ matrices. The null spaces of the node incidence matrices are equal to the numbers of unconnected subgraphs of the inductive, resistive, and capacitive networks respectively.
- For a simple electrical circuit without mutual inductances, the circuit matrices are illustrated in Fig. 6.1

We are now going to apply the spectral theory derived in Chapter 5 in order to obtain an explicit expression for the frequency-dependent impedance. Consider only the inner part, $\left(\widehat{\mathbf{L}^{-1}} + s\,\widehat{\mathbf{G}} + s^2\,\widehat{\mathbf{C}}\right)^{-1}$. This part really is the resolvent form of a

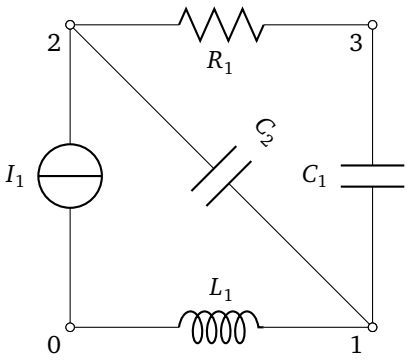

$$\mathbf{A}_s^{\mathrm{T}} = \begin{pmatrix} 0 & 1 & 0 \end{pmatrix}$$
$$\mathbf{A}_L^{\mathrm{T}} = \begin{pmatrix} 1 & 0 & 0 \end{pmatrix}$$
$$\mathbf{A}_R^{\mathrm{T}} = \begin{pmatrix} 0 & 1 & -1 \end{pmatrix}$$
$$\mathbf{A}_C^{\mathrm{T}} = \begin{pmatrix} -1 & 0 & 1 \\ 1 & -1 & 0 \end{pmatrix}$$

$$\widehat{\mathbf{L}^{-1}} = \begin{pmatrix} \frac{1}{L_1} & 0 & 0 \\ 0 & 0 & 0 \\ 0 & 0 & 0 \end{pmatrix} \quad \widehat{\mathbf{G}} = \begin{pmatrix} 0 & 0 & 0 \\ 0 & \frac{1}{R_1} & -\frac{1}{R_1} \\ 0 & -\frac{1}{R_1} & \frac{1}{R_1} \end{pmatrix} \quad \widehat{\mathbf{C}} = \begin{pmatrix} C1+C2 & -C_2 & -C_1 \\ -C_2 & C_2 & 0 \\ -C_1 & 0 & C_1 \end{pmatrix}$$

Figure 6.1.: Circuit matrices for exemplary electrical circuit

real symmetric quadratic matrix polynomial. Such polynomials are discussed in detail in Sect. 5.1.5. In particular, we showed that the resolvent form can be written in terms of eigenvectors Φ_k of the matrix polynomial as

$$\left(\widehat{\mathbf{L}^{-1}} + s\,\widehat{\mathbf{G}} + s^2\,\widehat{\mathbf{C}}\right)^{-1} = \sum_{k=1}^{2n} \frac{\lambda_k}{s_k - s} \Phi_k \Phi_k^{\mathrm{T}}. \tag{6.3}$$

This representation of the impedance function already explains (6.1). In the following sections, we discuss in greater detail the spectral properties of this matrix polynomial and develop a physical interpretation of its eigenvalues and eigenvectors.

Eigenfrequencies

Let s be a (complex) eigenfrequency, let Φ be the corresponding eigenvector. In Sect. 5.1.3, we showed that a real matrix polynomial has eigenvalues which are either real or come in complex pairs. It follows that the eigenfrequencies of an electrical circuit are either real or form complex conjugate pairs. Furthermore, let Φ be an eigenmode with eigenfrequencies s. The real numbers $l^{-1} = \Phi^\dagger \widehat{\mathbf{L}^{-1}} \Phi$, $r^{-1} = \Phi^\dagger \widehat{\mathbf{G}} \Phi$, $c = \Phi^\dagger \widehat{\mathbf{C}} \Phi$ are all non-negative due to the positive semi-definiteness

of the circuit matrices. From the matrix polynomial, the following relationship can be established:

$$0 = \Phi^\dagger \left(\widehat{\mathbf{L}^{-1}} + s\,\widehat{\mathbf{G}} + s^2\,\widehat{\mathbf{C}} \right) \Phi = l^{-1} + sr^{-1} + s^2 c. \tag{6.4}$$

This second order equation for the eigenfrequency is solved by

$$s = -\frac{1}{2rc} \pm \sqrt{\frac{1}{4(rc)^2} - \frac{1}{lc}}. \tag{6.5}$$

In general, only one of the two solutions is an eigenfrequency, [99]. The important point, however, is that either solution for the (complex) eigenfrequency s has a negative real part, $\Re(s) < 0$. In particular, it follows that electrical circuits are stable according to the analysis in Sect. 2.2.

Eigenmodes

In Sect. 2.3.3 we showed that the matrix polynomial acts on a space $\mathbb{C}^n$ which describes the node potentials Φ. An eigenmode Φ_k associated to an eigenfrequency s_k describes the node potentials of an eigenmode, i.e., in a state of resonance. From the node potentials, all information about edge voltages and edge currents can be computed using the node incidence matrices and the constitutive equations.

The normalization of an eigenvector Φ_k is a priori arbitrary. For the formulation of the resolvent form, an additional normalization coefficient λ_k is needed, see (5.24). Let Φ_k, Φ_l be eigenmodes with corresponding eigenfrequencies s_k, s_l. Then

$$\delta_{kl}\lambda_k^{-1} = \langle \Phi_k, \widehat{\mathbf{G}}\,\Phi_l + 2s_k\,\widehat{\mathbf{C}}\,\Phi_l \rangle = \Phi_k^{\mathrm{T}}\,\widehat{\mathbf{G}}\,\Phi_l + 2s_k \Phi_k^{\mathrm{T}}\,\widehat{\mathbf{C}}\,\Phi_l. \tag{6.6}$$

In order to rewrite the normalization in a more intuitive form, we reconsider the expressions for the resistive losses, (2.28), and the capacitive energy, (2.30). The total Ohmic losses and the total capacitive energy can be decomposed into contributions which are due to the eigenmodes,

$$P_{kl} = \Phi_k^{\mathrm{T}}\,\widehat{\mathbf{G}}\,\Phi_l \tag{6.7}$$

$$E_{C,kl} = \Phi_k^{\mathrm{T}}\,\widehat{\mathbf{C}}\,\Phi_l. \tag{6.8}$$

With this definitions, the normalization can be expressed in terms of the Ohmic losses P_{kl} and the change in capacitive energy $sE_{C,kl}$ by

$$\delta_{kl}\lambda_k^{-1} = P_{kl} + 2s_k E_{C,kl}. \tag{6.9}$$

The unit of the normalization coefficient λ is accordingly given by $[\lambda^{-1}] = 1\,\mathrm{V\,A}$.

Impedance Function

Using (5.26) to express the resolvent form in terms of eigenvectors, the impedance function for an electrical circuit can be computed by

$$\mathbf{Z}(s) = -s\,\mathbf{A}_s^{\mathrm{T}}\left(\widehat{\mathbf{L}^{-1}} + s\,\widehat{\mathbf{G}} + s^2\,\widehat{\mathbf{C}}\right)^{-1}\mathbf{A}_s = -s\,\mathbf{A}_s^{\mathrm{T}}\left[\sum_{k=1}^{2n}\frac{\lambda_k}{s_k - s}\Phi_k\Phi_k^{\mathrm{T}}\right]\mathbf{A}_s\,. \tag{6.10}$$

Checking the units yields $[Z] = [s][\lambda][\Phi]^2/[s] = 1\,\mathrm{V/\,A}$ as required.

6.1.2 Constructing an Electrical Circuit from its Impedance

As discussed above, the impedance function is a good link between electrical circuit models and electromagnetic field models because it can be defined for both. In this section, we are interested in whether a given impedance function can be represented by an electrical circuit, if this electrical circuit is unique and how it can be found. More precisely, we are interested in reconstructing an electrical circuit from an impedance function of the form (6.10). In later sections, we will compute the impedance function from a field-theoretical model and construct the electrical circuit to reproduce the impedance.

Reconstructing an electrical circuit from its impedance function is a two-step procedure. In the first step, the node voltage vectors Φ_k are recovered from the impedance function. In the second step, the electrical circuit is reconstructed from its node potential eigenvectors. In the following sections, we discuss the following questions:

- Under what conditions can the circuit eigenmodes Φ_k be recovered from the frequency-dependent impedance function? Mathematically, what conditions have to be satisfied for the node incidence matrix $\mathbf{A}_s$ of the source network to be invertible?

- What conditions have to be satisfied for the set of eigenmodes to uniquely describe an electrical circuit. More precisely, under what conditions does a unique electrical circuit exist which has the given eigenmodes?

Inverting the $\mathbf{A}_s$ matrix

In this section we discuss necessary conditions for the $\mathbf{A}_s$ matrix to be invertible. More precisely, we are interested in a right pseudo-inverse matrix $\mathbf{A}_s^+$ such that $\mathbf{A}_s \mathbf{A}_s^+ = \mathbf{1}_n$. In this case, the resolvent form can be recovered from the impedance function. When the resolvent form is known as a broad band function of frequency, the eigenmodes can be obtained from the resolvent form[1].

Consider an electrical circuit consisting of $n+1$ nodes[2]. Furthermore, let m denote the number of sources in the current source network. In general, the current source network may contain loops,. The number of independent loops is given by c. In this case, A_s is an $m \times n$ matrix. According to Thm. 2.4, the rank of the indicence matrix is given by $\mathrm{rank}(\mathbf{A}_s) = m - c$ and the nullity by $\dim\ker(\mathbf{A}_s) = n - m + c$. It follows that

- If $(m-c) < n$, $\dim\ker(\mathbf{A}_s) > 0$ and a pseudo-inverse matrix $\mathbf{A}_s^+$ cannot exist.
- If $(m-c) = n$, $\dim\ker(\mathbf{A}_s) = 0$ and there exists a pseudo-inverse matrix $\mathbf{A}_s^+$ such that $\mathbf{A}_s \mathbf{A}_s^+ = \mathbf{1}$.
- If, in particular, $m = n$ and $c = 0$, the $\mathbf{A}_s$ matrix is square and invertible, and the pseudo-inverse is equal to the inverse matrix, $\mathbf{A}_s^+ = \mathbf{A}_s^{-1}$.

These results can be illustrated very intuitively on the level of electrical circuits. First note that $(n+1)-(m-c)$ is the number of connected subsets of the source network. It follows that

- If $(m-c) < n$, there are at least two subsets of nodes which are not connected by the source network. The potentials assigned to the nodes in different subsets can all be offset relative to each other without altering the impedance function. Conversely, it is not possible to retrieve unique node potentials from the impedance function. This situation is depicted in Fig. 6.2a.

[1] If the resolvent form is given as a matrix valued function of complex frequency, the eigenmodes can be extracted using, e.g., the vector fitting method, [126]. In this work, the resolvent form is constructed from explicitly computed eigenvectors and the eigenfrequencies and residues already appear explicitly.

[2] n is the number of independent node potentials as the potential of the ground node is zero by definition.

- If $c > 0$, the source network contains loops. Due to Kirchhoff's voltage law, Thm. 2.2, which states that all voltages along closed loops add up to zero, some entries of the impedance function are linearly dependent.This situation is depicted in Fig. 6.2b.

- If $m = n$ and $c = 0$, the maximum number of independent voltages is determined and all linear dependencies are removed. The source network forms a spanning tree for the electrical circuit. This situation is depicted in Fig. 6.2c.

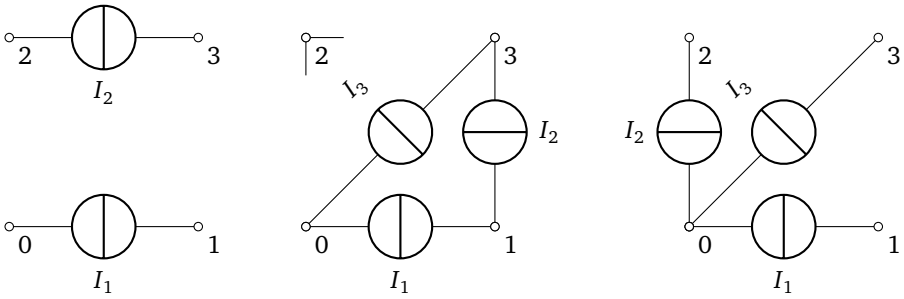

$$\mathbf{A}_s = \begin{pmatrix} 1 & 0 & 0 \\ 0 & -1 & 1 \end{pmatrix}$$

(a) Unconnected source network

$$\mathbf{A}_s = \begin{pmatrix} 1 & 0 & 0 \\ -1 & 1 & 0 \\ 0 & -1 & 0 \end{pmatrix}$$

(b) Source network with loops

$$\mathbf{A}_s = \begin{pmatrix} 1 & 0 & 0 \\ 0 & 1 & 0 \\ 0 & 0 & 1 \end{pmatrix}$$

(c) Tree network

Figure 6.2.: Source network configurations

To sum up, the circuit eigenmodes Φ_k can be recovered from the impedance function (6.10) if the source network comprises all nodes of the circuit. If a tree network is chosen, inversion is particularly simple. A very convenient choice for the source network is to define all voltages w.r.t the common ground node, i.e., all ports start at the same node. In this case, $\mathbf{A}_s = \mathbf{1}_n$. This situation is depicted in Fig. 6.2c.

In the previous section we showed the requirements for the circuit eigenmodes Φ_k to be recovered from the impedance function. The next step is to construct an electrical circuit from a set of eigenmodes and eigenfrequencies. We divide our approach in two steps

- In the first step, we use the circuit eigenmodes to construct the circuit matrices $\mathbf{R}$, $\widehat{\mathbf{L}^{-1}}$, and $\widehat{\mathbf{C}}$.
- In the second step, we use the circuit matrices $\tilde{\mathbf{L}}$, $\tilde{\mathbf{R}}$, and $\tilde{\mathbf{L}}$ to construct both the topology of the electrical circuit and the element values in explicit form.

We begin with the first step: For an electrical circuit with $n+1$ nodes, a set of $2n$ eigenmodes Φ_k with corresponding eigenfrequencies s_k and normalization coefficients λ_k is given. We need to find real symmetric matrices $\tilde{\mathbf{L}}$, $\tilde{\mathbf{R}}$, and $\tilde{\mathbf{C}}$, such that

$$\left(\widehat{\mathbf{L}^{-1}} + s\,\widehat{\mathbf{G}} + s^2\,\widehat{\mathbf{C}}\right)^{-1} = \sum_{k=1}^{2n} \frac{\lambda_k}{s_k - s} \Phi_k \Phi_k^{\mathrm{T}}.$$

We know that for the resolvent form to take this form, the normalization condition (5.24) has to be satisfied. Denoting by Φ the matrix whose k-th column is the eigenmode Φ_k and by $\mathbf{S}$ the diagonal matrix of eigenfrequencies s_k, this normalization condition takes the form

$$\begin{pmatrix} \Phi \\ \Phi\mathbf{S} \end{pmatrix}^{\mathrm{T}} \begin{pmatrix} \widehat{\mathbf{G}} & \widehat{\mathbf{C}} \\ \widehat{\mathbf{C}} & 0 \end{pmatrix} \begin{pmatrix} \Phi \\ \Phi\mathbf{S} \end{pmatrix} = \Lambda^{-1}$$

For most generalized eigenvalue problems, the coefficient matrices, i.e., $\widehat{\mathbf{L}^{-1}}$, $\widehat{\mathbf{G}}$ and $\widehat{\mathbf{C}}$, are known and the spectrum has to be found. In contrary, the spectrum is given here and the corresponding generalized eigenvalue problem has to be specified. In this case, the normalization condition really is a linear system of equations for the coefficient matrices $\widehat{\mathbf{G}}$ and $\widehat{\mathbf{C}}$. It follows that the matrices $\widehat{\mathbf{G}}$ and $\widehat{\mathbf{C}}$ can be constructed from the circuit eigenmodes by solving a linear system of equations. Pulling all known information to the right-hand side, an explicit expression for the circuit matrices can be formulated,

$$\begin{pmatrix} \widehat{\mathbf{G}} & \widehat{\mathbf{C}} \\ \widehat{\mathbf{C}} & 0 \end{pmatrix} = \begin{pmatrix} \Phi \\ \Phi\mathbf{S} \end{pmatrix}^{-\mathrm{T}} \Lambda^{-1} \begin{pmatrix} \Phi \\ \Phi\mathbf{S} \end{pmatrix}^{-1}. \tag{6.11}$$

Having computed two coefficient matrices, $\widehat{\mathbf{G}}$ and $\widehat{\mathbf{C}}$, we have to determine the missing coefficient matrix, $\widehat{\mathbf{L}^{-1}}$ in the next step. To do so, we exploit the left identity from (5.11). In terms of the coefficient matrices, the first companion matrix $\mathbf{C}_1$ is given by

$$\mathbf{C}_1 = \begin{pmatrix} 0 & \mathbf{1} \\ -\widehat{\mathbf{C}}^{-1}\widehat{\mathbf{L}^{-1}} & -\widehat{\mathbf{C}}^{-1}\widehat{\mathbf{G}} \end{pmatrix}.$$

As the $\widehat{\mathbf{C}}$ matrix is already known from the previous step, the $\widehat{\mathbf{L}^{-1}}$ matrix can be computed by solving the linear system of equations (5.11). Using the expression for the companion matrix given above and pulling all known information to the right hand side results in

$$\begin{pmatrix} 0 & \mathbf{1} \\ -\widehat{\mathbf{C}}^{-1}\widehat{\mathbf{L}^{-1}} & -\widehat{\mathbf{C}}^{-1}\widehat{\mathbf{G}} \end{pmatrix} = \begin{pmatrix} \Phi \\ \Phi\mathbf{S} \end{pmatrix} \mathbf{S} \begin{pmatrix} \Phi \\ \Phi\mathbf{S} \end{pmatrix}^{-1}.$$

The unknown quantity, $\widehat{\mathbf{L}^{-1}}$ is in the lower left block of the matrix. It can be extracted from the large matrix by

$$\widehat{\mathbf{L}^{-1}} = \begin{pmatrix} 0 & -\widehat{\mathbf{C}} \end{pmatrix} \begin{pmatrix} \Phi \\ \Phi\mathbf{S} \end{pmatrix} \mathbf{S} \begin{pmatrix} \Phi \\ \Phi\mathbf{S} \end{pmatrix}^{-1} \begin{pmatrix} 0 \\ \mathbf{1} \end{pmatrix}. \tag{6.12}$$

In summary, if a full set of $2n$ eigenfrequencies and eigenmodes with corresponding normalization coefficients λ are known, circuit matrices for an electrical circuit model with the correct spectral properties can be computed. In particular, the circuit matrices are unique.

The final step towards an electrical circuit model is the explicit computation of topology and element values from the circuit matrices. By definition in (2.27), the circuit matrices are products of incidence matrices, describing the topologies of the subcircuits, and the element matrices, $\widehat{\mathbf{L}^{-1}} = \mathbf{A}_L\,\mathbf{L}^{-1}\,\mathbf{A}_L^{\mathrm{T}}$, $\widehat{\mathbf{G}} = \mathbf{A}_R\,\mathbf{R}^{-1}\,\mathbf{A}_R^{\mathrm{T}}$, and $\widehat{\mathbf{C}} = \mathbf{A}_C\,\mathbf{C}\,\mathbf{A}_C^{-T}$. Consider first the resistive and capacitive subcircuits: The matrices $\mathbf{R}$ and $\mathbf{C}$ are diagonal. The circuit matrices $\widehat{\mathbf{G}}$ and $\widehat{\mathbf{C}}$ then take a simple form, [127], which is depicted exemplarily in Fig. 6.1:

- If $\widehat{\mathbf{C}}_{kl} = 0$ for $k \neq l$, the k-th and the l-th node are not connected by a capacitor.
- If $\widehat{\mathbf{C}}_{kl} \neq 0$ for $k \neq l$, the k-th and the l-th node are connected by a capacitor with capacitance $-\widehat{\mathbf{C}}_{kl}$.

- The diagonal element $\widehat{\mathbf{C}}_{kk}$ contains the sum of all capacitances which are connected to the k-th node, $\widehat{\mathbf{C}}_{kk} = C_{k0} + \sum_{l=1}^{n} C_{kl}$. It follows that if $\sum_{l=1}^{n} \widehat{\mathbf{C}}_{kl} \neq 0$, the k-th node is connected to the ground node by a capacitor with this capacitance.

- The same structure is also valid for the resistive circuit matrix $\widehat{\mathbf{G}}$.

From this structure, both the topology and the element values of the capacitive and resistive subcircuits can be read.

Constructing the inductive subcircuit from the $\widehat{\mathbf{L}^{-1}}$ matrix is considerably more complex and the inductive subcircuit is usually not unique. The higher complexity is due to mutual inductances, i.e., the $\mathbf{L}$ matrix is dense. The $\widehat{\mathbf{L}^{-1}}$ matrix therefore has a different structure than the $\widehat{\mathbf{G}}$ and the $\widehat{\mathbf{C}}$ matrices and the inductance matrix $\mathbf{L}$ cannot be read from $\widehat{\mathbf{L}^{-1}}$ by the above procedure. In order to extract the $\mathbf{L}$ matrix from the relationship $\widehat{\mathbf{L}^{-1}} = \mathbf{A}_L \, \mathbf{L}^{-1} \, \mathbf{A}_L^{\mathrm{T}}$, (2.27), we have to construct a pseudo-inverse $\mathbf{A}_L^{+}$ such that $\mathbf{A}_L^{+} \, \mathbf{A}_L = \mathbf{1}$ instead. This pseudo-inverse exists if and only if the inductive subcircuit does not contain loops. If the inductive subcircuit contains loops, the definition of the inductive subcircuit is possible, but it is not unique. In practice, the topology of the inductive subcircuit, i.e., the $\mathbf{A}_L$ matrix, is determined by the geometric structure of conductors. The following convention leads to a well-defined, unique inductive subcircuit: Two nodes which are located on disjoint conductors cannot be connected by an inductance. Two nodes which are located on the same conductor are by default connected by an inductance. If there are more than two nodes on the same conductor, the inductive subcircuit can be adapted to the requirements of the user as long as it does not contain loops. With this convention, the explicit formula for the inductance matrix $\mathbf{L}$ reads

$$\mathbf{L} = \left(\mathbf{A}_L^{+} \, \widehat{\mathbf{L}^{-1}} (\mathbf{A}_L^{+})^{\mathrm{T}} \right)^{-1} . \tag{6.13}$$

Last but not least, we emphasize the different conditions for the existence of pseudo-inverses for the $\mathbf{A}_s$ and the $\mathbf{A}_L$ matrices: In order to compute the circuit eigenmodes from the impedance function, we need a right pseudo-inverse for the $\mathbf{A}_s$ matrix, i.e., $\mathbf{A}_s \, \mathbf{A}_s^{+} = \mathbf{1}$. This pseudo-inverse exists if the graph described by $\mathbf{A}_s$ is spanning, however, it may contain loops. In order to compute the $\mathbf{L}$ matrix from the $\widehat{\mathbf{L}^{-1}}$ matrix, we need a left pseudo-inverse for the $\mathbf{A}_L$ matrix, i.e., $\mathbf{A}_L^{+} \, \mathbf{A}_L = \mathbf{1}$. This pseudo-inverse exists if the graph described by $\mathbf{A}_L$ does not contain loops, however, it need not be spanning.

6.1.3 Lossless Electrical Circuits

An electrical circuit without resistive circuit elements is called a lossless electrical circuit. In a lossless electrical circuit, $\widehat{\mathbf{G}} = 0$. In general, particularly at low frequencies, a lossless electrical circuit is a bad model for a real electromagnetic system. However, it can be a sufficiently accurate model at higher frequencies, when the impedance is dominated by inductive rather than resistive effects. The spectral properties of a lossless electrical circuit cannot be read directly from the spectral properties of a general electrical circuit. The missing linear term transforms the quadratic matrix polynomial into a linear matrix polynomial in s^2, i.e., the structure of the matrix polynomial is changed. An eigenmode Φ with eigenvalue s of a lossless electrical circuit satisfies

$$(\widehat{\mathbf{L}^{-1}} + s^2\,\widehat{\mathbf{C}})\Phi = 0. \tag{6.14}$$

The eigenvalues of this polynomial are all real. If Φ is an eigenvector with eigenvalue s^2, it follows

$$0 = \Phi^{\dagger}\left(\tilde{\mathbf{L}} + s^2\,\widehat{\mathbf{C}}\right)\Phi = l^{-1} + s^2 c, \tag{6.15}$$

i.e., $s = \pm i/\sqrt{lc}$, the eigenfrequencies are purely imaginary. In time domain, these solutions correspond to undamped oscillations. A lossless electrical circuit is not stable according to the definition in Sect. 2.2. However, as the solution remains bounded for all times, it is called weakly stable, [99].

The normalization condition (5.21) for lossless electrical circuits reads

$$\delta_{kl}\lambda_k^{-1} = \Phi_k^{\mathrm{T}}\,\widehat{\mathbf{C}}\,\Phi_l = \Phi_k^{\mathrm{T}}\,\mathbf{Q}_l = E_{C,kl}. \tag{6.16}$$

Note that the unit of λ differs from the unit of the normalization constant of lossy electrical circuits, (6.6). For lossless electrical circuits, $[\lambda^{-1}] = 1\,\mathrm{V\,A\,s}$. With this normalization, the resolvent form for a lossless electrical circuit is given by

$$\left(\widehat{\mathbf{L}^{-1}} + s^2\,\widehat{\mathbf{C}}\right)^{-1} = \sum_{k=1}^{n} \frac{\lambda_k}{s_k^2 - s^2}\Phi_k\Phi_k^{\mathrm{T}}. \tag{6.17}$$

This expression differs from (6.3) in the quadratic term in frequency and in the lower number of modes. The impedance function of a lossless electrical circuit can be written as

$$\mathbf{Z}(s) = -s\,\mathbf{A}_s^{\mathrm{T}}\left[\sum_{k=1}^{n}\frac{\lambda_k}{s_k^2 - s^2}\Phi_k\Phi_k^{\mathrm{T}}\right]\mathbf{A}_s\,. \tag{6.18}$$

Checking the units yields $[Z] = [s][\lambda][\Phi]^2/[s]^2 = 1\,\mathrm{V/\,A}$ as required. The circuit matrices $\widehat{\mathbf{L}^{-1}}$ and $\widehat{\mathbf{C}}$ can be computed from the matrix of eigenmodes Φ, the diagonal matrix of eigenfrequencies $\mathbf{S}$, and the diagonal matrix of normalization coefficients Λ by

$$\widehat{\mathbf{C}} = \Phi^{-T}\Lambda\Phi^{-1} \qquad \widehat{\mathbf{L}^{-1}} = \Phi^{-T}\Lambda\,\mathbf{S}^2\,\Phi^{-1}. \tag{6.19}$$

In order to construct the explicit form of the electrical circuit from the circuit matrices, the procedure from Sect. 6.1.2 can be reused.

6.2 The Physical Model behind Electrical Circuits

In the previous section, we highlighted the crucial importance of circuit eigenmodes for the analysis of electrical circuits. The eigenmodes completely specify the resolvent form and, in this way, the impedance function. In this section, we develop a field-theoretical model which is equivalent to electrical circuit theory on a 3D basis. This physical model will be shown to be equal to Darwin's model. We then discuss the properties of the impedance function in Darwin's model. The main result of this section will be an expression of the impedance function in terms of eigenmodes of Darwin's model, i.e., 3D field eigenmodes. The 3D eigenmodes of Darwin's model will be shown to have very similar properties to the discrete eigenmodes of electrical circuits.

6.2.1 Equations of Motion

In general, electromagnetism is governed by Maxwell's equations. The full set of Maxwell's equations exhibits properties which cannot be reproduced by electrical circuits, wave propagation and retardation, [37, 64]. In this section, we derive a field-theoretical model which exactly describes the electromagnetic properties incorporated in electrical circuit theory. This model is exactly Darwin's model from Sect. 3.4.3.

Constitutive Equations

The first set of equations will arise from the generalization of the constitutive equations for the circuit elements, shown in Sect. 2.1.1. We begin our investigation with the description of conductors. On the level of electrical circuits, a conductor is described by a resistor, an inductor or a combination of both. More generally, a conductor is described by specifying a conduction current as function of an applied voltage. On the level of electromagnetic fields, this corresponds to specifying a current density as function of an applied electric field. Such a relation is given by (3.8),

$$\vec{j}_\sigma = \sigma \vec{E}.$$

The subscript σ indicates that the conduction current inside a conductor will only be part of the total current. In order to make the connection between circuits and fields more evident, we use (3.23) to rewrite the electromagnetic field in terms of the scalar potential ϕ and the vector potential $\vec{A}$,

$$-\nabla\phi = \frac{\vec{j}_\sigma}{\sigma} + \partial_t \vec{A}. \tag{6.20}$$

Identifying the scalar potential Φ as the field-theoretical equivalent to the vector of node potentials and comparing this equation with (2.20) and (2.21), we can make the following identifications:

- For low frequencies, i.e. $\sigma \partial_t \vec{A} \ll \vec{j}_\sigma$, (6.20) describes an Ohmic resistor.
- For high frequencies, i.e. $\vec{j}_\sigma \ll \sigma \partial_t \vec{A}$, (6.20) describes an inductor.
- For frequencies between the two limits, (6.20) describes a series connection of inductor and resistor.

In order to complete the derivation, the defining equations for the vector potential $\vec{A}$ have to be specified. In particular, a gauge has to be chosen in order to render the potentials unique. As discussed in Sect. 4.4.1, each choice of gauge changes the definition of partial inductance. In order to comply with the definition used in the PEEC method, the following definition for the vector potential is chosen

$$\nabla \times \left(\frac{1}{\mu} \nabla \times \vec{A} \right) + \epsilon \nabla \partial_t \phi = \vec{j}_\sigma \tag{6.21}$$

$$\nabla \cdot \left(\epsilon \vec{A} \right) + \epsilon^2 \mu \partial_t \phi = 0. \tag{6.22}$$

Removing the complication stemming from considering inhomogeneous electric and magnetic material distributions considerably simplifies the interpretation:

- Eq. (6.21) is essentially Ampere's law, which is written in terms of the vector potential. For spatially homogeneous materials, it can be simplified to read $\Delta\vec{A} = -\mu\vec{j}$, which is the well-established expression for the vector potential used in the PEEC method, (4.19).

- Eq. (6.22) is the gauge fixing condition. For spatially homogeneous materials, it reduces to the well known Lorenz gauge [34], $\nabla\cdot\vec{A}+\epsilon\mu\partial_t\phi = 0$. There are many possible generalizations of the Lorenz gauge for dielectric and permeable materials[3]. We have chosen Eq. (6.22) because it will eventually lead to a symmetric system of equations of motion, even in the presence of inhomogeneous dielectric and permeable materials (Sect. 6.2.2).

- Last but not least, we emphasize that (6.21) is a non-retarded expression for the vector potential. As desired, the physical model does not describe retardation and wave propagation.

The formulation (6.21) for Ampere's law already allows for current densities with non-zero divergence. At first sight, current densities with non-zero divergence seem to be incompatible with Kirchhoff's current law, (2.18). However, remember that in Sect. 2.1.1 we showed that already on the level of electrical circuits, Kirchhoff's current law only holds when the conduction currents are supplemented by displacement currents through capacitors in the definition of the total current. Also on the level of field equations, the conduction currents have to be supplemented by displacement currents to restore current continuity. In practice, there are two different situations in which displacement currents appear: First, when the terminals of a current source are connected to two disjoint conductors, there is no conductive current return path and the current must return by displacement currents. In this case, the two conductors carry non-zero total charge. Second, at high frequencies the impedance of a current return path by displacement currents can be lower than the impedance of a conductive return path, even if such a conductive return path exists. In this case, the total charge of the conductor is zero at all times, but there are local fluctuations in the charge density. At the frequency when the impedances of the two return paths are equal, the system enters a state of resonance.

To finalize the derivation, we start with an expression for the displacement current in terms of the electric field,

[3] See, e.g., [128] or [129] for a discussion.

$$\vec{j}_D = \partial_t \vec{D}_c = \partial_t(-\epsilon \nabla \phi). \tag{6.23}$$

Instead of the Maxwell displacement current, $\vec{j}_D = \partial_t \vec{D}$, we again use the reduced version introduced in Sect. 3.4.3 about Darwin's model. Inserting this expression into the existing equations of motion (6.21) and (6.22) yields

$$\nabla \cdot \epsilon \nabla \phi = -\rho = \int_{\infty}^{t} \nabla \cdot \vec{j}_\sigma \mathrm{d}t. \tag{6.24}$$

To sum up, we identify

$$\vec{j}_D = (-\epsilon)\partial_t(\nabla \phi) \tag{6.25}$$

as the 3D equivalent of capacitor currents, $\mathbf{I}_c = \mathbf{C}\frac{\mathrm{d}U_c}{\mathrm{d}t}$.

Kirchhoff's Laws

For the complete description of electrical circuits, we need the constitutive equations for the circuit elements and Kirchhoff's equations. In this section, we generalize Kirchhoff's equations to 3D electromagnetic systems and show that the equations of motion satisfy these generalized Kirchhoff's equations.

Kirchhoff's current law, (2.18), is a continuity equation for the electric current. The continuity equation can be generalized to the 3D domain. Defining the total current as the sum of conductive currents $\vec{j}_\sigma$ and displacement current $\vec{j}_D$, this continuity equation directly follows from (6.24). In circuit and field domain respectively, Kirchhoff's current law reads

$$\mathbf{A}\mathbf{I} = \mathbf{A}(\mathbf{I}_R + \mathbf{I}_L + \mathbf{I}_C) = 0 \qquad \Leftrightarrow \qquad \nabla \cdot \vec{j} = \nabla \cdot \left(\vec{j}_\sigma + \vec{j}_D\right) = 0. \tag{6.26}$$

Kirchhoff's voltage law, (2.19), is already satisfied implicitely by using the node potential approach. We have already identified the node potential vector with the scalar potential. Further identifying the "algebraic sum of edge voltages" by line integrals of the $\nabla\phi$ field yields

$$0 = \mathbf{B}\mathbf{V} = \mathbf{B}\mathbf{A}^{\mathrm{T}}\Phi \qquad \Leftrightarrow \qquad 0 = \oint \vec{E}_c \cdot \mathrm{d}\vec{s} = \oint -\nabla\phi \cdot \mathrm{d}\vec{s} \tag{6.27}$$

because a loop integral of a gradient field is always zero.

The equations of motion (6.21), (6.22) and (6.24) were constructed as generalizations of electrical circuit theory to the 3D domain. What remains to be modeled are the "external interfaces" of the circuit, i.e., current sources to excite the electromagnetic system and voltage probes to measure the response.

On the level of electrical circuits, a current source is a device which extracts current from one node and injects it at another node of the electrical circuit. In other words, the current source can be seen as a violation of the continuity equation (2.18) for the passive subcircuit, i.e., the subcircuit consisting of only passive circuit elements:

$$\mathbf{A}_L\,\mathbf{I}_L + \mathbf{A}_R\,\mathbf{I}_R + \mathbf{A}_C\,\mathbf{I}_C = -\mathbf{A}_s\,\mathbf{I}_s. \tag{6.28}$$

In the 3D domain, we therefore model lumped current sources accordingly as an inhomogeneity of the continuity equation for the conduction and displacement currents, [130]:

$$\nabla\cdot\vec{j} = \nabla\cdot(\vec{j}_\sigma + \vec{j}_D) \equiv -\nabla\cdot\vec{j}_s = j_s\left(\delta^{(3)}(x-x_1) - \delta^{(3)}(x-x_0)\right). \tag{6.29}$$

In Eq. (6.29), the points x_1 and x_0 are the 3D equivalents to the terminal nodes of the current source. $\delta^{(3)}(x-x')$ is the three-dimensional Dirac delta function.

In order to make the definition compatible with the already established system of equations, we introduce an auxiliary field g such that

$$\vec{j}_s = \epsilon\nabla g. \tag{6.30}$$

Comparison with (6.29) shows that g is the solution of a Poisson equation

$$\nabla\cdot(\epsilon\nabla g) = \nabla\cdot\vec{j}_s = -j_s\left(\delta^{(3)}(x-x_1) - \delta^{(3)}(x-x_0)\right). \tag{6.31}$$

With this definition we can incorporate current sources into the equations of motion (6.21), (6.22), and (6.24):

$$\nabla\times\left(\frac{1}{\mu}\nabla\times\vec{A}\right) + \epsilon\nabla\partial_t\phi = \vec{j}_\sigma + \epsilon\nabla g \tag{6.32}$$

$$\nabla\cdot\left(\epsilon\vec{A}\right) + \epsilon^2\mu\partial_t\phi = \epsilon^2\mu g. \tag{6.33}$$

While the derivation is rather straightforward, the ansatz (6.30) is only one possible ansatz to satisfy (6.29) and needs some further motivation. We will therefore derive it in a different way. For simplicity, let us work under the assumption of homogeneous materials where Darwin's equations take the form

$$\Delta\vec{A} = -\mu\vec{j} = -\mu\sigma\vec{E} - \mu\vec{j}_s \qquad \nabla\cdot\vec{A} + \epsilon\mu\partial_t\phi = 0.$$

In the physical reality, the source current has to be treated on equal footing with the conduction currents, i.e., they both contribute to the vector potential $\vec{A}$. In order to study the impact of the current source, we decompose the vector potential into two contributions, $\vec{A} = \vec{A}_\sigma + \vec{A}_s$, stemming from the conduction current and the source current respectively. The equations of motion can similarly be decomposed into two systems of equations:

$$\begin{aligned} \Delta\vec{A}_\sigma &= -\mu\vec{j}_\sigma & \Delta\vec{A}_s &= -\mu\vec{j}_s \\ \nabla\cdot\vec{A}_\sigma + \epsilon\mu\partial_t\phi &= \epsilon\mu g & \nabla\cdot\vec{A}_s + \epsilon\mu g &= 0. \end{aligned} \tag{6.34}$$

From this system of equations, the following can be concluded:

- The system of equations on the right hand side can be solved immediately for the unknowns $\vec{A}_s$ and g. This definition of g agrees with (6.31).
- The system of equations on the left hand side depends on $\mathbf{A}_s$ and g in two ways: First, there is an explicit dependence on g. Second, there is a hidden dependence on $\mathbf{A}_s$ in the definition of the conductive current, $\vec{j}_\sigma = \sigma\vec{E} = \sigma\left(-\nabla\phi - \partial_t\vec{A}_s\right) - \sigma\partial_t\vec{A}_s$. Apart from the last term, (6.34) is identical to (6.32) and (6.33). The additional term can be interpreted as a mutual inductance between the current source and the conductor currents.

In classical electrical circuit theory and using ideal current sources, the self- and mutual inductances of current sources are not included[4]. Also removing them from our 3D model for electromagnetic circuit exactly yields (6.32) and (6.33).

[4] Even though they physically exist. Neglecting the inductances of current sources is an implicit approximation in the framework of electrical circuit theory. The approximation is mostly justified because in any meaningful measurement setup, the (physical) lengths of the current sources are short compared to the (physical) lengths of the conductors.

Voltage Probes

For the definition of voltage probes, we recall the previous identification of the node potential vector with the scalar potential. On the level of electrical circuits, a voltage probe measures potential differences of the node potentials of different nodes. For a voltage probe between the k-th and l-th node, the voltage is thus given by

$$V = \Phi(k) - \Phi(l) = \sum_{i=1}^{n} \Phi(i)(\delta_{ik} - \delta_{il}). \tag{6.35}$$

$\Phi(i)$ is the i-th component of the node potential vector, δ_{ij} is the discrete Kronecker delta. Similarly, on the level of electromagnetic fields, a voltage probes measures potential differences of the scalar potential between different points. For a voltage probe between the x_k and x_l, the voltage is thus given by

$$\begin{aligned} V = \phi(x_k) - \phi(x_l) &= \int \phi(x')(\delta^{(3)}(x' - x_k) - \delta^{(3)}(x' - x_l))\mathrm{d}^3x \\ &= \delta_k^{\mathrm{T}}\phi - \delta_l^{\mathrm{T}}\phi. \end{aligned} \tag{6.36}$$

$\delta^{(3)}(x' - x)$ is the three-dimensional Dirac delta function. The last equality defines a short-hand notation for the convolution of the scalar potential and the delta function, which we will frequently use in following sections.

6.2.2 Eigenmode Analysis

In this section, we perform a spectral analysis of the 3D model for electrical circuits, (6.32) and (6.33). We will show that the 3D eigenmodes and eigenfrequencies have very similar properties to the circuit eigenmodes and eigenfrequencies of electrical circuits. Furthermore, we will derive an expression for the impedance function in terms of 3D eigenmodes which is very similar to the expression for the impedance in terms of circuit eigenmodes, (6.10).

In order to perform the spectral analysis, the equations of motion have to be transformed into frequency domain. This is possible by means of the Fourier transform (Sect. 2.2). In the complex frequency s, the equations of motion read

$$\nabla \times \left(\frac{1}{\mu}\nabla \times \vec{A}\right) + s\epsilon\nabla\phi = \vec{j}_\sigma + \epsilon\nabla g \tag{6.37}$$

$$\nabla \cdot \left(\epsilon\vec{A}\right) + s\epsilon^2\mu\phi = \epsilon^2\mu g. \tag{6.38}$$

Symmetrization

The properties of real symmetric polynomial eigenvalue problems (Sect. 5.1.3 and Sect. 5.1.5) greatly simplify the spectral analysis. Furthermore, numerical algorithms for the solution of real symmetric (or, more generally, hermitian) eigenvalue problems are in general better conditioned than numerical algorithms for non-hermitian eigenvalue problems. The equations of motion in frequency domain, (6.37) and (6.38) can be symmetrized by changing variables,

$$\left[\begin{pmatrix} \nabla\cdot\epsilon\nabla & 0 \\ 0 & \nabla\times\mu^{-1}\nabla\times \end{pmatrix} + s\begin{pmatrix} 0 & \nabla\cdot\epsilon \\ -\epsilon\nabla & \sigma \end{pmatrix} + s^2\begin{pmatrix} -\epsilon^2\mu & 0 \\ 0 & 0 \end{pmatrix}\right] \cdot \begin{pmatrix} s\phi \\ \vec{E} \end{pmatrix} = \begin{pmatrix} -\epsilon^2\mu s^2 g \\ -\epsilon s\nabla g \end{pmatrix}. \tag{6.39}$$

With this change of variables, Darwin's model is described by a real symmetric matrix polynomial. In the next sections, we apply results from Sect. 5.1.5 in order to study the spectral properties of Darwin's model.

Eigenfrequencies

According to the investigation in Sect. 5.1.3, all eigenvalues appear in complex conjugate pairs. It remains to check that all eigenvalues are located in the left complex half plane to ensure the stability of the physical model. Assume that $\left(\phi, \vec{E}\right)$ is an eigenmode with complex eigenfrequency s. Inserting into the equations of motion yields

$$\begin{aligned} 0 &= \phi^\dagger\left(\nabla\cdot\epsilon\vec{E} + \nabla\cdot\epsilon\nabla\phi - \epsilon^2\mu s^2\phi\right) &&= -\epsilon|\nabla\phi|^2 - s^2\epsilon^2\mu|\phi|^2 - (\nabla\phi)^\dagger\,\epsilon\vec{E} \\ 0 &= \vec{E}^\dagger\left(\nabla\times\left(\tfrac{1}{\mu}\nabla\times\vec{E}\right) + s\sigma\vec{E} - s^2\nabla\phi\right) &&= \tfrac{1}{\mu}|\nabla\times\vec{E}|^2 + s\sigma|\,\mathbf{E}\,|^2 - s^2\left(\epsilon\vec{E}\right)^\dagger\nabla\phi. \end{aligned}$$

which can be combined to yield

$$0 = \left\{\frac{1}{\mu}|\nabla\times\vec{E}|^2 + \epsilon^2\mu|s|^4|\phi|^2\right\} + s\left\{\sigma|\vec{E}|^2\right\} + s^2\left\{\epsilon|\nabla\phi|^2\right\}. \tag{6.40}$$

Analyzing (6.40) in the same way as (6.4) shows that all eigenfrequencies are indeed in the left half plane, $\Re(s) < 0$. The locations of the eigenfrequencies in the complex plane thus agree with the locations of the eigenfrequencies of an electrical circuit model.

The normalization of the eigenvectors is a priori arbitrary. In order to express the resolvent form in terms of eigenmodes, a normalization matrix Λ is needed. Denoting by $(\phi_i, \vec{E}_i)$ the eigenmode with eigenfrequency s_i and inserting the coefficient matrices from (6.39) into the normalization condition (5.24) yields

$$\delta_{kl}\lambda_k^{-1} = \vec{E}_k^{\mathrm{T}}\sigma\vec{E}_l - 2s_k\phi_k^{\mathrm{T}}\nabla\epsilon\nabla\phi_l. \tag{6.41}$$

In the discussion of the normalization condition for circuit eigenmodes, (6.9), the normalization was expressed in terms of energy related quantities, the Ohmic losses and the change in capacitive energy. The same considerations can also be applied to (6.41). Again consider a field distribution,

$$\left(\phi(x), \vec{E}(x)\right) = \sum_{k=1}^{N} a_k \left(\phi_k(x), \vec{E}(x)\right).$$

The Ohmic loss rate according to (3.39) and the capacitive energy according to (3.40) are given by

$$P = \sum_{k,l=1}^{N} a_k a_l P_{kl} \qquad P_{kl} = \int \vec{E}_k(x) \underbrace{(\sigma\vec{E}_l(x))}_{\vec{j}_l(x)} \mathrm{d}^3x \tag{6.42}$$

$$E_C = \sum_{k,l=1}^{N} a_k a_l E_{C,kl} \quad E_{C,kl} = \int \phi_k(x) \underbrace{(-\nabla\cdot\epsilon\nabla\phi_l)}_{\rho_l} \mathrm{d}^3x. \tag{6.43}$$

and $\vec{j}_\sigma$ and ρ are the Ohmic current and the space charge density. With these definitions, the normalization condition (6.41) can be reformulated

$$\delta_{kl}\lambda_k^{-1} = \int \vec{E}_k^{\mathrm{T}}\vec{j}_k + 2s_k\phi_k^{\mathrm{T}}\rho_l \mathrm{d}^3x = P_{kl} + 2s_k E_{C,kl}. \tag{6.44}$$

This normalization condition is equivalent to a similar normalization condition for the circuit eigenmodes of electrical circuits, (6.9).

On the level of electrical circuits, the impedance function is computed by exciting the system with a time-harmonic current source and computing the voltages or, equivalently, the potential differences. In Sect. 6.2.1 we generalized the definition of current sources for electrical circuits to the 3D domain.

According to the derivation in Sect. 6.2.1, let the current source be described by the scalar field g, defined by (6.31). The electromagnetic fields can be computed using the equations of motion (6.39),

$$\begin{pmatrix} s\phi \\ \vec{E} \end{pmatrix} = \left[\begin{pmatrix} \nabla\cdot\epsilon\nabla & 0 \\ 0 & \nabla\times\mu^{-1}\nabla\times \end{pmatrix} + s\begin{pmatrix} 0 & \nabla\cdot\epsilon \\ -\epsilon\nabla & \sigma \end{pmatrix} + s^2\begin{pmatrix} -\epsilon^2\mu & 0 \\ 0 & 0 \end{pmatrix} \right]^{-1} \cdot \begin{pmatrix} -\epsilon^2\mu s^2 g \\ -\epsilon s\nabla g \end{pmatrix}.$$

The resolvent form can be expressed in terms of field eigenmodes $(\phi_k, \vec{E}_k)$ using (5.26). The scalar potential can then be written

$$\phi = \sum_{k=1}^{2N} \frac{\lambda_k}{s_k - s} \left[-\epsilon^2\mu s_k s \phi_k^{\mathrm{T}} g + (\nabla\cdot\epsilon\vec{E}_k)^{\mathrm{T}} g \right] \phi_k,$$

which can be reformulated using the equations of motion,

$$\phi = s\sum_{k=1}^{2N} \frac{\lambda_k}{s_k - s} \left[\phi_k^{\mathrm{T}} \nabla\cdot(\epsilon\nabla g) \right] \phi_k.$$

In order to obtain the final form, we recall the definition of the g field, $\nabla\cdot(\epsilon\nabla g) = -j_s\left(\delta^{(3)}(x-x_1) - \delta^{(3)}(x-x_0)\right) = -j_s\delta$. It follows

$$\phi = sj_s\sum_{k=1}^{2N} \frac{\lambda_k}{s_k - s} \left[-\phi_k^{\mathrm{T}}\delta \right] \phi_k.$$

In order to define voltages, we have to use the voltage probes according to Sect. 6.2.1. We directly proceed to the definition of the impedance matrix. Let the k-th current source be described by g_k where $\nabla\cdot\epsilon\nabla g_k = -j_{s,k}(\delta^3(x-x_{k,1}) - \delta^3(x-$

$x_{k,0}) = -j_{s,k}\delta_k$. The k-th voltage probe measures the voltage drop produced by the k-th source current and is accordingly described by δ_k, i.e., $\delta_k^{\mathrm{T}}\phi = \phi(x_{k,1}) - \phi_(x_{k,0})$. The voltage drop along the l-th voltage probe due to the current in the k-th current source is thus given by

$$\mathbf{Z}_{kl} = -s\sum_{i=1}^{2M}\frac{\lambda_k}{s-s_i}\left[\delta_l^{\mathrm{T}}\phi_i\right]\left[\phi_i^{\mathrm{T}}\delta_k\right].$$

Denoting by δ the matrix whose columns are given by the δ_k functions, the impedance matrix can be written as

$$\mathbf{Z} = -s\delta^{\mathrm{T}}\left[\sum_{i=1}^{2N}\frac{\lambda}{s-s_i}\phi_i\phi_i^{\mathrm{T}}\right]\delta. \tag{6.45}$$

This equation is very similar to the equivalent expression for the impedance function of electrical circuits, (6.10).

6.2.3 Lossless systems

In Sect. 6.1.3 we introduced lossless electrical circuits as an approximation of electrical circuit theory. It is also possible to define a lossless system on the level of Darwin's model. In this case, all conductivities are set to infinity, $\sigma = \infty$. In practice, lossless conductors are modeled by a perfectly conducting (PEC) boundary condition $\vec{E} \times \vec{n} = 0$ instead of a conductivity. For the lossless Darwin model, a different change of variables than in (6.39) leads to a symmetric matrix polynomial with lower order,

$$\left[\begin{pmatrix} \nabla\cdot\epsilon\nabla & 0 \\ 0 & 0 \end{pmatrix} + s^2\begin{pmatrix} -\epsilon^2\mu & \nabla\cdot\epsilon \\ -\epsilon\nabla & \nabla\times\mu^{-1}\nabla\times \end{pmatrix}\right]\begin{pmatrix} s^2\phi \\ \vec{E} \end{pmatrix} = \begin{pmatrix} -\epsilon^2\mu s^3 g \\ -\epsilon s^3\nabla g \end{pmatrix}. \tag{6.46}$$

It can be shown that the eigenvalues s^2 of this system of equations are real and negative, i.e., the eigenfrequencies are purely imaginary. The location of the eigenfrequencies in the complex plane thus agree with the locations of the eigenfrequencies of a lossless electrical circuit model.

Due to the lower order of the polynomial eigenvalue problem, the normalization condition for the eigenmodes of lossless electrical circuits has a simpler form than the general expression (6.41). Denoting by $(\phi_i, \vec{E}_i)$ the eigenmode with eigenfrequency s_i and inserting the coefficient matrices for the lossless Darwin model,

(6.46), into the normalization condition for linear eigenvalue problems, (5.21), can be shown to yield

$$\lambda_k^{-1}\delta_{kl} = -\phi_k^{\mathrm{T}}\nabla\epsilon\nabla\phi_l = \phi_k^{\mathrm{T}}\rho_l = E_{C,kl}. \tag{6.47}$$

This normalization condition is equivalent to a similar normalization condition for the circuit eigenmodes of lossless electrical circuits, (6.16). With this normalization, the impedance function is given by

$$\mathbf{Z} = -s\delta^{\mathrm{T}}\left[\sum_{k=1}^{n}\frac{\lambda_k}{s_k^2 - s^2}\phi_k\phi_k^{\mathrm{T}}\right]\delta. \tag{6.48}$$

.

6.2.4 Connection to Ampere's law

In the previous section, we used the Lorenz gauge to derive an expression of the vector potential (and, hence, the magnetic field) which depends only on the conduction current. Combining (6.37) and (6.38) yields

$$\nabla\times\frac{1}{\mu}\nabla\times\vec{A} - \epsilon\nabla\frac{1}{\epsilon^2\mu}\nabla\cdot(\epsilon\vec{A}) = -\frac{1}{\mu}\Delta\vec{A} = \vec{j}_\sigma,$$

where we assumed homogeneous materials in the first identity. This equation has an explicit solution in terms of Green's functions, (3.31),

$$\vec{A} = -\frac{\mu}{4\pi}\int\frac{\vec{j}_\sigma(x')}{|x-x'|}\mathrm{d}^3x'.$$

If the conduction current is solenoidal, $\nabla\cdot\vec{j}_\sigma = 0$, it has been shown that the magnetic field $\vec{B} = \nabla\times\vec{A}$ is consistent with Ampere's law, [131]. More precisely, applying Ampere's law yields $\nabla\times\vec{B} = \nabla\times\nabla\times\vec{A} = \mu\vec{j}_\sigma$. If, however, the conduction current is not solenoidal, it has been shown, [131], that

$$\nabla\times\vec{B} = \nabla\times\nabla\times\vec{A} = \mu\vec{j}_\sigma + \mu\nabla\underbrace{\frac{1}{4\pi}\int\frac{\nabla\cdot\vec{j}_\sigma(x')}{|x-x'|}\mathrm{d}^3x'}_{g'}. \tag{6.49}$$

In order to render the magnetic field constistent with Ampere's law, the current path is closed by a genric current return path $\vec{j}_{\text{return}} = \nabla g'$, [132]. Further using the Green function identity (3.31) yields

$$\Delta g' = \nabla \cdot \vec{j}_\sigma = -\nabla \cdot \vec{j}_s.$$

The definition of g' therefore agrees with the definition (6.31) for the auxiliary g field. In particular, our formulation for inductance-free current sources, (6.30), agrees with the generic current return path appearing in (6.49).

6.2.5 Connection to the PEEC Method

The PEEC method (Sect. 4.4) is the state-of-the-art method for the construction of electrical circuit models. In this section, we explore similarities and differences between our method and the PEEC method.

Both the PEEC method and our method start from a field-theoretical (3D) model for an electromagnetic system. Both methods use Darwin's model as the field-theoretical equivalent to electrical circuit theory. There is a difference in the modeling of current sources, however: In the PEEC method, current sources are included on the level of electrical circuits, i.e., after the discretization process. In the physical system underlying our method, current sources are modeled in the 3D domain and included in the discretization process. As such, the models for current sources cannot be readily compared. However, when a discretized PEEC model including current sources is transformed back into a continuous system of integro-differential equations, i.e., the PEEC discretization process is reversed, a formulation to include lumped current sources in a 3D model. This process is explained in detail in Sect. 4.4.5. It turns out that the two formulations are equivalent. Mathematically, the equations of motion used in our method, (6.32) and (6.33), are equal to the equations of motion used in the PEEC method, (4.30).

The PEEC method starts from the equations of motion and discretizes them in such a way that the result has the form of an electrical circuit. The discretized equations of motion can be solved to compute, e.g., transfer functions and eigenmodes. On the other hand, our method starts from eigenmodes of the equations of motion and constructs the electrical circuit from the eigenmodes. In this thesis, the eigenmodes are computed numerically using the FEM. However, it is also possible to use, e.g., analytical expression for the eigenmodes (if available) or even use the PEEC method to compute the eigenmodes. While the electrical circuits constructed

by the PEEC method are usually very large[5], our method aims at constructing very compact equivalent circuit with as few circuit elements as possible to reach sufficient accuracy in the frequency range of interest. In short, the PEEC method is a discretization scheme which yields large electrical circuits, our method is a model order reduction scheme which yields very compact electrical circuit models.

So far, the PEEC method was the only method available for the numerical computation of partial inductances, which have proven very useful for the description of multiconductor systems. Our formulation opens a different path: Starting from the equations of motion in differential form, (6.32)-(6.33), the discretization process can be performed with essentially all methods suitable for the discretization of systems of partial differential equations. In particular, instead of a discretization in terms of integral equations, e.g., the PEEC method, the system of equations can also be discretized directly from the differential equations using, e.g., the FEM or the Finite Integration Technique. Compared with the PEEC discretization, our approach has the following advantages:

- The FEM can be implemented with a wide range of different mesh types. In particular, it can handle unstructred, tetrahedral meshes which offer a great flexibility in the description of complex geometries. Furthermore, the FEM can be extended in a straightforward way[6] to handle curvilinear meshes. Using higher order ansatz functions on the same mesh leads to faster convergence. In comparison, the standard PEEC method was defined for rectangular, orthonormal meshes. Generalizing the PEEC method to different mesh types is possible, [133, 134], but requires considerably more implementational and computational effort. To our knowledge, there is no extension of the PEEC method to higher order ansatz functions.

- The FEM can handle complex, spatially inhomogeneous material distributions. Most importantly, permeable and dielectric materials can be described without additional computational effort. In the PEEC method, such materials have to be modeled by additional degrees of freedom because of the lack of Green's functions for inhomogeneous material distributions (see Sect. 4.4.4).

- The PEEC method can describe systems with lots of vacuum space very efficiently because there are no degrees of freedom assigned to the vacuum.

[5] The number of circuit elements is equal to the number of discretization elements. Therefore, already a large number of elements is needed to achieve moderate accuracy.

[6] By 'straightforward' we indicate that the basic structure of the discretization procedure remains the same. Added complexity arises only from increased book-keeping due to the higher number of degrees of freedom.

The FEM, on the other hand, operators on a mesh filling all space, leading to a much higher number of degrees of freedom in this case.

6.3 The Connection between Electrical Circuits and Electromagnetic Fields

6.3.1 Connections between Circuit Quantities and Field Quantities

In the previous sections, we discussed electrical circuits and their field-theoretical equivalent, Darwin's model. We analyzed the spectral properties of both models in order to separate relevant physical processes (i.e., eigenmodes in the frequency range of interest) from irrelevant physical processes (i.e., eigenmodes far outside the frequency range of interest which contribute only weakly). We then defined a special transfer function, the impedance, for both models and expressed it in terms of eigenmodes. We showed that the impedance can be written as a rational function with poles given by the eigenfrequencies in the spectrum.

In this section, we discuss similarities between the two models. We highlight equivalent expressions within the two models and identify field quantities with circuit quantities:

- The current density is identfied with the vector of edge currents and the charge density is identified with the vector of node charges,

$$\left(\vec{j}, \rho\right) \qquad \Leftrightarrow \qquad (\mathbf{I}, \mathbf{Q}) .$$

- The scalar potential is identified with the vector of node potentials,

$$\phi(x) \qquad \Leftrightarrow \qquad \Phi .$$

- The divergence operator is identified with the node incidence matrix; the gradient operator is identified with its transpose,

$$(\mathrm{div} = \nabla\cdot, \nabla) \qquad \Leftrightarrow \qquad \left(\mathbf{A}, -\mathbf{A}^{\mathrm{T}}\right) .$$

  The minus sign stems from the fact that the nabla operator has to be seen as the negative transpose of the divergence operator. This can be understood from the result $\langle \vec{v}, \nabla f \rangle = \int \vec{v}^{\mathrm{T}} \nabla f \, \mathrm{d}^3x = -\int (\nabla \cdot \vec{v}) f \, \mathrm{d}^3x = -\langle \nabla \cdot \vec{v}, f \rangle$.

- It follows from the previous identfication that the longitudinal part of the electric field is identified with the vector of edge voltages,

$$\vec{E}_L = -\nabla\phi \qquad \Leftrightarrow \qquad \mathbf{V} = \mathbf{A}^{\mathrm{T}}\,\phi\,.$$

- The set of path integrals around closed loops is identified with the fundamental loop matrix[7],

$$\oint_\gamma \mathrm{d}\vec{s} \qquad \Leftrightarrow \qquad \mathbf{B}\,.$$

- The three-dimensional Dirac delta function is identified with the discrete Kronecker delta,

$$\delta^{(3)}(x_k - x_l) \qquad \Leftrightarrow \qquad \delta_{kl}\,.$$

The above identifications can all be understood very intuitively. Already with this set of equations, we arrive at the following equivalences:

- The constitutive equation for the current, $\vec{j} = -\sigma\partial_t\vec{A} - \sigma\nabla\phi$ is identified with the voltage-current relationship of resistors and inductors,

$$-\nabla\phi = \frac{\vec{j}}{\sigma} + \partial_t\vec{A} \qquad \Leftrightarrow \qquad \mathbf{A}^{\mathrm{T}}\,\Phi = \mathbf{R}\,\mathbf{I} + \mathbf{L}\,\frac{\mathrm{d}\,\mathbf{I}}{\mathrm{d}t}.$$

- Coulomb's law is identified with the charge-voltage relationship of a capacitor,

$$\rho = -\nabla\cdot(\epsilon\nabla\phi) \qquad \Leftrightarrow \qquad \mathbf{Q} = \widehat{\mathbf{C}}\,\Phi.$$

- The continuity equation (3.18) is identified with Kirchhoffs current law (2.31),

$$\nabla\cdot\vec{j}_\sigma + \nabla\cdot\vec{j}_D = -\nabla\cdot\vec{j}_s \qquad \Leftrightarrow \qquad \mathbf{A}\,\mathbf{I} + \partial_t\,\mathbf{Q} = -\mathbf{A}\,\mathbf{I}_s\,.$$

[7] Recall that multiplying a vector by the fundamental loop matrix is equivalent to forming algebraic sums of closed loops in the corresponding graph.

- The conservativeness of the gradient field $\nabla\phi$ is identified with Kirchhoff's voltage law,

$$\oint_\gamma \nabla\phi \, \mathrm{d}\vec{s} = 0 \qquad \Leftrightarrow \qquad \mathbf{B}\mathbf{V} = \mathbf{B}\mathbf{A}^{\mathrm{T}}\Phi = 0.$$

- A 3D voltage probe is identified with the discrete voltage probe,

$$V = \delta^{\mathrm{T}}\phi \qquad \Leftrightarrow \qquad \mathbf{V} = \mathbf{A}_{\mathrm{s}}\Phi.$$

The similarities between circuits and field theory can be carried even further when the eigenmodes of the respective systems are compared:

- Eigenfrequencies of Darwin's model are identified with the eigenfrequencies of electrical circuits. In Sect. 6.2.2 and Sect. 6.1.1 respectively, we showed that the eigenfrequencies of Darwin's model and electrical circuits both appear in complex conjugate pairs in the complex half plane with negative real part.

- For both the lossless Darwin system and lossless electrical circuits, the eigenfrequencies are purely imaginary.

- Eigenmodes ϕ of Darwin's model are identified with eigenmodes Φ of electrical circuits. The normalization conditions used in this work, (6.44) and (6.9) respectively, read

$$P_{kl} + 2s_k E_{C,kl} = \lambda_k^{-1}\delta_{kl} \qquad \Leftrightarrow \qquad P_{kl} + 2s_k E_{C,kl}) = \lambda_k^{-1}\delta_{kl}.$$

  The normalization conditions are thus equivalent.

- For the lossless Darwin system and lossless electrical circuits, the normalization condition for the eigenmodes, (6.47) and (6.16) respectively, read

$$E_{C,kl} = \lambda_k^{-1}\delta_{kl} \qquad \Leftrightarrow \qquad E_{C,kl} = \lambda_k^{-1}\delta_{kl}.$$

  For lossless electromagnetic systems, the normalization conditions also agree.

- When the eigenmodes satisfy the normalization conditions above, the impedance for the Darwin model (6.45) and electrical circuits (6.10) can be written in terms of the eigenmodes

$$Z = -s\delta^{\mathrm{T}}\left[\sum_{k=1}^{\infty}\frac{\lambda_k}{s-s_k}\phi_k\phi_k^{\mathrm{T}}\right]\delta \qquad \Leftrightarrow \qquad \mathbf{Z} = -s\,\mathbf{A}_s^T\left[\sum_{k=1}^{N_n}\frac{\lambda_k}{s-s_k}\Phi_k\Phi_k^{\mathrm{T}}\right]\mathbf{A}_s\,. \tag{6.50}$$

  For lossless systems, this expression has to be replaced by (6.48) and (6.18) respectively,

$$Z = -s\delta^{\mathrm{T}}\left[\sum_{k=1}^{\infty}\frac{\lambda_k}{s^2-s_k^2}\phi_k\phi_k^{\mathrm{T}}\right]\delta \qquad \Leftrightarrow \qquad \mathbf{Z} = -s\,\mathbf{A}_s^T\left[\sum_{k=1}^{N_n}\frac{\lambda_k}{s^2-s_k^2}\Phi_k\Phi_k^{\mathrm{T}}\right]\mathbf{A}_s\,. \tag{6.51}$$

6.4 An Automated Method for the Construction of Electrical Circuit Models

Field theoretical models in terms of, e.g., Darwin's model or Maxwell's model, and electrical circuit models are both valid models for the description of electrical components in a certain frequency domain. In the previous section, we showed that the frequency range of validity of electrical circuits agrees with the frequency range of Darwin's model. Due to this fact and the great similarity between the two models worked out in the previous section, Darwin's model can be seen as the field theoretical generalization of electrical circuits [37, 64].

Based on this observation, we propose in this section a procedure to automatically generate electrical circuit models from an existing field-theoretical model in terms of Darwin's equations. More precisely, we condense the 3D Darwin eigenmodes into a form which can be interpreted as circuit eigenmodes of the associated electrical circuit. The explicit form of this equivalent electrical circuit can be constructed using the procedure in Sect. 6.1.2.

6.4.1 The Basic Method

Our method for the construction of electrical circuit models for electromagnetic components is based on the following axiom:

Axiom 6.1. *The nodes of the electrical circuit model can be associated with points in the 3D geometry.*

We call a point x_k which is associated to the k-th node of the electrical circuit an **electrode**. In other words, if an electromagnetic component or system is equipped with a set of electrodes, these electrodes correspond to the nodes of the electrical circuit model. For the sake of clarity, we shift the detailed discussion about the significance and the physical interpretation of the electrodes to Sect. 6.4.3 and assume for the moment that a set of electrodes is given.

Let $\{x_0, x_1, \cdots, x_n\}$ be this set of electrodes. Further consider a scalar potential distribution $\phi(x)$. We define a vector of potentials by evaluating $\phi(x)$ only at the positions of the electrodes. Mathematically,

$$\tilde{\Phi} = \begin{pmatrix} \phi(x_1) - \phi(x_0) \\ \phi(x_2) - \phi(x_0) \\ \vdots \\ \phi(x_n) - \phi(x_0) \end{pmatrix} = \delta^{\mathrm{T}} \phi. \tag{6.52}$$

For simplicity, we again used the short-hand notation from Sect. 6.2 for the application of a vector of delta functions, $\delta_k = \delta^{(3)}(x - x_k) - \delta^{(3)}(x - x_0)$. The main idea of our procedure is to interpret the resulting vector of potentials as the vector of node potentials for the electrical circuit model. More precisely, let

$$S_{\mathrm{Darwin}} = \left\{ \left(s_k, \phi_k, \vec{E}_k \right), k = 1, \cdots, N \right\} \tag{6.53}$$

be the spectrum of the Darwin equations of motion for some electromagnetic component (i.e., for some distribution of conducting, dielectric and magnetic materials). Then for each eigenmode in the spectrum, we can define a vector of node potentials by projecting them in the electrodes according to (6.52). The projected Darwin eigenmodes should then be interpreted as circuit eigenmodes of the electrical circuit model with the same eigenfrequencies. At this point, one thing prevents us from proceeding:

- The maximum number of independent eigenfrequencies which is supported by the equations of motion of an electrical circuit is equal to n, $n+1$ being the number of nodes of the electrical circuit[8]. For typical electrical circuit models, $n \lesssim 10$.

[8] For a lossy electrical circuit, the total number is $2n$ However, we count each complex conjugate pair of eigenfrequencies as one independent eigenfrequency only.

- The Darwin equations of motion as a continuous system of equations support an infinite amount of eigenfrequencies. After the discretization procedure, the number becomes finite. While the numerical number N of Darwin eigenmodes depends on the mesh size of the discretization, for any practical application, $n \ll N$.

Due to these considerations, only a very limited number of Darwin eigenmodes can be reproduced by the electrical circuit model. The choice of eigenmodes is a priori arbitrary. However, in order to realistically describe the component at low frequncies, i.e., starting at DC up to some maximum frequency and without skipping resonances in the frequency range of validity, the n lowest eigenfrequencies have to be chosen. Therefore,

$$\begin{aligned} S_{\mathrm{ec}} &= \{(s_k, \Phi_k), k = 1, \cdots n\} \\ &= \left\{ \left(s_k, \tilde{\Phi}_k = \int \delta^{\mathrm{T}} \phi_k \mathrm{d}^3 x \right) \middle| \begin{array}{l} s_k \text{ are } n \text{ lowest Darwin} \\ \text{eigenfreq. with } \tilde{\Phi}_k \neq 0 \end{array} \right\}. \end{aligned} \tag{6.54}$$

As a final step, we interpret S_{ec} as the spectrum of the corresponding electrical circuit model. The electrical circuit model is uniquely determined by its spectrum and can be constructing by the procedure in Sect. 6.1.

It remains to discuss the properties of the electrical circuits constructed by the procedure above.

- According to (6.50) and (6.51), the first n poles and residues of the impedance functions computed from the 3D Darwin model and the electrical circuit model respectively agree with each other.

- According to (6.54), apart from the first n Darwin eigenmodes, no more eigenmodes are reproduced by the electrical circuit. The corresponding poles and residues of the Darwin impedance function do not appear in the impedance function computed from the electrical circuit. The electrical circuit model is **compact**.

- In other words, an electrical circuit is a mode-reduced representation of the field-theoretical Darwin model. Such mode-reduced representations frequently appear in the context of model order reduction [135, 136].

- Even though all singularities of the impedance function are correctly modeled in the frequency range of validity, neglecting all eigenmodes outside

the frequency range of interest can lead to a significant offset error, negatively affecting the accuracy of the electrical circuit model. In Sect. 6.4.3, we show that the accuracy depends solely on the positions of the electrodes. The **accuracy can be controlled**.

- The nodes of the electrical circuit exist as electrodes in the 3D reality. The electrical circuit has a **physical meaning**.

It follows that all requirements on valid electrical circuit models which were formulated in the Introduction are satisfied.

6.4.2 Electrode Positioning and the Accuracy of Electrical Circuits

An electrical circuit is, above all, a model for a real electromagnetic device. Before it can be used in practical applications, its accuracy has to be assessed and possible sources for inaccuracies have to be identified. Instead of comparing the circuit model directly with measurement results, we define the field-theoretical model of Maxwell's equations as reference. Effects which are not included in Maxwell's equations usually do not play any significant role in the devices covered in this work.

In order to compare an electrical circuit model with the field-theoretical model of Maxwell's equations, some quantity has to be used which exists for both models. We choose this quantity to be the frequency-dependent impedance function, which can be defined for both models and which has a well-defined physical meaning. Furthermore, the impedance function is usually the quantity of interest for the characterization of electrical components in an industrial environment. A given electrical circuit model is accurate, therefore, when it correctly reproduces an impedance function predicted by Maxwell's equations. Repeating the steps needed for the construction of an electrical circuit from a 3D field theoretical models, the following sources for inaccuracies can be detected:

- The underlying physical model for the construction of electrical circuit models is Darwin's model (Sect. 3.4). Darwin's model is a low-frequency approximation of Maxwell's equations. The frequency range of validity for quasistatics in terms of the quasistatic parameter $\alpha = Lf/c$, see (3.16), is given by $\alpha \ll 1$. Within the range of validity, the error of Darwin's model with respect to Maxwell's model grows as $\mathcal{O}(\alpha^2)$, [137, 138, 139].

- When the physical eigenmodes are computed using a numerical method, the reduction of degrees of freedom leads to a discretization error, [140]. If the

equations of motion of Darwin's model are discretized using the FEM, it can be shown that the result converges with increasing mesh size [141].

- Only a limited set of eigenmodes of the field-theoretical model are used for the construction of the electrical circuit model. When the impedance functions are written as a rational function, it follows that the impedance function of the electrical circuit, (6.10), is equal to the impedance function of the Darwin model, (6.45), with all terms removed which have poles outside the frequency range of interest. Removing these terms gives rise to another error.

The error due to using Darwin's system of equations is an intrinsic error of electrical circuit modeling, i.e., it appears independently of the method used to construct electrical circuit models. It follows that the maximum frequency of validity for Darwin's model defines the frequency above which an electrical circuit model cannot be defined in a meaningful way. The error induced by the discretization of a physical system of equations is well understood and discussed in the literature. In the following, we will assume that the discretization is sufficiently fine such that no significant numerical errors are induced.

In this section, we concentrate on the error which is due to the finite number of eigenmodes. First note that if we allowed the electrical circuit model to become arbitrarily large, we would be able to take into account an arbitrary number of eigenmodes and thus reach an arbitarily accurate representation of the Darwin impedance function. In fact, this procedure is followed in some model order reduction techniques, [142]. However, the circuits constructed in this way lose their physical significance and become mathematical expressions reproducing the pole terms of the impedance function. In this thesis, we restrict ourselves to circuits of limited size, describing only a limited number of eigenmodes (in practical cases $\lesssim 10$). The error of the electrical circuit representation of impedance with respect to the full Darwin model is given by

$$\begin{aligned} \Delta\mathbf{Z}(s) &= \mathbf{Z}_{\text{circuit}}(\omega) - \mathbf{Z}_{\text{Darwin}}(\omega) \\ &= \delta^T \left(\sum_{k=n+1}^{N} \frac{\lambda_k}{s_k - s} \phi_k \phi_k^{\mathrm{T}} \right) \delta. \end{aligned} \tag{6.55}$$

where we have used the fact that the first n terms of the impedance functions agree by construction. In order to condense the matrix-valued, frequency dependent error into a figure of merit which can be handled more easily, we define the quality [143] of an electrical circuit by

$$
\begin{aligned}
Q = Q(\delta) &= \frac{\det(\mathbf{Z}_{\text{circuit}}(s=0))}{\det(\mathbf{Z}_{\text{Darwin}}(s=0))} \\
&= \frac{\det\left(\delta^{\mathrm{T}}\left(\sum_{k=1,s_k\neq 0}^{n} \frac{\lambda_k}{s_k}\phi_k\phi_k^{\mathrm{T}}\right)\delta\right)}{\det\left(\delta^{\mathrm{T}}\left(\sum_{k=1,s_k\neq 0}^{N} \frac{\lambda_k}{s_k}\phi_k\phi_k^{\mathrm{T}}\right)\delta\right)} \\
&= 1 - \frac{\det(\Delta\,\mathbf{Z}(s=0))}{\det(\mathbf{Z}_{\text{Darwin}}(s=0)}.
\end{aligned}
\tag{6.56}
$$

The quality has the following properties:

- By the properties of the determinant, the scalar quality is independent of the topology of the current source network and depends only on the positions of the electrodes. In other words, if the nodes of the circuit are renumbered or if the topology of the source network is changed, the corresponding permutation of rows and columns in δ leaves the determinant invariant.
- The quality is contained in the interval between 0 and 1. Increasing the quality to a value close to 1 induced an increased accuracy of the electrical circuit model.
- Intuitively speaking, the quality is maximized if the electrodes are at positions where the electric scalar potential ϕ is strong. In other words, the electrodes should be located at the minima and maxima of the scalar potential eigenmodes.

In the following section we discuss how the properties of the quality allow to define a procedure to automatically define optimal electrode positions.

6.4.3 The Importance of Electrode Positioning

In the previous section, we showed that the quality, i.e., the accuracy of an electrical circuit model, is a function of the electrode positions only. In practice, two situations have to be distinguished:

- The positions of the electrodes are unknown and the node positions should be determined using an algorithmic scheme.
- The positions of the electrodes have been specified by the user, e.g., because the user wants to evaluate the impedance function at specific positions.

In the first case, the optimal positions for the electrodes are exactly those which maximize the quality, i.e., the resulting electrical circuit model provides the best accuracy of all possible electrical circuit models. More specifically, it there are N eigenmodes in the frequency range of interest, the $n+1 = N+1$ nodes needed for the construction of an electrical circuit with exactly N eigenmodes have to be chosen according to

$$\{x_1, \cdots, x_n\} = \arg\left(\max_{\tilde{x}_1, \cdots, \tilde{x}_n \in \mathbb{R}^3} Q(\delta(\tilde{x}_1, \cdots, \tilde{x}_n) \right). \tag{6.57}$$

In the second case, experience indicates that the user defined nodes can only be used if their quality is sufficiently high. Otherwise, the electrical circuit elements can take unphysical values. If the user nevertheless needs to include the electrodes in the electrical circuit model, the user defined set of electrodes has to be augmented by electrodes at the correct positions. Furthermore, a very large set of electrodes can lead to the situation that there is not an equal number of eigenmodes in the frequency range of interest. Adding eigenmodes from outside the frequency range of interest usually only leads to deterioration of the quality instead of restoring the correct relationship. In this case, the procedure from Sect. 6.4.4 should be applied.

6.4.4 The Relationship between Modes and Nodes

In Sect. 6.4.1 we showed that the number m of eigenmodes used for the construction of the electrical circuit is related to the number $n+1$ of nodes of the electrical circuit model by $m = n$. In this section, we discuss the situation when the two numbers are not equal. We restrict ourselves to lossless electrical circuits.

If $m > n$, there are too many eigenmodes than can be reproduced by the electrical circuit. The problem can easily be remedied by adding further nodes (while maintaining good quality).

The opposite case, $m+1 < n$ appears more frequently and there is no obvious solution. If $m < n$, the matrices Φ in (6.19) cannot be inverted or, in other words, the linear systems of equations for the circuit matrices $\widehat{\mathbf{L}^{-1}}$ and $\widehat{\mathbf{G}}$ in terms of eigenmodes Φ,

$$\Phi^{\mathrm{T}} \widehat{\mathbf{C}} \Phi = \Lambda \qquad \Phi^{\mathrm{T}} \widehat{\mathbf{L}^{-1}} \Phi = \Lambda \mathbf{S}^2,$$

are underdetermined. This means that an electrical circuit with the desired spectral properties is not unique and the circuit elements can take arbitrary, even unphysical

values. In this section, we propose a procedure to recover uniqueness in a well-defined, physical way. The main idea is to decompose the electrical circuit into a resonant subcircuit and a non-resonant supply circuit. By definition, the resonant circuit has to be a complete LC circuit. On the other hand, the supply circuit consists of indutors only and does not have resonances of its own. The mathematical way of constructing a non-resonant circuit is to (formally) set the eigenfrequencies of the circuit to infinity (Sect. 5.1.6). An example of the topology of the resulting circuit is shown in Fig. 6.3.

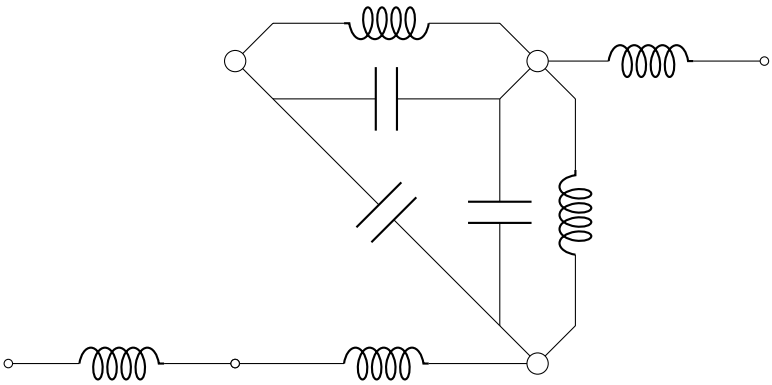

Figure 6.3.: Electrical circuit with unequal number of (finite) eigenmodes and electrodes: The capacitive subcircuit comprises the nodes with highest quality (large circles) only, nodes with low quality (small circles) are connected by inductors only.

More rigorously, the procedure can be decomposed in two steps. The first step is to choose $m+1$ nodes to form the resonant electrical circuit. The obvious choice are the $m+1$ nodes offering the best accuracy,

$$\{x_{i_0}, \cdots, x_{i_m}\} = \arg\left(\max_{y_0,\cdots,y_m \in \{x_0,\cdots,x_n\}} Q(\delta(y_0, \cdots, y_m) \right). \tag{6.58}$$

Eq. (6.58) is a special case of (6.57) when only existing electrodes are taken into account. By construction, the reduced electrical circuit exhibits the correct relationship between the number of nodes and modes. After renumbering if necessary, we can assume that $x_{i_j} = x_j, j = 0 \cdots m$.

In the next step, the reduced electrical circuit model will be enlarged by the remaining electrodes. In order to maintain the equality between the number of nodes

and the number of modes without introducing further resonances, each additional electrode is accompanied by an additional eigenmode with (formal) infinite eigenfrequency. These eigenmodes are constructed in the following way: Decompose all potential eigenmodes in the following way

$$\Phi_k = \Phi_{k,f} \oplus \Phi_{k,\infty} = \begin{pmatrix} \Phi_{k,f} \\ \Phi_{k,\infty} \end{pmatrix}, \qquad k = 1, \cdots, m,$$

where $\Phi_{k,f} = (\phi_k(x_1) - \phi_k(x_0), \cdots, \phi_k(x_m) - \phi_k(x_0))$ and $\Phi_{k,\infty} = (\phi_k(x_{m+1}) - \phi_k(x_0), \cdots, \phi_k(x_n) - \phi_k(x_0))$. The additional infinite eigenvalues are specifically set to zero at the reduced set of nodes,

$$\Phi_k = 0 \oplus \Phi_{k,\infty} = \begin{pmatrix} 0 \\ \Phi_{k,\infty} \end{pmatrix}, \qquad k = m+1, \cdots, n.$$

With the additional eigenmodes, the impedance function reads

$$\mathbf{Z} = -s\,\mathbf{A}_s^{\mathrm{T}} \Bigg[\underbrace{\sum_{k=1}^{m} \frac{\lambda_k}{s^2 - s_k^2} \Phi_k \Phi_k^{\mathrm{T}}}_{\left(\begin{array}{c|c} * & * \\ \hline * & * \end{array}\right)} + \underbrace{\sum_{k=m+1}^{n} \lambda_k \Phi_k \Phi_k^{\mathrm{T}}}_{\left(\begin{array}{c|c} 0 & 0 \\ \hline 0 & * \end{array}\right)} \Bigg] \mathbf{A}_s\,.$$

In the pictorial matrices, each star indicates a non-zero block submatrix. For the construction of the circuit matrices, (6.19) have to be altered,

$$\widehat{\mathbf{L}^{-1}} = \Phi^{-T} \left(\begin{array}{c|c} \mathbf{S}_f^2 \Lambda_f & 0 \\ \hline 0 & \Lambda_\infty \end{array} \right) \Phi^{-1} \quad \widehat{\mathbf{C}} = \Phi^{-T} \left(\begin{array}{c|c} \Lambda_f & 0 \\ \hline 0 & 0 \end{array} \right) \Phi^{-1}. \tag{6.59}$$

By construction, the capacitance matrix contains zero blocks at the positions of the additional electrodes. In pictorial form,

$$\widehat{\mathbf{C}} = \left(\begin{array}{c|c} * & 0 \\ \hline 0 & 0 \end{array} \right).$$

In other words, only the nodes $\{x_0, \cdots, x_m\}$ are connected to the capacitive circuit as desired. The corresponding subcircuit describes exactly the m eigenmodes.

In Chapter 7, this procedure is used in several applications:

- In Sect. 7.4.2, a battery pack is modeled as an electrical circuit. Only the batteries themselves form the resonant subcircuit. The external connectors are modeled as inductors and not connected to the capacitive subcircuit.

- In Sect. 7.3.1, a commutation cell for a solar inverter is modeled as an electrical circuit. In this extreme case, there are no non-zero eigenfrequencies in the frequency domain of interest. The electrical circuit is thus purely inductive in nature. Capacitors only exist between nodes on disjoint conductors.

6.4.5 Electrical Circuit Models for Lossy Systems

Our method for the construction of equivalent electrical circuits described in the previous section depends on the basic assumption that the nodes of the electrical circuit exist as distinguished points in the 3D geometry. Now consider the geometry of a simple 3D conductor, e.g. a round wire, and its equivalent electrical circuits: It is well known, e.g., from the description of a conductor in the PEEC method (Sect. 4.4), that a real conductor can be described as a series connection of a resistor and an inductor. The middle node seems to be a violation of the basic assumption that all nodes of the electrical circuit exist in reality. Clearly, there is no physical point which can be associated with it.

In order to remedy this seemingly flaw in the theory, we first note that the middle node does not have any physical significance and is only needed in order to assign to the conductor an impedance which can be written as a series connection of an inductor and a resistor, $R + sL$. Such a node can thus be safely ignored in the 3D computation. For the simple conductor geometry, for example, the scalar potential is evaluated at the end points only. Instead of directly interpreting the resulting vector of scalar potentials as the vector of node potentials of the equivalent electrical circuit, however, it has to be altered by some auxiliary nodes. More precisely, for each pair of nodes k and l which are located on the same conductor, an auxiliary node (k,l) is introduced which is assigned a scalar potential $\Phi(k,l) = \Re(\Phi(k)) + j\Im(\Phi(l)$. On the level of electrical circuits, the auxiliary node (k,l) is connected to the node k by an inductor and to the node l by a resistor only, i.e., the auxiliary node (k,l) is exactly the middle node introduced above.

7 Tests and Applications

In this chapter, our method is tested and applied to realistic examples. As sanity check, we compute electrical circuit models for conductor geometries for which analytical expression are known and prove the validity of both our method and the implemention. Our method is then applied to realistic examples describing real products from an industrial partner, Robert Bosch GmbH, [28].

7.1 Convergence Test

Before starting with practical examples, we check the implementation of the Finite Element discretization by computing the Maxwell eigenmodes of a rectangular resonator with perfectly conducting boundaries. The analytical solution for the eigenfrequencies of a rectangular resonator with side-length L read

$$f_{klm} = \frac{c}{2L}\sqrt{k^2 + l^2 + m^2}.$$

The lowest eigenfrequency is three-fold degenerated and given by

$$f_{110} = f_{101} = f_{011} = \frac{\sqrt{2}c}{L}.$$

In order to study the convergence of our implementation, we compute the triple of eigenfrequencies using different meshes and using first and second order basis functions for discretization. The meshes cover the computational domain homogeneously, i.e., there is no adaptive mesh refinement. The accuracy is defined by the maximum relative error of the triple of eigenfrequencies.

In Fig. 7.1a we show the accuracy relative to different mesh sizes for first and second order basis functions. For a mesh with N tetrahedral elements, the characteristic edge length is given by $l = L/\sqrt[3]{N}$. Convergence is plotted with respect to the dimensionless quantity $h = l/L$. The numerical result agrees remarkably well with the theoretically predicted rates of convergence.

For practical purposes, it is even more important to evaluate the efficiency of the method by comparing the accuracy relative to the number of degrees of freedom. In 7.1b we show that with the same number of degrees of freedom, the second order FEM provides significantly higher accuracy.

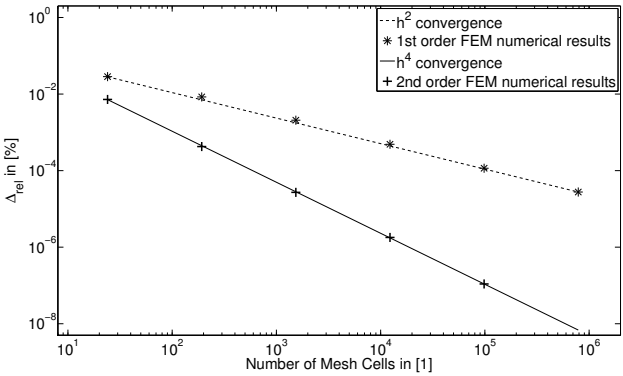

(a) Convergence vs. number of mesh cells

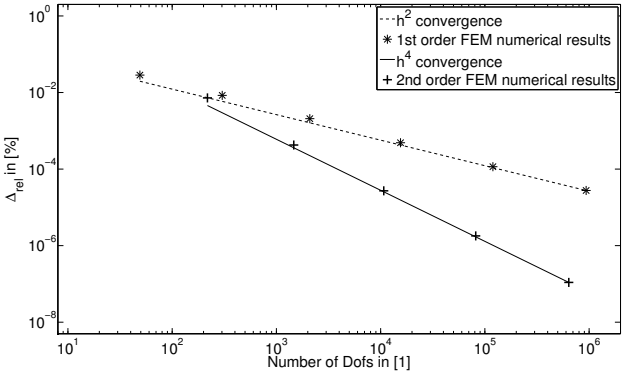

(b) Convergence vs. number of degrees of freedom

Figure 7.1.: Convergence of the triple of lowest eigenfrequencies of a rectangular resonator

7.2 Inductive Components

In this section, we discuss inductive components, i.e., components which can be described by a purely inductive electrical circuit model. Such a description is valid if two conditions are satisfied:

- All non-zero eigenfrequencies of the component are far above the frequency domain of interest. In this case, the $1/(s-s_k)$ terms in (6.45) can be replaced by the frequency-independent approximation $1/(s-s_k) \sim -1/s_k$.
- If there are static eigenmodes, i.e., $s_k = 0$, they do not play a role for the final analysis. This is usually the case when the component is a bare geometry, e.g., a Printed Circuit Board (PCB), which has to be populated for the final analysis. Recall that in this case, the static eigenmodes describe the capacitances of the bare geometry. When the PCB is populated with lumped semiconductor devices and lumped capacitors, the capacitances of the lumped elements are much larger than the capacitances of the bare geometry. The latter can therefore be neglected without significant loss of accuracy.

We emphasize that the above considerations do not imply that an eigenmode analysis of the populated component is not needed, e.g., for EMC analysis. However, the eigenmode analysis only leads to meaningful results when it is performed for the final, populated device. In practice, we therefore create an inductive circuit model for the bare geometry. This inductive circuit model can then be populated by additional lumped elements on the level of electrical circuits. The eigenmode analysis is then also performed on the level of electrical circuits.

Before studying practical examples, we also use this section to show results for some reference geometries where analytical formulae for partial inductances exist. In addition to the analytical proof in Sect. 6.2.5, we show that the definition of partial inductances provided by our method agrees with the reference definition in the PEEC method. More examples for inductance calculations can be found in [144].

7.2.1 Reference Geometries

Straight Round Wire

The first example is the computation of the partial self inductance and the partial resistance of a straight, round wire, as illustrated in Fig. 7.2. In order to

compute the partial resistance and inductance at low frequencies (i.e., when the total impedance is dominated by the resistance and the current flows homogeneously through the wire), the wire is modeled as conductor with homogeneous, finite conductivity of $6 \times 10^7\,\mathrm{S\,m^{-1}}$. In order to compute the partial inductance at high frequencies (i.e., total impedance is dominated by the inductance and current flow is restricted to the surface of the wire), the wire is modeled using perfectly conducting boundary conditions. In the high-frequency limit, no resistance is extracted. The excitation currents are impressed through facial electrodes (marked in red) at the end faces of the wire. The partial inductances and resistances are computed for different radius to length ratios r/l.

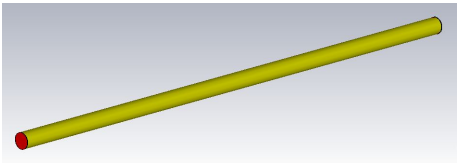

Figure 7.2.: Computer Aided Design (CAD) geometry of a straight round wire with electrodes (red)

For this geometry, an analytical expression for the partial self inductance (4.14) exists for both the low- and the high-frequency limit, [145],

$$\begin{aligned} \frac{L_{LF}(l,r)}{l} &= \frac{\mu_0}{2\pi}\left(\log\left(\frac{2l}{r}-\frac{3}{4}\right)\right) \\ \frac{L_{HF}(l,r)}{l} &= \frac{\mu_0}{2\pi}\left(\log\left(\frac{2l}{r}-1\right)\right) \\ \frac{R_{LF}(l,r)}{l} &= \frac{1}{\pi r^2 \sigma}. \end{aligned} \tag{7.1}$$

The comparison between computed and analytical values is shown in Fig. 7.3.

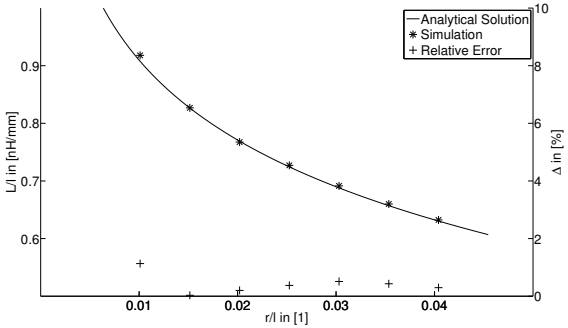

(a) Per length partial inductance at low frequencies

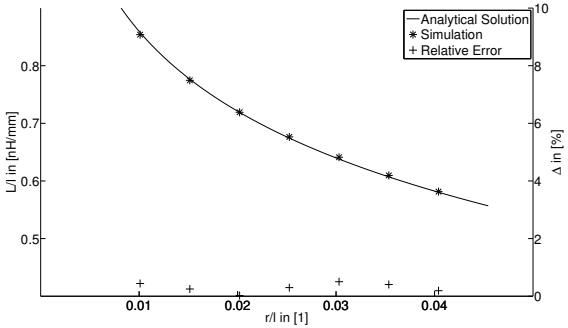

(b) Per length partial inductance at high frequencies

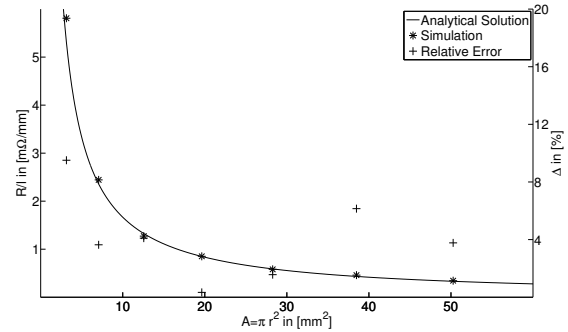

(c) Per length partial resistance at low frequencies

Figure 7.3.: Partial inductance and resistance of a straight round wire

Busbar

The second example is the computation of the partial self inductance and partial resistance of a busbar, as illustrated in Fig. 7.4. The busbar is modeled as a conductor with homogeneous, finite conductivity of $6 \times 10^7\,\mathrm{S\,m^{-1}}$. The excitation currents are impressed through facial electrodes (marked in red) at the end faces of the busbar.

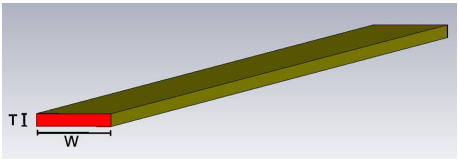

Figure 7.4.: CAD geometry of a busbar with electrodes (red)

To our knowledge, an analytical expression for the partial self inductance (4.14) of this geometry exists only in the low frequency limit, [145]. At high frequencies, there is current crowding at the edges of the conductor and the exact form of the current is not known, [146]. In the low frequency limit, the partial self inductance is a function of the aspect ratio $\omega = T/W$, where T and W are the width and height of the busbar as illustrated in Fig. 7.4. The comparison between computed and analytical values is shown in Fig. 7.5.

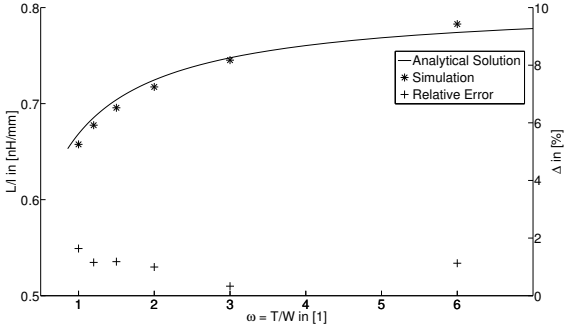

(a) Per length partial inductance at low frequencies

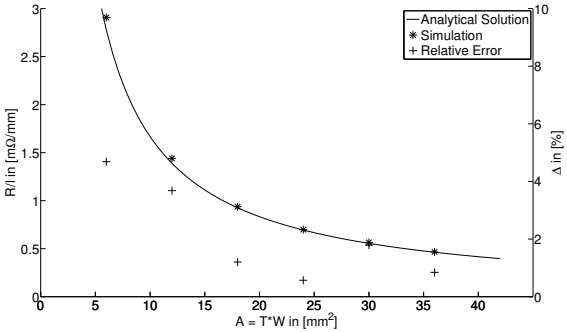

(b) Per length partial resistance at low frequencies

Figure 7.5.: Partial inductance and resistance of a busbar

7.2.2 Wireframe Package for Integrated Circuit

Fig. 7.6 shows a wireframe package which is used for the packaging of an integrated circuit (IC). The CAD model was taken from [65]. For signal integrity analysis, the knowledge of the partial self inductances of the wires and, in particular, the partial mutual inductances between neighbouring wires are of crucial importance.

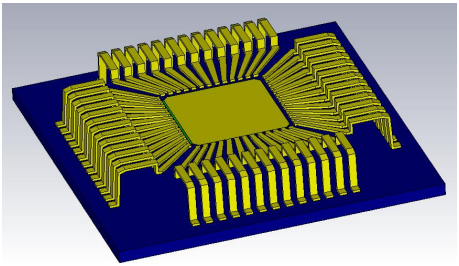

Figure 7.6.: CAD geometry of a wireframe package for an IC

For this geometry, an analytical formula for the partial self inductances of the wires and the partial mutual inductances between the wires does not exist. We therefore compare our results with results from a commercial inductance solver, ANSYS Q3D [147], which uses the PEEC method.

For the comparison in Fig. 7.7b, we fix one wire (which is marked red in Fig. 7.7a) and compute all partial mutual inductances to the other wires in the wireframes. For this purpose, the wires are numbered such that with increasing wire number, we circle the package once (as indicated by the red arrow in Fig. 7.7a). The comparison shows that the values of partial mutual inductance for neighboring wires agree very well. For wires with large spatial separation, the difference is larger. This is due to the fact that the PEEC method as an integral method excels at describing long-range interactions. Our implementation is based on a differential method, the FEM, and excels at describing short-range interactions of complex current densities. Such geometries are presented in the following sections. The absolute errors are very small.

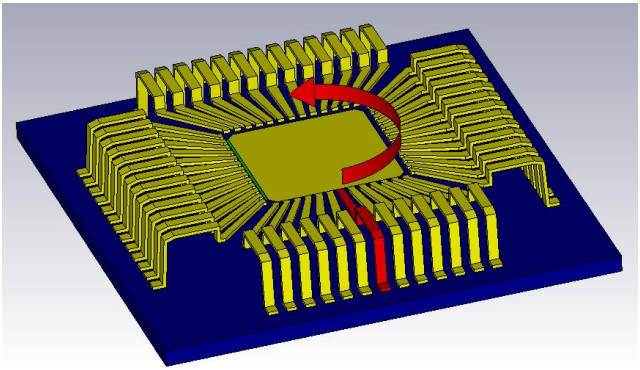

(a) Counting scheme for partial mutual inductances

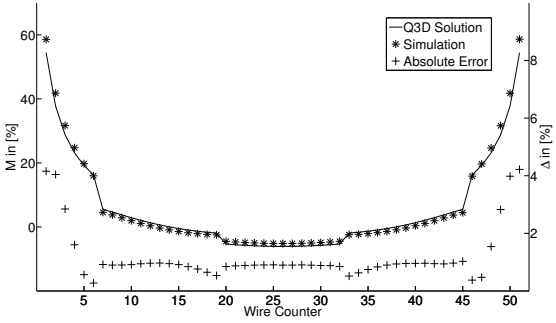

(b) Partial mutual inductances of wires

Figure 7.7.: Wireframe package results

7.3 Inductive Components with Static Capacitances

We proceed in this section to the study of inductive components where the capacitances between the disjoint conductors are also important, i.e., the static eigenmodes have to be included in the analysis. This is usually the case when the capacitances arising from the geometric arrangement of the conductors have the same order of magnitude as the lumped capacitors used to populate the component. An important field of application are multi-layered PCBs, where considerable capacitances can arise between the different layers of the board.

7.3.1 Commutation Cell for Photovoltaic Inverter

Fig. 7.8 shows a CAD model of a commutation cell for a photovoltaic inverter. This component was developed as part of the publicly funded project “ögP SOlar” [148].

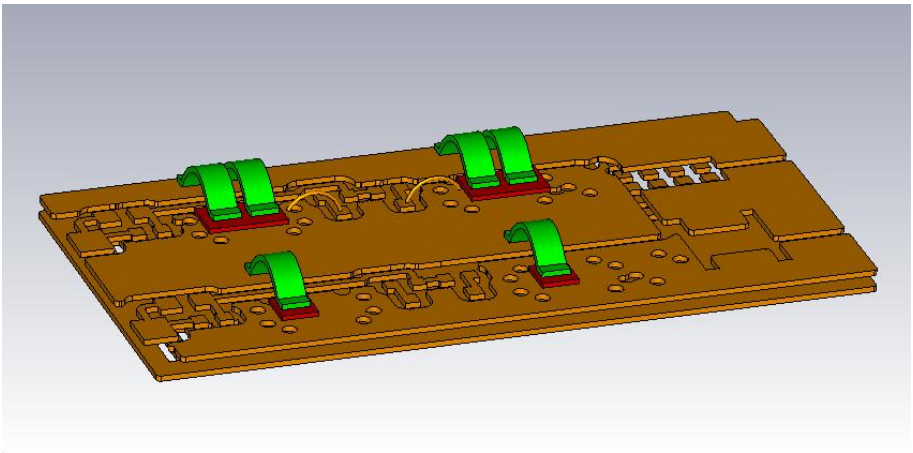

Figure 7.8.: CAD model of commutation cell

EMC Problems in Commutation Cell

In general, an inverter transforms an Alternating Current (AC) signal to a Direct Current (DC) signal or vice versa. For example, a photovoltaic inverter transforms a DC voltage from the solar cells to an AC current which can be fed into the electric power grid. An inverter consists of two basic components: The commutation cell

chops the DC signal into a periodic series of pulses, a filter then smooths the pulse functions into a sinusoidal signal.

In this example, analysis is restricted to the commutation cell. The basic functioning of the commutation cell is visualized in Fig. 7.9. The voltage source charges the voltage link capacitors C_l such that there is a voltage drop of $V/2$ at each of the two capacitors. When T_1 is switched on and T_0 is switched off, the current flows along the blue line and there is a voltage drop $V/2$ at the load. In the opposite case, T_1 off and T_0 on, the current flows along the red line and there is a voltage drop $-V/2$ at the load. In particular, the direction of the current flow through the load is reversed. When the two configurations are applied alternatingly, there is an effective AC current through the load.

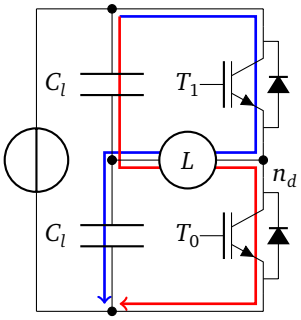

Figure 7.9.: Electrical circuit for ideal commutation cell: voltage link capacitors C_l, dynamical node n_d, IGBTs T_0 and T_1, load L

A real commutation cell suffers from different parasitic effects, deteriorating device performance. The two most frequent parasitic processes are visualized in Fig. 7.10 and Fig. 7.11: In Fig. 7.10a, it is shown that parasitic capacitances in parallel with the IGBTs offer an alternate path for the time-dependent current (dashed). This leads to an increase of the current through the IGBTs, Fig. 7.10b and a deterioration of efficiency. In Fig. 7.11a, the connection between the link capacitors and the IGBTs is modeled by a parasitic inductor to account for a conductor with non-zero physical length. During the switching process, the currents through the inductor change from zero to full current or vice versa. This leads to an induced voltage overshoot at the IGBTs. In order to keep the peak voltage below the breakdown voltage of the semiconductor and prevent damage of the IGBTs, the switching times cannot become arbitrarily short. Slow switching, however, again leads to deterioration of the efficiency of the inverter.

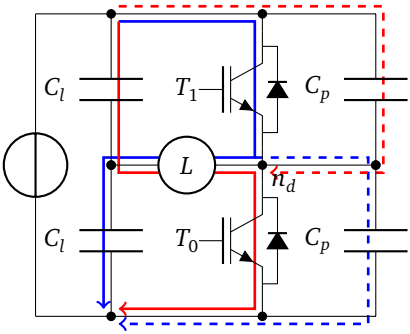

(a) Displacement currents in parasitic capacitors (dashed)...

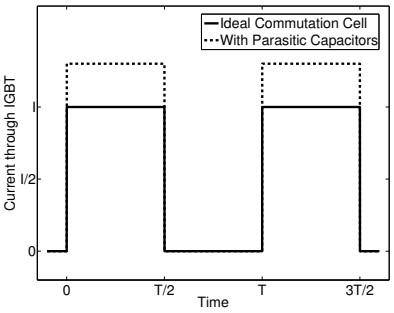

(b) ... lead to higher current through the IGBTs.

Figure 7.10.: EMC problems in commutation cell I: parasitic capacitors

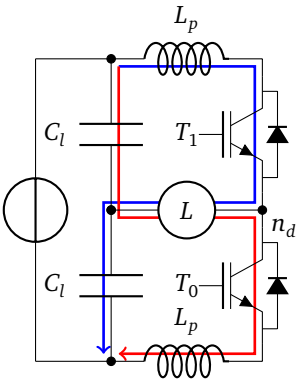

(a) Parasitic inductors L_p in commutation cell...

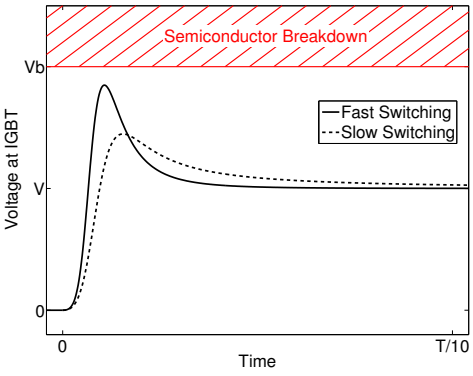

(b) ... lead to voltage overshoots at IGBTs.

Figure 7.11.: EMC problems in commutation cell II: parasitic inductors

Equivalent Electrical Circuit

In the above section, we showed that the main parasitic processes in a commutation cell can be explained on the level of electrical circuits. The values of the parasitic elements are determined by the 3D design of the commutation cell only. This enables us to compute them in a 3D simulation of the bare geometry, i.e., without the need to include the lumped elements (e.g., link capacitors, IGBTs). The behavior of the complete commutation cell can be simulated on the level of electrical circuits, i.e., by inserting the lumped elements in the equivalent electrical circuit for the 3D geometry.

In this section, we construct an electrical circuit model for the bare geometry of the commutation cell in Fig. 7.8. An eigenmode analysis shows that the lowest eigenfrequency is $\approx 500\,\mathrm{MHz}$ which is far higher than the highest frequency of interest given by the typical rise time of the current pulses, $\tau_{\mathrm{rise}} \approx 100\,\mathrm{ns}$, $f_{\mathrm{max}} \approx 0.35\tau^{-1}_{\mathrm{switching}} = 3.5\,\mathrm{MHz}$. It thus suffices to construct an electrical circuit consisting of inductances and augmented by those capacitances which belong to static eigenmodes only.

The positions of the electrodes are shown in Fig. 7.12a. The electrodes correspond to the nodes of the equivalent electrical circuit model in Fig. 7.12b. The electrical circuit can be decomposed into two subcircuits, an inductive subcircuit and a capacitive subcircuit. The inductive subcircuit consists of four disjoint parts. Each disjoint part corresponds to one disjoint conductor. According to Sect. 6.1, the inductive subcircuit does not form closed loops. The capacitive subcircuit, on the other hand, connects the disjoint conductors, i.e., it connects the inductive subcircuits. Note, first, that the capacitive subcircuit is connected. In the physical reality, each pair of separate conductors shares a common capacitance. Note, second, that from the set of all nodes on the same conductor, only one node is chosen to be part of the capacitive subcircuit. The full circuit therefore does not have cycles containing both inductive and capacitive elements, i.e., by construction, the circuit does not exhibit resonances at finite, non-zero frequencies. The values of the partial self inductances and capacitances of the electrical circuit are tabulated in Fig. 7.13. The values for the partial mutual inductances are tabulated in Appendix A.

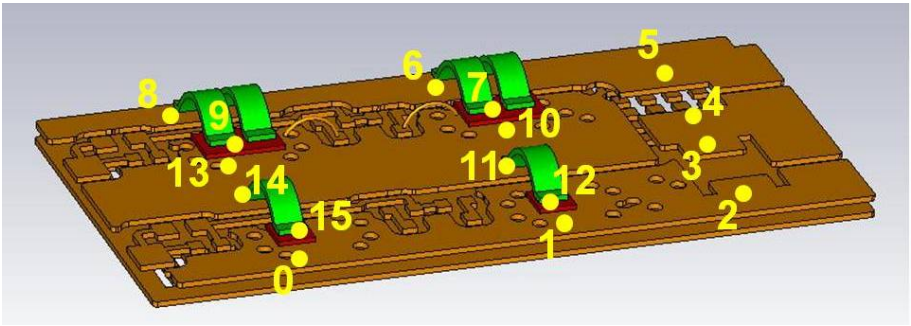

(a) Electrode positions for commutation cell

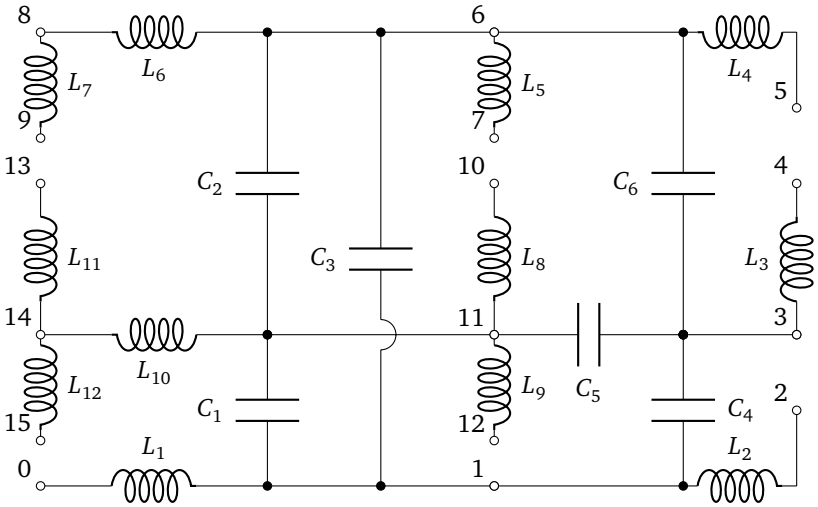

(b) Electrical circuit model for commutation cell

Figure 7.12.: Commutation cell: electrodes and equivalent electrical circuit

	$\mathbf{L}$ [nH]	$\mathbf{L}_{Q3D}$ [nH]	Δ [%]
L_1	5.3	5.3	1
L_2	3.4	3.3	3
L_3	1.2	1.1	8
L_4	3.5	3.4	3
L_5	1.4	1.5	4
L_6	5.8	6.0	3
L_7	1.5	1.5	6
L_8	1.1	1.0	11
L_9	2.0	2.1	7
L_{10}	4.5	4.5	1
L_{11}	1.1	0.9	13
L_{12}	2.0	2.2	6

	$\mathbf{C}$ [pF]	$\mathbf{C}_{Q3D}$ [pF]	Δ [%]
C_1	2.19	2.05	7
C_2	2.45	2.65	9
C_3	0.82	0.87	6
C_4	0.40	0.37	10
C_5	0.34	0.33	3
C_6	0.43	0.43	1

Figure 7.13.: Commutation cell: electrical circuit element values

7.4 Components exhibiting LC resonances

In the examples discussed in this section, the frequency range of interest reaches beyond the first non-zero eigenfrequency. This is the most general case and the electrical circuit models also have to describe the resonant behavior of the device.

7.4.1 Transformer

Fig. 7.14 shows a CAD model of a typical transformer for power electronics applications. In general, a transformer consists of two windings, a primary winding which is connected to an electrical energy source, and a secondary winding which is connected to an electrical load. When an AC voltage is applied to the primary winding, an AC voltage is induced in the secondary winding. For an ideal transformer, the voltage ratio $\alpha = V_2/V_1$ between the primary and the secondary winding is determined by the ratio of winding turns N_1 and N_2 respectively, $\alpha = N_2/N_1$. A real transformer exhibits loss mechanisms, e.g. stray magnetic fields and magnetic losses in the core, leading to a lower voltage ratio. In order to increase the maximum current supported by the transformer, a transformer can be constructed by connecting several identical transformer in parallel.

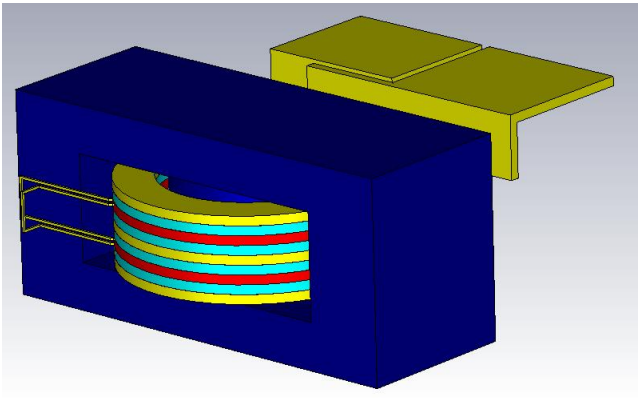

Figure 7.14.: CAD drawing of transformer

The primary winding of the transformer considered in this work consists of two parallel coils, which are stacked above each other. Each coil has 13 turns. The secondary side consists of three parallel coils, each coil having one turn. The winding ratio is thus $N_2/N_1 = 1/13$. In order to minimize stray magnetic fields, the trans-

former is equipped with a highly permeable core consisting of N97 material with constant permeability $\mu_r = 2300$.

A description of transformers including parasitic elements is important whenever the transformer is used to transform high-frequent signals. For example, in [149], a detailed model is derived to model the parasitic capacitances of transformer used for very short voltage pulses.

Eigenmode Computation

In order to numerically compute eigenmodes, the Darwin system (3.19) is discretized using the second order FEM. The eigenmodes of the resulting generalized eigenvalue problem were computed using the Lanczos method, described in Sect. 5.2.3. The eigenmode plots were generated using Paraview, [150]. Only the scalar potential part ϕ_k of the Darwin eigenmodes $(\phi_k, \mathbf{E}_k)$ was plotted.

The first eigenmodes have eigenfrequencies 0.34 MHz, 44.7 MHz, and 64.3 MHz. The corresponding eigenmodes are shown in Fig. 7.15. Note that there is a gap of two orders of magnitude between the first eigenmode in the spectrum and all following eigenmodes. This gap is due to the symmetrical nature of the transformer, which is essentially a parallel connection of several coils. It can be seen from Fig. 7.15 that the first eigenmode is symmetrical with respect to the parallel coils while all higher eigenmodes are asymmetrical.

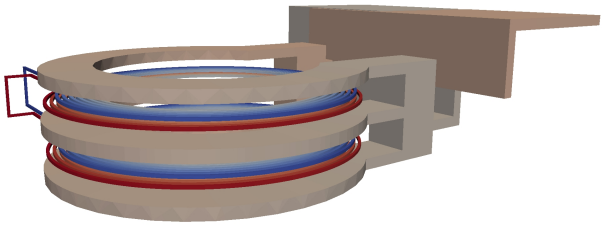

(a) 0.34 MHz

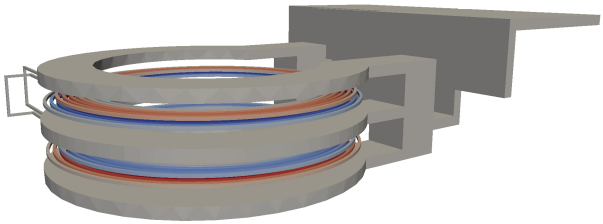

(b) 44.7 MHz

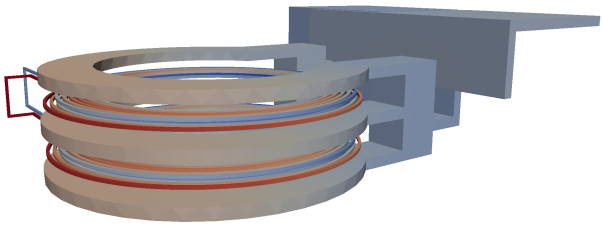

(c) 64.3 MHz

Figure 7.15.: Transformer: scalar potential of Darwin eigenmodes with lowest eigenfrequency

Computation of node positions

From Fig. 7.15 we can see that while there are large voltage variations of the eigenmodes on the primary winding, there is only little variation on the secondary winding. Intuitively, this can be understood by noting that the higher number of turns on the primary side and the smaller distance between the turns leads to higher values for the inductances and capacitances associated to the primary windings than to the secondary windings. The eigenfrequencies being of the order $1/\sqrt{LC}$, we conclude that the low-frequency eigenmodes are essentially due to the primary winding only.

Based on the above considerations, we assign two nodes to the secondary side, at each end point of the windings. The nodes on the secondary winding allow to express the voltage along the secondary winding in terms of the equivalent electrical circuit. The number of nodes assigned to the primary winding depends on the frequency range of interest:

- If only the first resonance is of interest, it suffices to choose two nodes on the primary windings. Inspecting the first eigenmode (Fig. 7.15a), we conclude that the nodes have to be chosen at the terminal points of the primary windings, where the potential associated to the first eigenmode is extremal.

- If more resonances are of interest, further nodes have to be added. In this investigation, we construct an equivalent electrical circuit which is valid up to the third resonance. In Fig. 7.15, we see that the high-frequency eigenmodes arise from oscillations between the different layers of the primary windings. We thus assign one node to each layer.

We will treat both cases and show, how the frequency range of validity depends on the number and position of the nodes. The positions of the nodes for the two cases are shown in Fig. 7.16.

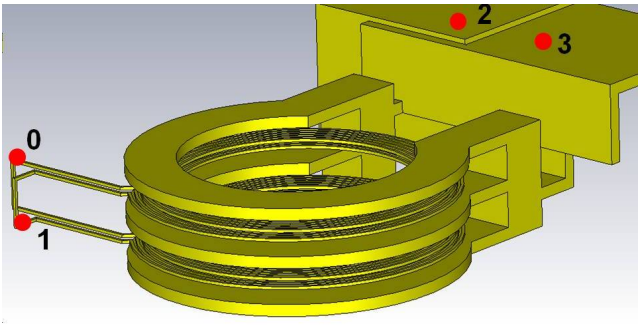

(a) Node positions for equivalent electrical circuit describing the first dynamical resonance

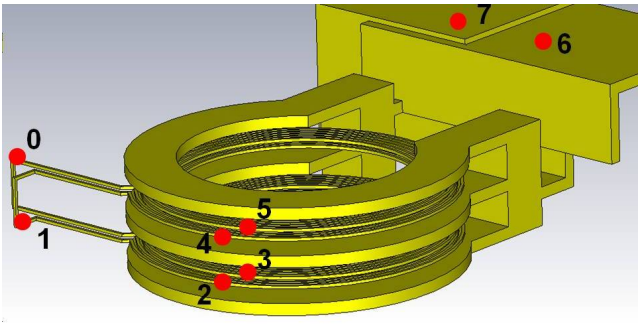

(b) Node positions for equivalent electrical circuit describing the first three dynamical resonances

Figure 7.16.: Node positions for the transformer

The equivalent electrical circuit for the transformer can be constructed from the eigenmodes computed in the previous section. We construct first the most simple equivalent electrical circuit describing the first eigenmode with non-zero eigenfrequency only. For this, we use the first eigenmode in Fig. 7.15a only and choose the node positions as in Fig. 7.16a. The resulting electrical circuit model is shown in Fig. 7.17. Note that only three nodes are part of the capacitive subcircuit according to the analysis in Sect. 6.4.4. This is because only two eigenmodes are taken into account - one static eigenmode and one eigenmode with non-zero eigenfrequency.

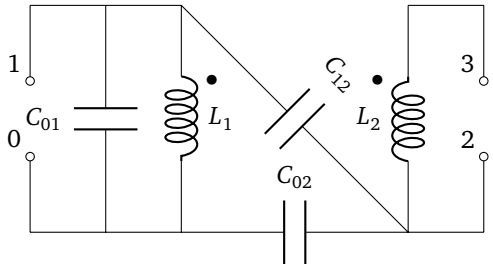

(a) Topology

L	μH
L_1	2580
L_2	15

K	%
K_{12}	99.1

C	pF
C_{01}	78.5
C_{02}	12.2
C_{12}	13.5

(b) Element values

Figure 7.17.: Electrical circuit model for the transformer (1 resonance)

We next construct an equivalent electrical circuit with a larger frequency range of validity. In particular, we want the equivalent electrical circuit to describe the resonances at 44.7 MHz and 64.3 MHz also. The equivalent circuit in Fig. 7.17 then necessarily has to be enlarged by adding further nodes. As argued above, we use the node positions in Fig. 7.16b. The equivalent electrical circuit then takes a more complicated form shown in Fig. 7.18. For simplicity, in Fig. 7.18 we only show the inductive subcircuit. We implicitely assume that for each pair (k,l) of nodes, there exists a capacitor C_{kl} between them and we refrain from showing them explicitly in Fig. 7.18.

Note that in the equivalent electrical circuit in Fig. 7.18 the parallel structure of the real transformer in Fig. 7.14 is resolved, unlike the first equivalent electrical

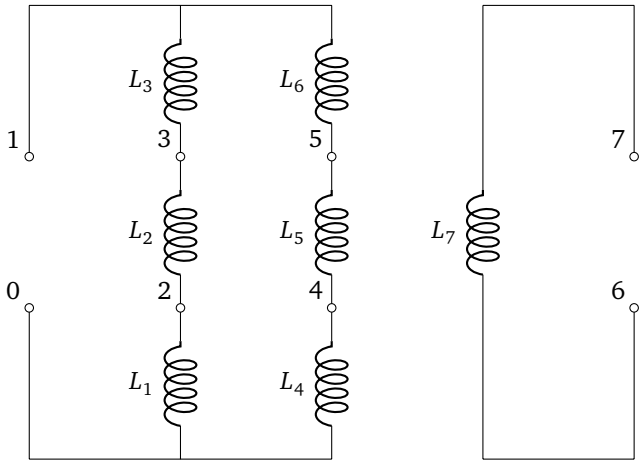

(a) Topology: It is assumed implicitly that for each pair of nodes (k, l) there exists a capacitance $C_{k,l}$. Each pair of inductors shares a mutual inductance.

L	μH
L_1	305
L_2	381
L_3	190
L_4	305
L_5	381
L_6	190
L_7	15

K	%
K_{12}	99.0
K_{13}	99.8
K_{14}	99.7
K_{15}	99.4
K_{16}	99.7
K_{17}	99.1
K_{23}	99.4
K_{24}	99.4
K_{25}	99.4
K_{26}	99.7

K	%
K_{27}	99.0
K_{34}	99.7
K_{35}	99.7
K_{36}	99.7
K_{37}	99.2
K_{45}	99.0
K_{46}	99.8
K_{47}	99.1
K_{56}	99.4
K_{57}	99.0
K_{67}	99.2

C	pF
C_{01}	13.4
C_{02}	44.5
C_{03}	2.7
C_{04}	43.2
C_{05}	3.5
C_{06}	3.2
C_{07}	0
C_{12}	2.7
C_{13}	0.4
C_{14}	38.9
C_{15}	20.5
C_{16}	6.2
C_{17}	0
C_{23}	22.3

C	pF
C_{24}	20.8
C_{25}	9.8
C_{26}	3.3
C_{27}	0
C_{34}	2.7
C_{35}	0.4
C_{36}	5.9
C_{37}	0
C_{45}	23.0
C_{46}	3.3
C_{47}	0
C_{56}	3.7
C_{57}	0
C_{67}	0

(b) Element values

Figure 7.18.: Electrical circuit model for the transformer: 3 resonances

circuit from Fig. 7.17. This is because the eigenmodes at higher frequencies, Fig. 7.15b and 7.15c, are asymmetrical with respect to the parallel structure of the

transformer, while the first eigenmode in Fig. 7.15a respects the symmetry of the parallel structure and therefore cannot resolve it.

Impedance Comparison

In order to check the accuracy of the equivalent circuit, we compute the impedances at the terminal ports of the primary and secondary windings and compare the result with a 3D field simulation using the Darwin model. For brevity, we restrict ourselves to Z_{12}, the transfer function from the primary to the secondary winding. For the simple electrical circuit model in Fig. 7.17, the results are plotted in Fig. 7.19.

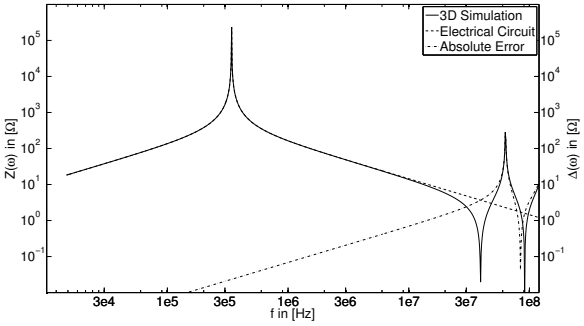

Figure 7.19.: Transformer: comparison of the equivalent electrical circuit in Fig. 7.17 with 3D simulations

As expected, there is very good agreement in the low-frequency regime up to approximately 10 MHz. By construction, the equivalent electrical circuit correctly reproduces the first singularity in the impedance function. In order to describe resonances at higher frequencies, the more complex equivalent electrical circuit in Fig. 7.18 has to be used. By construction, it extends the range of validity beyond the second and third singularity. For verification, we again compute Z_{12} and compare the result with a 3D simulation using the Darwin model, Fig. 7.20.

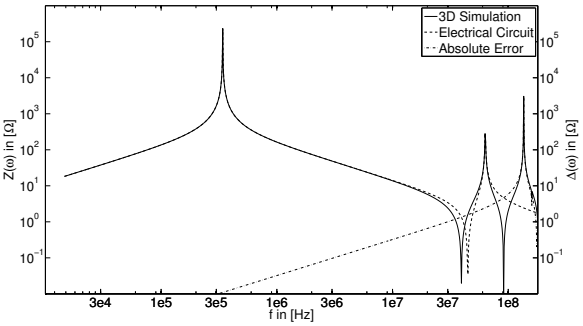

Figure 7.20.: Transformer: comparison of the equivalent electrical circuit in Fig. 7.18 with 3D simulations

7.4.2 Battery Pack

Fig. 7.21 shows a battery pack from the automotive industry. In general, a battery pack consists of several identical battery cells which are connected in parallel or in series in order to maximize current or voltage respectively. In a real battery pack, the battery cells may behave differently due to manufacturing tolerances or degradation. In order to optimize the overall performance of the battery pack, i.e. in order to have maximum flexibility regarding load profiles at maximum lifetime, it is crucial that the load is distributed among the cells such that each battery cell is used most efficiently. This requires that each battery cell is monitored individually. For this, each battery cell is equipped with a sensor operating at a sufficiently high frequency to avoid interference with the operating mode of the battery. We are thus interested in the behavior of the battery pack at relatively high frequencies, especially in resonance effects which might interefere with sensor signals. In particular, in order to make the sensor signals robust to interference, we aim at specifying an operating frequency which is far away from any resonance of the battery pack system. The operating frequency therefore has to be defined either below the first eigenfrequency or, if it exists, in a gap in the spectrum.

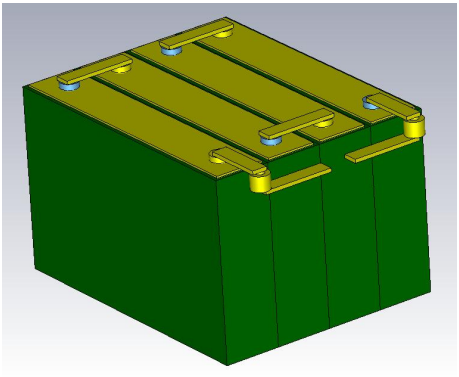

Figure 7.21.: CAD drawing of battery pack

The battery pack considered in this work consists of four battery cells which are connected in series. Each battery cell is packed into a metallic housing of 15 cm times 9.0 cm times 3 cm. The housings are 4 mm apart, the gaps between the battery cells are filled with non-conducting, dielectric lacquer. The series connection of the battery cells is formed by conducting bars connecting the electrodes. Additionally, the first and the last electrode are connected to a terminal port. Our

investigations concentrate on frequencies which are much higher than the typical time-scales of the chemical processes in the batteries. The batteries are therefore modeled as conductors, the DC currents are not included in the investigations. Furthermore, damping is unimportant for our investigations. All conductors, i.e. the housings and the connecting bars of the battery cells, are modeled as perfect electric conductors.

Eigenmode Computation

In order to numerically compute eigenmodes, we discretized the Darwin system (3.19) using the second order FEM. The eigenmodes of the resulting generalized eigenvalue problem were computed using the Lanczos method, described in Sect. 5.2.3.

The lowest eigenmodes have eigenfrequencies 77 MHz, 82 MHz, 83 MHz, and 330 MHz, [143]. While the first three eigenfrequencies are closely clustered, there is a gap of roughly one order of magnitude between the third and the fourth eigenfrequency. It is advisable to choose the operating frequency inside this gap. Above the fourth eigenfrequency, the spectrum becomes increasingly dense. Only the first three eigenfrequencies are in the frequency range of interest. The corresponding eigenmodes are shown in Fig. 7.22. The eigenmode plots were generated using Paraview, [150]. Only the scalar potential part ϕ_k of the Darwin eigenmodes $(\phi_k, \mathbf{E}_k)$ was plotted.

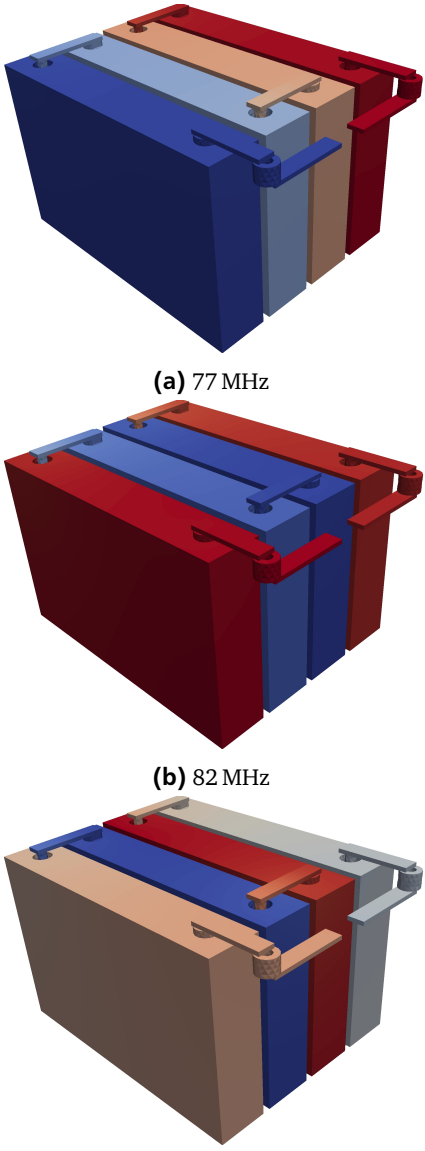

(a) 77 MHz

(b) 82 MHz

(c) 83 MHz

Figure 7.22.: Battery pack: scalar potential of Darwin eigenmodes with lowest eigenfrequency

Studying the eigenmodes in Fig. 7.22a-7.22c, we see that the eigenmodes are essentially oscillations of the battery cells relative to each other. In particular, each cell itself is an equipotential volume. We therefore assign one electrode to each of the battery cells. According to Sect. 6.4.4, these four nodes can be used to construct an electrical circuit with exactly three eigenfrequencies. The electrodes are numbered as 0-3 in Fig. 7.23.

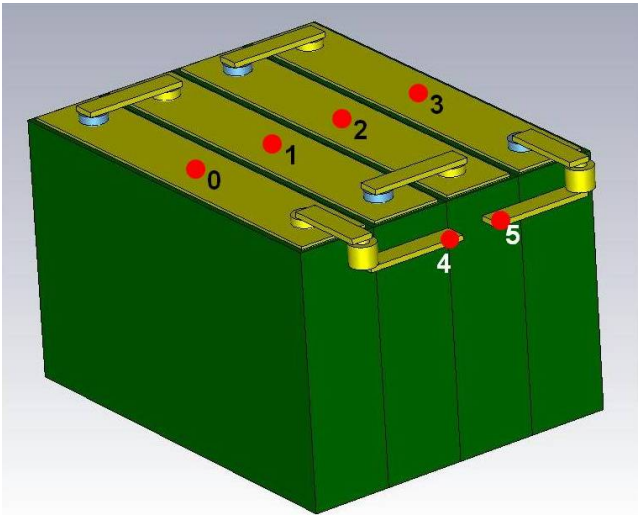

Figure 7.23.: Battery pack: electrode positions

We add two more nodes, labeled 4 and 5 in Fig. 7.23, at the end points of the terminal port. While these nodes do not participate in the resonant behavior, they can be used to compute the impedance at the terminal.

The equivalent electrical circuit for the battery pack can be constructed from the eigenmodes computed in the previous section. We emphasize that the resonant behavior can be described entirely by the subcircuit comprising nodes 0-3 only, [143]. According to the discussion in Sect. 6.4.4, nodes 4 and 5 are not included in the capacitive network and are connected to nodes 0-3 by inductors only.

The inductance matrix **L** and the capacitance matrix **C** are computed from the 3D eigenmodes according to the procedure in Sect. 6. The resulting circuit is shown in Fig. 7.24.

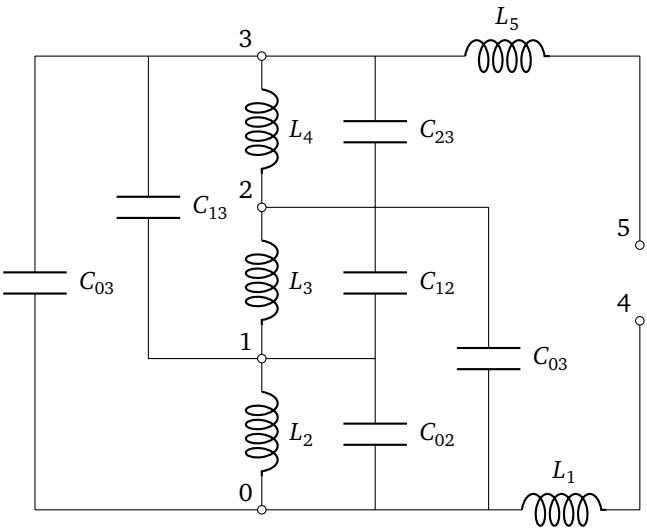

(a) Topology: It is assumed implicitly that each pair of inductors shares a common partial mutual inductance.

L	nH
L_1	50.2
L_2	32.8
L_3	32.8
L_4	32.9
L_5	27.0

C	pF
C_{01}	113
C_{02}	2.4
C_{03}	4.3
C_{12}	111
C_{13}	2.2
C_{23}	113

K	%
K_{12}	3.4
K_{13}	-2.2
K_{14}	1.2
K_{15}	-0.8
K_{23}	0.1
K_{24}	-0.1
K_{25}	1.2
K_{34}	0.01
K_{35}	-3.1
K_{45}	3.1

(b) Element values

Figure 7.24.: Electrical circuit model for the battery pack

Impedance comparison

In order to check the accuracy of the equivalent circuit, we compute the impedance at the terminal port and compare the result with a 3D field simulation using the Darwin model. The results are plotted in Fig. 7.25.

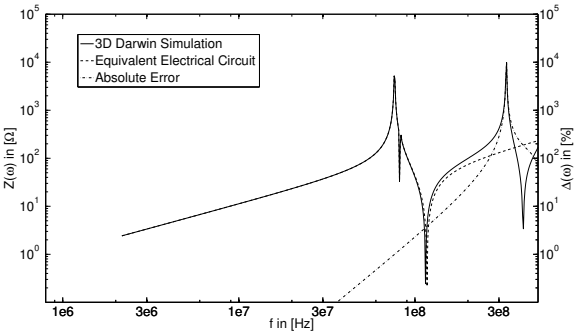

Figure 7.25.: Battery pack: Comparison of the impedance from the 3D simulations and the equivalent electrical circuit

As expected, there is very good agreement in the low-frequency regime up to 100 MHz. By construction, the equivalent electrical circuit correctly reproduces the first three singularities in the impedance function. The equivalent circuit does not reproduce singularities at higher frequencies. If needed, further resonances can be included by adding further nodes, thus enlarging the equivalent circuit.

8 Conclusion

In this thesis, we presented an automated procedure to construct electrical circuit models for electromagnetic components or systems. The method is formulated on the level of field equations, i.e., it is very general and can be implemented numerically using any scheme for the discretization of partial differential equations. With a reference implementation using the FEM, the validity and feasibility of the procedure was shown. In this chapter, we will shortly reiterate the necessary steps for the method. We will sum up the main contributions of this work and show future extensions and fields of applications.

8.1 Summary

In Chapter 1, we formulated three requirements for electrical circuit models to be valid and useful models for electromagnetic components and systems:

- Compactness: The electrical circuit model is as compact as possible while reproducing all relevant interactions in the frequency range of interest.
- Physicality: The elements of the electrical circuit model can be related to physical properties of the electric component or system.
- Accuracy: The accuracy of the electrical circuit is controllable and respects with user-defined limits.

In this thesis, we proposed an automated procedure for the construction of such models. The main steps of our method are:

1. Taking as input a **3D CAD model** of the electromagnetic component or system, including material data and boundary conditions.
2. Equipping the 3D model with **electrodes**. These electrodes will become the **nodes** of the electrical circuit model. The relationship between electrodes and nodes provides the link between the circuit model and the 3D model, i.e., the circuit satisfies the physicality requirement. The locations of the nodes depend on the application, they can be defined by the user or they can be determined by an automated procedure (Sect. 6.4.3).

3. Describing the electromagnetic properties of the component or system by an appropriate **physical model**. Instead of Maxwell's equations, we use a quasistatic approximation, Darwin's model (Sect. 3.4.3). Darwin's approximate model removes from Maxwell's equations all phenomena which cannot be explained by electrical circuit models (Sect. 6.2).

4. Computing the **electromagnetic eigenfrequencies and eigenmodes** of the component or system. Comparing the eigenfrequencies with the frequency range of interest allows us to separate relevant from irrelevant interactions (Sect. 6.4.4). Removing irrelevant effects allows us to construct very compact circuit models, i.e., the circuit models satisfy the compactness requirement.

5. Using a projection procedure to map the 3D eigenmodes on **circuit eigenmodes** of the corresponding electrical circuit model (Sect. 6.4).

6. The projection procedure can be controlled strictly to yield a very **direct measure for accuracy** of the electrical circuit model, thus guaranteeing the accuracy requirement. The accuracy is a function of two parameters only, the number and the locations of the electrodes.

7. Computing the **explicit form of the electrical circuit model** from the circuit eigenmodes (Sect. 6.1.2).

Our procedure is formulated on the basis of electromagnetic field equations and circuit equations. This allows for very general numerical analysis. More precisely, the procedure can be implemented using any numerical scheme for the discretization of partial differential equations, thereby exploiting the advantages of the individual schemes. In particular, the computation of partial inductances has been made available to numerical schemes different from the PEEC method.

In the course of this thesis, a reference implementation was developed based on the FEM. Using the FEM, complex geometries and dielectric or permeable materials can be described very easily. The implementation uses first or second order basis functions for the scalar potential, and, correspondingly, first and second order Nedelec basis functions for the vector potential. An eigenmode solver was implemented based on the Lanczos method. This eigenmode solver handles linear eigenvalue problems only, thereby restricting the field of application to lossless electromagnetic systems. The extension of the formalism to quadratic eigenvalue problems for lossy electromagnetic components or systems was described in the course of this work. However, the numerical implementation goes beyond the

scope of the work. By interfaces to commercial software, the implementation can be embedded in the simulation workflow at industrial companies. Selected use-cases were shown in this work. The validity and functionality of the approach was proven. At present, the implementation is in use at Robert Bosch GmbH, [28], for purposes of EMC analysis of existing and future products.

8.2 Contributions

In the course of this work, many techniques and results have been used. Not all of them are new and innovative. In this section, we point out our own contributions and contributions taken from other authors.

- The relationship between Darwin's model and electrical circuits is well known in literature. Some references are given in the corresponding sections. Similarly, the description of electromagnetic components and devices using partial circuit elements has been the subject of long-time research. The definitions and properties of partial circuit elements in Sect. 4.4 were taken from the cited references in the section.

- The definition of partial circuit elements using a system of partial differential equations (Sect. 6.2) has not been stated in this form before. More precisely, the method of incorporating lumped current sources into the field-theoretical equations of motion, (6.32) and (6.33), has not been stated explicitely before.

- The theory of polynomial eigenvalue problems, Chap. 5, is well known in the literature. However, to our knowledge, the juxtaposition of the spectral content of electrical circuits and the spectral content of Darwin's model, Sect. 6.3, and the similarities of the spectral content have not been shown before.

- Electrical circuit models have been constructed from model-order reduced representations of an impedance function in the literature. However, these models usually suffer from a lack of physicality. The novel feature in this work is the construction of electrical circuits from circuit eigenmodes which guarantee the physicality of the electrical circuit models.

- In the course of this work, numerical methods have been used for the discretization of the field-theoretical model and for the computation of 3D eigenmodes. Third-party software is referenced at the appropriate positions in the thesis. The Finite Element discretization for Darwin's model

and the Lanczos algorithm for the solution of the matrix eigenvalue problem have been implemented by the author. The implementation is largely based on existing procedures from the literature cited in this thesis.

8.3 Outlook

The method presented in this paper can be applied to a wide range of electromagnetic problems in an academic and industrial environment.

- The restriction of the implementation to lossless systems is sufficient for EMC analysis, concentrating on high-frequency effects. Extending the implementation to describe lossy systems requires the solution of quadratic eigenvalue problems. However, with the additional numerical effort, electrical circuit models can be constructed which are valid from the DC regime to high-frequencies, i.e., the entire frequency domain of operation can be covered.

- In order to use electrical circuit models in multi-domain optimizations of electricomagnetic components and systems, it is highly desirable to express the circuit elements in terms of geometry parameters. With this knowledge, any sensitivity analysis on the level of electrical circuits can immediately be generalized to a sensitivity analysis of design parameters. It is promising, therefore, to combine the method presented in this work with existing work on parametric model order reduction.

A Mutual Inductances of Commutation Cell

	$\mathbf{M}$ [%]	$\mathbf{M}_{Q3D}$ [%]	Δ_{abs} [%]		$\mathbf{M}$ [%]	$\mathbf{M}_{Q3D}$ [%]	Δ_{abs} [%]
M_{1-2}	22.7	24.5	1.8	M_{4-8}	-11.6	-14.3	2.7
M_{1-3}	-5.9	-6.6	0.7	M_{4-9}	-7.4	-8.1	0.7
M_{1-4}	-25.5	-25.5	0.1	M_{4-10}	27.7	27.4	0.3
M_{1-5}	3.9	2.6	1.4	M_{4-11}	-8.1	10.1	2.0
M_{1-6}	-37.1	36.3	0.7	M_{4-12}	-6.0	-6.8	0.8
M_{1-7}	-4.5	-5.8	1.3	M_{5-6}	10.8	12.8	2.0
M_{1-8}	2.5	4.1	1.6	M_{5-7}	10.5	12.3	1.8
M_{1-9}	4.9	3.8	1.1	M_{5-8}	21.7	29.4	7.7
M_{1-10}	-59.0	-58.4	0.5	M_{5-9}	8.6	10.4	1.8
M_{1-11}	-14.8	-13.3	1.5	M_{5-10}	-5.5	-3.3	2.2
M_{1-12}	-5.2	-4.5	0.8	M_{5-11}	12.7	14.8	2.1
M_{2-3}	-9.5	-9.8	0.3	M_{5-12}	7.2	8.5	1.3
M_{2-4}	-32.3	-32.2	0.1	M_{6-7}	-10.6	-9.6	1.0
M_{2-5}	-1.7	-3.0	1.3	M_{6-8}	17.5	15.7	1.8
M_{2-6}	-26.8	-26.6	0.2	M_{6-9}	3.4	3.5	0.1
M_{2-7}	-3.5	-4.4	0.9	M_{6-10}	49.5	48.5	0.9
M_{2-8}	-14.8	-14.4	0.4	M_{6-11}	-7.7	-9.4	1.8
M_{2-9}	-5.6	-5.1	0.5	M_{6-12}	-5.3	-5.0	0.2
M_{2-10}	-28.8	-29.0	0.2	M_{7-8}	13.5	16.4	2.9
M_{2-11}	-7.3	-7.1	0.2	M_{7-9}	7.6	9.3	1.7
M_{2-12}	-2.9	-3.3	0.4	M_{7-10}	5.8	7.5	1.7
M_{3-4}	1.5	3.7	2.2	M_{7-11}	23.2	30.	7.3
M_{3-5}	-13.1	-16.2	3.1	M_{7-12}	8.9	10.7	1.8
M_{3-6}	-6.9	-7.2	0.3	M_{8-9}	19.6	21.4	1.8
M_{3-7}	-7.0	-9.6	2.6	M_{8-10}	-8.0	-10.6	2.6
M_{3-8}	-23.6	-28.3	4.7	M_{8-11}	20.2	23.4	3.2
M_{3-9}	-14.6	-17.3	2.6	M_{8-12}	11.7	13.8	2.2
M_{3-10}	1.4	1.6	0.2	M_{9-10}	2.5	2.9	0.4
M_{3-11}	-10.1	-13.2	3.1	M_{9-11}	12.7	14.5	1.8
M_{3-12}	-6.8	-8.9	2.1	M_{9-12}	9.3	10.5	1.2
M_{4-5}	-20.7	-21.4	0.7	M_{10-11}	24.2	22.4	1.8
M_{4-6}	17.2	16.4	0.8	M_{10-12}	-3.0	-3.0	0.0
M_{4-7}	-6.6	-7.4	0.8	M_{11-12}	20.5	22.3	1.8

B Curriculum Vitae

December 3, 2013	Ph.D. Defense in Electrical Engineering Technische Universität Darmstadt
2010	Master of Science in Physics with distinction Eidgenössische Technische Hochschule Zürich
2008	Bachelor of Science in Physics Eidgenössische Technische Hochschule Zürich
2005	Abitur Parler Gymnasium, Schwäbisch Gmünd

C Lists of Abbreviations and Symbols

Abbreviations

3D	3-dimensional.
AC	Alternating Current.
CAD	Computer Aided Design.
DC	Direct Current.
DG	Discontinuous Galerkin.
EMC	Electromagnetic Compatibility.
EMI	Electromagnetic Interference.
FEM	Finite Element Method.
HPC	High-Performance Computing.
IGBT	Insulated-Gate Bipolar Transistor.
MKL	Math Kernel Library.
MPI	Message Passing Interface.
CST MWS	CST Microwave Studio ®.
PCB	Printed Circuit Board.
PEEC	Partial Element Equivalent Circuit.
PETSc	Portable Extensible Toolkit for Scientific Computation.
rPEEC	Retarded Partial Element Equivalent Circuit.
SI Lanczos	Shift-and-Invert Lanczos.
RFID	Radio-Frequency Identification.
VLSI	Very Large Scale Integrated.

Mathematical Symbols and Operators

$\mathbb{R}$	Set of Real Numbers.
$\mathbb{C}$	Set of Complex Numbers.
j	Imaginary Unit.
$\Re$	Real Part of a Number.
$\Im$	Imaginary Part of a Number.

t	Time.
x	Point in 3D Space.
$\mathscr{F}$	Fourier Transform.
ω	Angular Frequency.
s	Complex Frequency, $s = j\omega$.
δ_{kl}	Kronecker Delta.
$\delta(t - t')$	Dirac Delta Function.
$\delta^{(3)}(x - x')$	Dirac Delta Function in 3D.
$\mathscr{X}$	Finite-Dimensional Vector Space.
$\oplus$	Direct Sum.
rank	Rank of a Matrix.
det	Determinant of a Matrix.
ker	Null Space of a Matrix.
$\langle \circ, \circ \rangle$	Scalar Product.
$\mathbf{1}$	Identity Matrix.
∇	Nabla Operator.
$\nabla\cdot$	Divergence Operator.
$\nabla\times$	Curl Operator.
Δ	Laplace Operator.
$\mathrm{d}a$	2D Surface Integration Element.
d^3x	3D Integration Element.
$\mathscr{O}$	Order of Magnitude.

Electrical Circuits

I	Electrical Current in Circuit.
V	Electrical Voltage in Circuit.
E	Electrical Energy.
P	Electrical Power.
R	Resistance.
L	Inductance.
C	Capacitance.
$\mathbf{A}$	Incidence Matrix of an Electrical Circuit.
$\mathbf{B}$	Fundamental Loop Matrix of an Electrical Circuit.
$\mathbf{I}$	Vector of Edge Currents.
$\mathbf{I}_R$	Vector of Currents in Resistors.
$\mathbf{I}_L$	Vector of Currents in Inductors.

$\mathbf{I}_C$	Vector of Currents in Capacitors.
$\mathbf{I}_s$	Vector of Currents in Sources.
$\mathbf{V}$	Vector of Edge Voltages.
$\mathbf{V}_R$	Vector of Voltages across Resistors.
$\mathbf{V}_L$	Vector of Voltages across Inductors.
$\mathbf{V}_C$	Vector of Voltages across Capacitors.
$\mathbf{V}_s$	Vector of Voltages across Sources.
$\mathbf{A}_R$	Incidence Matrix of the Resistive Subcircuit.
$\mathbf{R}$	Resistance Matrix.
$\widehat{\mathbf{G}}$	Resistive Circuit matrix, $\widehat{\mathbf{G}} = \mathbf{A}_R \mathbf{R}^{-1} \mathbf{A}_R^{\mathrm{T}}$.
$\mathbf{A}_L$	Incidence Matrix of the Inductive Subcircuit.
$\mathbf{L}$	Inductance Matrix.
$\widehat{\mathbf{L}^{-1}}$	Inductive Circuit Matrix, $\widehat{\mathbf{L}^{-1}} = \mathbf{A}_L \mathbf{L}^{-1} \mathbf{A}_L^{\mathrm{T}}$.
$\mathbf{A}_C$	Incidence Matrix of the Capacitive Subcircuit.
$\mathbf{C}$	Capacitance Matrix.
$\widehat{\mathbf{C}}$	Capacitive Circuit Matrix, $\widehat{\mathbf{C}} = \mathbf{A}_C \mathbf{C} \mathbf{A}_C^{\mathrm{T}}$.
$\mathbf{A}_s$	Incidence Matrix of the Source Subcircuit.
Φ	Vector of Node Potentials.
$\mathbf{Q}$	Vector of Node Charges.
$\mathbf{Z}$	Z Parameter Matrix.

Macroscopic Electrodynamics

ρ	Electric Charge Density.
$\vec{j}$	Electric Current Density.
$\vec{E}$	Electric Field Strength.
$\vec{B}$	Magnetic Field Strength.
$\vec{D}$	Electric Displacement Field.
$\vec{H}$	Magnetizing Field.
ϵ	Electric Permittivity.
ϵ_0	Dielectric Constant.
μ	Magnetic Permeability.
μ_0	Magnetic Constant.
σ	Electric Conductivity.
$\vec{A}$	Magnetic Vector Potential.

ϕ	Electric Scalar Potential.
u	Electromagnetic Energy Density.
$\mathbf{P}$	Potential Matrix.

Discrete Electrodynamics

$\mathscr{D}$	System of Partial Differential Equations.
u	Excitation Function.
f	Unknown Function.
Ω	Computational Domain.
$\partial\Omega$	Boundary of Computational Domain.
$\mathscr{H}(\Omega)$	Vector Space of Functions defined on Ω.
$\mathscr{H}^{\mathrm{D}}(\Omega)$	Discretization of $\mathscr{H}(\Omega)$.
f^{D}	Discretization of f, Element of $\mathscr{H}^{\mathrm{D}}(\Omega)$.
ϕ_i	Nodal FEM Basis Function.
$\vec{v}_{ij}$	FEM Edge Basis Function.
$\vec{m}_k$	PEEC Basis Function, Current Cell.
v_l	PEEC Basis Function, Charge Cell.

Spectral Theory

$\mathbf{L}(s)$	Matrix Polynomial.
$\mathbf{A}_k$	Coefficient Matrix in Matrix Polynomial.
σ	Spectrum of Matrix Polynomial.
s_k	k-th Eigenvalue.
$\mathbf{x}_k$	k-th Right Eigenvector.
$\mathbf{y}_k$	k-th Left Eigenvector.
α_k	Algebraic Multiplicity of k-th Eigenvalue.
β_k	Geometric Multiplicity of k-th Eigenvalue.
$\mathbf{C}_1$	First Companion Form.
$\mathbf{C}_2$	Second Companion Form.
$\mathbf{J}$	Jordan Matrix.
$(\mathbf{X},\mathbf{J},\mathbf{Y})$	Canonical Triple of Matrix Polynomial.
$\bar{\mathbf{x}}$	Element-Wise Complex Conjugate of $\mathbf{x}$.
$\mathbf{A}_k^{\dagger}$	Complex Conjugate of $\mathbf{A}_k$.
λ_k	Normalization Coefficient for the k-th Eigenvector.

Λ	Diagonal Matrix of Normalization Coefficients.
$\mathscr{K}_k$	Krylov Space after k Iterations.

Equivalent Electrical Circuits

s_k	k-th Complex Eigenfrequency.
$\mathbf{S}$	Diagonal Matrix of Eigenfrequencies.
Φ_k	Vector of Node Potentials of k-th Circuit Eigenmode.
Φ	Matrix of Circuit Eigenmodes.
ϕ_k	Scalar Potential of k-th Darwin Eigenmode.
λ_k	Normalization Coefficient for k-th Eigenmode.
Λ	Diagonal Matrix of Normalization Coefficients.
$\vec{j}_\sigma$	Conduction Current.
$\vec{j}_D$	Displacement Current.
g	Auxiliary Function for Current Source Modeling.
P_{kl}	Contribution from k-th and l-th Eigenmode to Total Dissipated Power.
$E_{C,kl}$	Contribution from k-th and l-th Eigenmode to Total Capacitive Energy.
L_{LF}	Low-Frequency Inductance.
L_{HF}	High-Frequency Inductance.

Bibliography

[1] A. Ruehli, "Inductance Calculations in a Complex Integrated Circuit Environment," *IBM Journal of Research and Development*, vol. 16, no. 5, pp. 470–481, 1972.

[2] Y. Ismail and E. Friedman, "Effects of inductance on the propagation delay and repeater insertion in VLSI circuits," *IEEE Transactions on Very Large Scale Integration (VLSI) Systems*, vol. 8, no. 2, pp. 195–206, 2000.

[3] A. E. Ruehli, "Equivalent Circuit Models for Three-Dimensional Multiconductor Systems," *IEEE Transactions on Microwave Theory and Techniques*, vol. 22, no. 3, pp. 216–221, 1974.

[4] M. Caponet, F. Profumo, R. De Doncker, and A. Tenconi, "Low stray inductance bus bar design and construction for good EMC performance in power electronic circuits," *IEEE Transactions on Power Electronics*, vol. 17, no. 2, pp. 225–231, 2002.

[5] R. Bayerer and D. Domes, "Power circuit design for clean switching," in *International Conference on Integrated Power Electronics Systems*, pp. 1–6, 2010.

[6] W. Tabisz and F. Lee, "Zero-voltage-switching multi-resonant technique-a novel approach to improve performance of high frequency quasi-resonant converters," in *19th Annual IEEE Power Electronics Specialists Conference*, vol. 1, pp. 9–17, 1988.

[7] B. Archambeault and A. Ruehli, "Analysis of power/ground-plane EMI decoupling performance using the partial-element equivalent circuit technique," *IEEE Transactions on Electromagnetic Compatibility*, vol. 43, no. 4, pp. 437–445, 2001.

[8] S. Wang, F. Lee, D. Chen, and W. Odendaal, "Effects of parasitic parameters on EMI filter performance," *IEEE Transactions on Power Electronics*, vol. 19, no. 3, pp. 869–877, 2004.

[9] S. Director and R. Rohrer, "The Generalized Adjoint Network and Network Sensitivities," *IEEE Transactions on Circuit Theory*, vol. 16, no. 3, pp. 318–323, 1969.

[10] P. Scholz, W. Ackermann, and T. Weiland, "Derivatives of partial inductances for the sensitivity analysis in PEEC systems," in *2010 URSI International Symposium on Electromagnetic Theory (EMTS)*, pp. 48–51, 2010.

[11] V. Ladogubets, O. Beznosyk, and O. Finogenov, "Presentation of a system of ordinary differential equations as an equivalent electrical circuit," in *Proceedings of VIth International Conference on Perspective Technologies and Methods in MEMS Design*, pp. 116–120, 2010.

[12] G. Antonini, "SPICE equivalent circuits of frequency-domain responses," *IEEE Transactions on Electromagnetic Compatibility*, vol. 45, no. 3, pp. 502–512, 2003.

[13] T. Wittig, *Zur Reduzierung der Modellordnung in elektromagnetischen Feldsimulationen*. Göttingen: Cuvillier Verlag, 2003.

[14] R. Johnson, C. Chang, P. Asbeck, M. Wood, G. Garcia, and I. Lagnado, "Comparison of microwave inductors fabricated on silicon-on-sapphire and bulk silicon," *IEEE Microwave and Guided Wave Letters*, vol. 6, no. 9, pp. 323–325, 1996.

[15] C. Yue and S. Wong, "On-chip spiral inductors with patterned ground shields for Si-based RF ICs," *IEEE Journal of Solid-State Circuits*, vol. 33, no. 5, pp. 743–752, 1998.

[16] B. Schweighofer, K. Raab, and G. Brasseur, "Modeling of high power automotive batteries by the use of an automated test system," *IEEE Transactions on Instrumentation and Measurement*, vol. 52, no. 4, pp. 1087–1091, 2003.

[17] M. Chen and G. Rincon-Mora, "Accurate electrical battery model capable of predicting runtime and I-V performance," *IEEE Transactions on Energy Conversion*, vol. 21, no. 2, pp. 504–511, 2006.

[18] P. Baudry, M. Neri, M. Gueguen, and G. Lonchampt, "Electro-thermal modelling of polymer lithium batteries for starting period and pulse power," *Journal of power sources*, vol. 54, no. 2, pp. 393–396, 1995.

[19] N. G. Elvin and A. A. Elvin, "A general equivalent circuit model for piezoelectric generators," *Journal of Intelligent Material Systems and Structures*, vol. 20, no. 1, pp. 3–9, 2009.

[20] W. Smith, H. Gerard, J. H. Collins, T. Reeder, and H. Shaw, "Analysis of Interdigital Surface Wave Transducers by Use of an Equivalent Circuit Model," *IEEE Transactions on Microwave Theory and Techniques*, vol. 17, no. 11, pp. 856–864, 1969.

[21] A. Bryant, P. Mawby, P. Palmer, E. Santi, and J. Hudgins, "Exploration of Power Device Reliability Using Compact Device Models and Fast Electrothermal Simulation," *IEEE Transactions on Industry Applications*, vol. 44, no. 3, pp. 894–903, 2008.

[22] J. T. Hsu and L. Vu-Quoc, "A rational formulation of thermal circuit models for electrothermal simulation. I. Finite element method," *IEEE Transactions on Circuits and Systems*, vol. 43, no. 9, pp. 721–732, 1996.

[23] J. T. Hsu and L. Vu-Quoc, "A rational formulation of thermal circuit models for electrothermal simulation. II. Model reduction techniques," *IEEE Transactions on Circuits and Systems*, vol. 43, no. 9, pp. 733–744, 1996.

[24] A. Hefner and D. Blackburn, "Thermal component models for electrothermal network simulation," *IEEE Transactions on Components, Packaging, and Manufacturing Technology*, vol. 17, no. 3, pp. 413–424, 1994.

[25] A. Ammous, S. Ghedira, B. Allard, H. Morel, and D. Renault, "Choosing a thermal model for electrothermal simulation of power semiconductor devices," *IEEE Transactions on Power Electronics*, vol. 14, no. 2, pp. 300–307, 1999.

[26] D. Cottet, U. Drofenik, and J.-M. Meyer, "A systematic design approach to thermal-electrical power electronics integration," in *Electronics System-Integration Technology Conference*, pp. 219–224, 2008.

[27] A. Morandi, M. Fabbri, and P. Ribani, "Coupled electromagnetic-thermal model and equivalent circuit of a magnetic shield type sfcl," *IEEE Transactions on Applied Superconductivity*, vol. 23, no. 3, p. 5602705, 2013.

[28] "Robert Bosch GmbH." `www.bosch.de`. Accessed 2013-09-30.

[29] M. Van Valkenburg, *Network Analysis*, ch. 2. Upper Saddle River: Prentice Hall, 1974.

[30] M. Van Valkenburg, *Network Analysis*, ch. 5. Upper Saddle River: Prentice Hall, 1974.

[31] M. Van Valkenburg, *Network Analysis*, ch. 7. Upper Saddle River: Prentice Hall, 1974.

[32] N. Deo, *Graph Theory*, ch. 7. Upper Saddle River: Prentice Hall, 1974.

[33] N. Deo, *Graph Theory*, ch. 13. Upper Saddle River: Prentice Hall, 1974.

[34] J. D. Jackson, *Electrodynamics*. Hoboken: Wiley, 3 ed., 1999.

[35] A. Ruehli and H. Heeb, "Circuit models for three-dimensional geometries including dielectrics," *IEEE Transactions on Microwave Theory and Techniques*, vol. 40, no. 7, pp. 1507–1516, 1992.

[36] P.-A. Raviart and E. Sonnendrücker, "A hierarchy of approximate models for the Maxwell equations," *Numerische Mathematik*, vol. 73, no. 3, pp. 329–372, 1996.

[37] J. Larsson, "Electromagnetics from a quasistatic perspective," *American Journal of Physics*, vol. 75, pp. 230–240, 2007.

[38] A. E. Ruehli and P. A. Brennan, "Efficient Capacitance Calculations for Three-Dimensional Multiconductor Systems," *IEEE Transactions on Microwave Theory and Techniques*, vol. 21, no. 2, pp. 76–82, 1973.

[39] K. Nabors and J. White, "FastCap: A multipole accelerated 3-D capacitance extraction program," *IEEE Transactions on Computer-Aided Design of Integrated Circuits and Systems*, vol. 10, no. 11, pp. 1447–1459, 1991.

[40] J. Ekman, G. Antonini, and A. Orlandi, "3D PEEC capacitance calculations," in *IEEE International Symposium on Electromagnetic Compatibility*, vol. 2, pp. 630–635, 2003.

[41] S. Koch, *Quasistatische Feldsimulationen auf der Basis von Finiten Elementen und Spektralmethoden in der Anwendung auf supraleitende Magnete*. PhD thesis, Technische Universität Darmstadt, 2009.

[42] M. Kamon, M. J. Tsuk, and J. K. White, "FastHenry: A multipole-accelerated 3-D inductance extraction program," *IEEE Transactions on Microwave Theory and Techniques*, vol. 42, no. 9, pp. 1750–1758, 1994.

[43] J.-M. Jin, *The finite element method in electromagnetics*, ch. 2. New York: Wiley, 2002.

[44] J.-M. Jin, *The finite element method in electromagnetics*. New York: Wiley, 2002.

[45] J. Zhu and O. Zienkiewicz, "Adaptive techniques in the finite element method," *Communications in applied numerical methods*, vol. 4, no. 2, pp. 197–204, 1988.

[46] R. Verfürth, "A posteriori error estimation and adaptive mesh-refinement techniques," *Journal of Computational and Applied Mathematics*, vol. 50, no. 1, pp. 67–83, 1994.

[47] I. Babuska, B. A. Szabo, and N. Katz, "The p-version of the finite element method," *SIAM journal on numerical analysis*, vol. 18, no. 3, pp. 515–545, 1981.

[48] M. Ainsworth and B. Senior, "Aspects of an adaptive hp-finite element method: Adaptive strategy, conforming approximation and efficient solvers," *Computer Methods in Applied Mechanics and Engineering*, vol. 150, no. 1, pp. 65–87, 1997.

[49] J. S. Hesthaven and T. Warburton, "Nodal high-order methods on unstructured grids: I. Time-domain solution of Maxwell's equations," *Journal of Computational Physics*, vol. 181, no. 1, pp. 186–221, 2002.

[50] D. N. Arnold, F. Brezzi, B. Cockburn, and L. D. Marini, "Unified analysis of discontinuous Galerkin methods for elliptic problems," *SIAM journal on numerical analysis*, vol. 39, no. 5, pp. 1749–1779, 2002.

[51] D. Sun, J. Manges, X. Yuan, and Z. Cendes, "Spurious modes in finite-element methods," *IEEE Antennas and Propagation Magazine*, vol. 37, no. 5, pp. 12–24, 1995.

[52] B. Rahman and J. Davies, "Finite-element solution of integrated optical waveguides," *Lightwave Technology, Journal of*, vol. 2, no. 5, pp. 682–688, 1984.

[53] A. Pinchuk, C. W. Crowley, and P. Silvester, "Spurious solutions to vector diffusion and wave field problems," *IEEE Transactions on Magnetics*, vol. 24, no. 1, pp. 158–161, 1988.

[54] K. Ise, K. Inoue, and M. Koshiba, "Three-dimensional finite-element solution of dielectric scattering obstacles in a rectangular waveguide," *IEEE Transactions on Microwave Theory and Techniques*, vol. 38, no. 9, pp. 1352–1359, 1990.

[55] B.-N. Jiang, J. Wu, and L. A. Povinelli, "The origin of spurious solutions in computational electromagnetics," *Journal of computational physics*, vol. 125, no. 1, pp. 104–123, 1996.

[56] G. Mur and A. de Hoop, "A finite-element method for computing three-dimensional electromagnetic fields in inhomogeneous media," *IEEE Transactions on Magneticsn*, vol. 21, no. 6, pp. 2188–2191, 1985.

[57] J.-C. Nédélec, "Mixed finite elements in R3," *Numerische Mathematik*, vol. 35, no. 3, pp. 315–341, 1980.

[58] A. Bossavit, "Whitney forms: a class of finite elements for three-dimensional computations in electromagnetism," *IEE Proceedings A (Physical Science, Measurement and Instrumentation, Management and Education, Reviews)*, vol. 135, no. 8, pp. 493–500, 1988.

[59] A. Chatterjee, J.-M. Jin, and J. Volakis, "Computation of cavity resonances using edge-based finite elements," *IEEE Transactions on Microwave Theory and Techniques*, vol. 40, no. 11, pp. 2106–2108, 1992.

[60] J. Wang and N. Ida, "Eigenvalue analysis in electromagnetic cavities using divergence free finite elements," *IEEE Transactions on Magnetics*, vol. 27, no. 5, pp. 3978–3981, 1991.

[61] G. Mur, "Edge elements, their advantages and their disadvantages," *IEEE Transactions on Magnetics*, vol. 30, no. 5, pp. 3552–3557, 1994.

[62] R. Abdul-Rahman and M. Kasper, "Orthogonal hierarchical Nedelec elements," *IEEE Transactions on Magnetics*, vol. 44, no. 6, pp. 1210–1213, 2008.

[63] P. Ingelstrom, "A new set of H (curl)-conforming hierarchical basis functions for tetrahedral meshes," *IEEE Transactions on Microwave Theory and Techniques*, vol. 54, no. 1, pp. 106–114, 2006.

[64] S. Koch, H. Schneider, and T. Weiland, "A Low-Frequency Approximation to the Maxwell Equations Simultaneously Considering Inductive and Capacitive Phenomena," *IEEE Transactions on Magnetics*, vol. 48, no. 2, pp. 511–514, 2012.

[65] "CST - Computer Simulation Technology." `www.cst.com`. Accessed 2013-08-20.

[66] C. Geuzaine and J.-F. Remacle, "Gmsh: A 3-D finite element mesh generator with built-in pre-and post-processing facilities," *International Journal for Numerical Methods in Engineering*, vol. 79, no. 11, pp. 1309–1331, 2009.

[67] S. Balay, J. Brown, K. Buschelman, W. D. Gropp, D. Kaushik, M. G. Knepley, L. C. McInnes, B. F. Smith, and H. Zhang, "PETSc Web page." `http://www.mcs.anl.gov/petsc`. Accessed 2013-09-14.

[68] S. Balay, J. Brown, , K. Buschelman, V. Eijkhout, W. D. Gropp, D. Kaushik, M. G. Knepley, L. C. McInnes, B. F. Smith, and H. Zhang, "PETSc Users Manual," Tech. Rep. ANL-95/11 - Revision 3.4, Argonne National Laboratory, 2013.

[69] S. Balay, W. D. Gropp, L. C. McInnes, and B. F. Smith, "Efficient Management of Parallelism in Object Oriented Numerical Software Libraries," in *Modern Software Tools in Scientific Computing*, (Boston), pp. 163–202, Birkhäuser Press, 1997.

[70] "Intel MKL." `software.intel.com/intel-mkl`. Accessed 2013-09-14.

[71] "Microsoft High Performance Computing Pack." `microsoft.com/hpc`. Accessed 2013-09-14.

[72] X. Li, J. Demmel, J. Gilbert, L. Grigori, M. Shao, and I. Yamazaki, "SuperLU Users Guide," Tech. Rep. 44289, Lawrence Berkeley National Laboratory, September 1999.

[73] X. S. Li and J. W. Demmel, "SuperLU_DIST: A Scalable Distributed-Memory Sparse Direct Solver for Unsymmetric Linear Systems," *ACM Trans. Mathematical Software*, vol. 29, pp. 110–140, June 2003.

[74] "LT Spice." `http://www.linear.com`. Accessed 2013-09-10.

[75] "LT Spice." `http://www.synopsys.com`. Accessed 2013-09-10.

[76] M. Popovich, A. Mezhiba, and E. Friedman, *Power Distribution Networks with On-Chip Decoupling Capacitors*, ch. 2. New York: Springer, 2010.

[77] H. Song, Y. Yoon, M. Steffka, J. Campbell, and R. Young, "A method for measuring partial inductance," in *IEEE International Symposium on Electromagnetic Compatibility*, pp. 335–340, 2011.

[78] G. Antonini, "The fast multipole method for PEEC circuits analysis," in *IEEE International Symposium on Electromagnetic Compatibility*, vol. 1, pp. 446–451, 2002.

[79] G. Antonini, "The fast multipole method for PEEC circuits analysis," in *IEEE International Symposium on Electromagnetic Compatibility*, vol. 1, pp. 446–451, 2002.

[80] S. Kochetov and G. Wollenberg, "Stability of full-wave PEEC models: reason for instabilities and approach for correction," *IEEE Transactions on Electromagnetic Compatibility*, vol. 47, no. 4, pp. 738–748, 2005.

[81] M. Chou, M. Kamon, K. Nabors, J. Phillips, and J. White, "3-d extraction techniques for signal integrity analysis," in *Proceedings of the IEEE Custom Integrated Circuits Conference*, pp. 379–382, 1995.

[82] S. Kochetov, G. Wollenberg, and M. Leone, "Peec-Models Based on Dyadic Green's Functions for Structures in Layered Media," in *International Symposium onElectromagnetic Compatibility and Electromagnetic Ecology*, pp. 179–182, 2007.

[83] H. Wang and J. Fan, "Modeling Local Via Structures Using Innovative PEEC Formulation Based on Cavity Green's Functions With Wave Port Excitation," *IEEE Transactions on Microwave Theory and Techniques*, vol. 61, no. 5, pp. 1748–1757, 2013.

[84] W. Shu and S. Xu, "Capacitance extraction for multiconductor transmission lines in multilayered dielectric media using the numerical Green's function," *Microwave and Optical Technology Letters*, vol. 40, no. 6, pp. 529–531, 2004.

[85] A. Ruehli and H. Heeb, "Circuit models for three-dimensional geometries including dielectrics," *IEEE Transactions on Microwave Theory and Techniques*, vol. 40, no. 7, pp. 1507–1516, 1992.

[86] H. Heeb and A. Ruehli, "Three-dimensional interconnect analysis using partial element equivalent circuits," *IEEE Transactions on Circuits and Systems I: Fundamental Theory and Applications*, vol. 39, no. 11, pp. 974–982, 1992.

[87] J. P. Keradec, E. Clavel, J. P. Gonnet, and V. Mazauric, "Introducing linear magnetic materials in PEEC simulations. Principles, academic and industrial applications," in *Conference Record of the 2005 Industry Applications Conference*, vol. 3, pp. 2236–2240, 2005.

[88] G. Antonini, M. Sabatini, and G. Miscione, "PEEC modeling of linear magnetic materials," in *IEEE International Symposium on Electromagnetic Compatibility*, vol. 1, pp. 93–98, 2006.

[89] Y. Massoud and J. White, "FastMag: a 3-D magnetostatic inductance extraction program for structures with permeable materials," in *IEEE/ACM International Conference on Computer Aided Design*, pp. 478–484, 2002.

[90] G. Antonini, A. E. Ruehli, and C. Yang, "PEEC modeling of dispersive and lossy dielectrics," *IEEE Transactions on Advanced Packaging*, vol. 31, no. 4, pp. 768–782, 2008.

[91] G. Antonini, A. Ruehli, and A. Haridass, "Including dispersive dielectrics in PEEC models," in *Electrical Performance of Electronic Packaging*, pp. 349–352, 2003.

[92] C.-W. Ho, A. E. Ruehli, and P. A. Brennan, "The modified nodal approach to network analysis," *IEEE Transactions on Circuits and Systems*, vol. 22, no. 6, pp. 504–509, 1975.

[93] I. Gohberg, P. Lancaster, and L. Rodman, "Spectral analysis of matrix polynomials I. Canonical forms and divisors," *Linear Algebra and its Applications*, vol. 20, no. 1, pp. 1–44, 1978.

[94] N. J. Higham, D. S. Mackey, N. Mackey, and F. Tisseur, "Symmetric linearizations for matrix polynomials," *SIAM Journal on Matrix Analysis and Applications*, vol. 29, no. 1, pp. 143–159, 2006.

[95] D. S. Mackey, N. Mackey, C. Mehl, and V. Mehrmann, "Vector spaces of linearizations for matrix polynomials," *SIAM Journal on Matrix Analysis and Applications*, vol. 28, no. 4, pp. 971–1004, 2006.

[96] I. Gohberg, M. Kaashoek, and D. Lay, "Equivalence, linearization, and decomposition of holomorphic operator functions," *Journal of Functional Analysis*, vol. 28, no. 1, pp. 102–144, 1978.

[97] I. Gohberg, P. Lancaster, and L. Rodman, "Spectral analysis of matrix polynomials II. The resolvent form and spectral divisors," *Linear Algebra and its Applications*, vol. 21, no. 1, pp. 65–88, 1978.

[98] P. Lancaster, "A fundamental theorem on lambda-matrices with applications. I. Ordinary differential equations with constant coefficients," *Linear Algebra and Its Applications*, vol. 18, no. 3, pp. 189–211, 1977.

[99] F. Tisseur and K. Meerbergen, "The quadratic eigenvalue problem," *SIAM review*, vol. 43, no. 2, pp. 235–286, 2001.

[100] K. Jaenich, *Lineare Algebra*. Heidelberg: Springer, 2010.

[101] I. Gohberg, P. Lancaster, and L. Rodman, "Spectral analysis of selfadjoint matrix polynomials," *The Annals of Mathematics*, vol. 112, no. 1, pp. 33–71, 1980.

[102] I. Gohberg, P. Lancaster, and L. Rodman, *Matrix polynomials*. Philadelphia: SIAM, 2009.

[103] B. Kågström and A. Ruhe, "An algorithm for numerical computation of the jordan normal form of a complex matrix," *ACM Transactions on Mathematical Software (TOMS)*, vol. 6, no. 3, pp. 398–419, 1980.

[104] G. Kalogeropoulos, P. Psarrakos, and N. Karcanias, "On the computation of the Jordan canonical form of regular matrix polynomials," *Linear algebra and its applications*, vol. 385, pp. 117–130, 2004.

[105] Z. Bai, *Templates for the solution of algebraic eigenvalue problems: a practical guide*. Philadelphia: Siam, 2000.

[106] D. S. Watkins, "The QR algorithm revisited," *SIAM review*, vol. 50, no. 1, pp. 133–145, 2008.

[107] A. Quarteroni, R. Sacco, and F. Saleri, *Numerical mathematics*, ch. 5. Berlin: Springer, 2007.

[108] J. M. Ortega and H. F. Kaiser, "The LLT and QR methods for symmetric tridiagonal matrices," *The Computer Journal*, vol. 6, no. 1, pp. 99–101, 1963.

[109] K. Braman, R. Byers, and R. Mathias, "The multishift QR algorithm. I. Maintaining well-focused shifts and level 3 performance," *SIAM Journal on Matrix Analysis and Applications*, vol. 23, no. 4, pp. 929–947, 2002.

[110] K. Braman, R. Byers, and R. Mathias, "The multishift QR algorithm. II. Aggressive early deflation," *SIAM Journal on Matrix Analysis and Applications*, vol. 23, no. 4, pp. 948–973, 2002.

[111] E. Anderson, *LAPACK Users' guide*, vol. 9. Philadelphia: Siam, 1999.

[112] Y. Saad, *Iterative methods for sparse linear systems*. Philadelphia: Siam, 2003.

[113] W. Arnoldi, "The principle of minimized iteration in the solution of the matrix eigenvalue problem," *Quart. Appl. Math. 9*, pp. 17–29, 1951.

[114] A. Ruhe, "Implementation aspects of band Lanczos algorithms for computation of eigenvalues of large sparse symmetric matrices," *Mathematics of Computation*, vol. 33, pp. 680–687, 1979.

[115] J. Cullum and W. Donath, "A block Lanczos algorithm for computing the q algebraically largest eigenvalues and a corresponding eigenspace of large, sparse, real symmetric matrices," in *IEEE Conference on Decision and Control*, vol. 13, pp. 505–509, 1974.

[116] H. Simon, "Analysis of the symmetric Lanczos algorithm with reorthogonalization methods," *Linear Algebra and its Applications*, vol. 61, pp. 101–131, 1984.

[117] C. C. Paige, "Computational variants of the Lanczos method for the eigenproblem," *IMA Journal of Applied Mathematics*, vol. 10, no. 3, pp. 373–381, 1972.

[118] H. D. Simon, "The Lanczos algorithm with partial reorthogonalization," *Mathematics of Computation*, vol. 42, no. 165, pp. 115–142, 1984.

[119] B. Parlett and D. Scott, "The Lanczos Algorithm with selective orthogonalization," *Mathematics of Computation*, vol. 33, pp. 217–238, 1979.

[120] J. K. Cullum and R. A. Willoughby, *Lanczos Algorithms for Large Symmetric Eigenvalue Computations: Volume 1, Theory*. Philadelphia: SIAM, 2002.

[121] V. Hernandez, J. E. Roman, and A. Tomas, "Evaluation of several variants of explicitly restarted Lanczos eigensolvers and their parallel implementations," in *High Performance Computing for Computational Science*, pp. 403–416, 2007.

[122] D. Calvetti, L. Reichel, and D. C. Sorensen, "An implicitly restarted Lanczos method for large symmetric eigenvalue problems," *Electronic Transactions on Numerical Analysis*, vol. 2, no. 1, p. 21, 1994.

[123] D. Sorensen, "Implicitly Restarted Arnoldi/Lanczos Methods for Large Scale Eigenvalue Calculations," in *Parallel Numerical Algorithms*, pp. 119–165, Dordrecht: Kluwer, 1997.

[124] K. Wu and H. Simon, "Thick-restart Lanczos method for large symmetric eigenvalue problems," *SIAM Journal on Matrix Analysis and Applications*, vol. 22, no. 2, pp. 602–616, 2000.

[125] T. Wittig, I. Munteanu, R. Schuhmann, and T. Weiland, "Two-step Lanczos algorithm for model order reduction," *IEEE Transactions on Magnetics*, vol. 38, no. 2, pp. 673–676, 2002.

[126] B. Gustavsen and A. Semlyen, "Rational approximation of frequency domain responses by vector fitting," *IEEE Transactions on Power Delivery*, vol. 14, no. 3, pp. 1052 –1061, 1999.

[127] L.-P. Schmidt, G. Schaller, and M. Siegfried, *Grundlagen der Elektrotechnik 3: Netzwerke*. Bonn: Addison-Wesley, 2006.

[128] A. Bossavit, "On the Lorenz gauge," *COMPEL: The International Journal for Computation and Mathematics in Electrical and Electronic Engineering*, vol. 18, no. 3, pp. 323–336, 1999.

[129] O. Biro and K. Preis, "Finite element analysis of 3-D eddy currents," *IEEE Transactions on Magnetics*, vol. 26, no. 2, pp. 418–423, 1990.

[130] F. Traub, J. Hansen, W. Ackermann, and T. Weiland, "Generation of physical equivalent circuits using 3D simulations," in *IEEE International Symposium on Electromagnetic Compatibility*, pp. 486–491, 2012.

[131] J. D. Jackson, *Electrodynamics*, ch. 5. Hoboken: Wiley, 3 ed., 1999.

[132] G. Lehner, *Electromagnetic Field Theory for Engineers and Physicists*, ch. 5. Berlin: Springer, 2008.

[133] A. Ruehli, G. Antonini, and A. Orlandi, "Extension of the partial element equivalent circuit method to non-rectangular geometries," in *Electromagnetic Compatibility, 1999 IEEE International Symposium on*, vol. 2, pp. 728–733, 1999.

[134] A. Ruehli, G. Antonini, J. Esch, J. Ekman, A. Mayo, and A. Orlandi, "Nonorthogonal PEEC formulation for time- and frequency-domain EM and circuit modeling," *IEEE Transactions on Electromagnetic Compatibility*, vol. 45, no. 2, pp. 167–176, 2003.

[135] P. Feldmann and R. W. Freund, "Efficient linear circuit analysis by Pade approximation via the Lanczos process," *IEEE Transactions on Computer-Aided Design of Integrated Circuits and Systems*, vol. 14, no. 5, pp. 639–649, 1995.

[136] T. Wittig, R. Schuhmann, and T. Weiland, “Model order reduction for large systems in computational electromagnetics,” *Linear algebra and its applications*, vol. 415, no. 2, pp. 499–530, 2006.

[137] P. Degond and P. Raviart, “An analysis of the Darwin model of approximation to Maxwell’s equations,” *Forum Mathematicum*, vol. 4, pp. 13–44, 1992.

[138] P.-A. Raviart and E. Sonnendrücker, “Approximate models for the Maxwell equations,” *Journal of computational and applied mathematics*, vol. 63, no. 1, pp. 69–81, 1995.

[139] N. Fang, C. Liao, and L. Ying, “Darwin Approximation to Maxwell’s Equations,” in *Computational Science*, pp. 775–784, Berlin: Springer, 2009.

[140] A. Kost, *Numerische Methoden in der Berechnung elektromagnetischer Felder*, ch. 4.3. Berlin: Springer, 1994.

[141] P. Ciarlet Jr and J. Zou, “Finite element convergence for the Darwin model to Maxwell’s equations,” *RAIRO-M2AN Modelisation Mathematique et Analyse Numerique*, vol. 31, no. 2, pp. 213–250, 1997.

[142] T. Wittig, I. Munteanu, R. Schuhmann, and T. Weiland, “Model order reduction and equivalent circuit extraction for FIT discretized electromagnetic systems,” *International Journal of Numerical Modelling: Electronic Networks, Devices and Fields*, vol. 15, no. 5-6, pp. 517–533, 2002.

[143] F. Traub, J. Hansen, W. Ackermann, and T. Weiland, “Eigenmodes of electrical components and their relation to equivalent electrical circuits,” in *IEEE International Symposium on Electromagnetic Compatibility*, pp. 287–293, 2013.

[144] F. Traub, J. Hansen, W. Ackermann, and T. Weiland, “Automated construction of physical equivalent circuits for inductive components,” in *International Symposium on Electromagnetic Compatibility (EMC EUROPE)*, pp. 67–72, 2013.

[145] F. Grover, *Inductance Calculations*. Mineola: Dover Publications, 1946.

[146] C. R. Paul, *Inductance: Loop and Partial*. Hoboken: Wiley, 2011.

[147] “ANSYS Q3D Extractor.” `www.ansys.com`. Accessed 2013-10-23.

[148] BMBF Verbundprojekt SOlar, “Abschlussbericht,” to be published.

[149] J. Biela, D. Bortis, and J. Kolar, “Modeling of pulse transformers with parallel-and non-parallel-plate windings for power modulators,” *IEEE Transactions on Dielectrics and Electrical Insulation*, vol. 14, no. 4, pp. 1016–1024, 2007.

[150] A. Henderson, *ParaView Guide, A Parallel Visualization Application*. Kitware Inc., 2007.